

**Surface Chemistry Modification of Glass and  
Gold for Low Density Neural Cell Culture**

Darren James Albutt

Thesis submitted to the University of Nottingham  
for the degree of Doctor of Philosophy

December 2013

## Abstract

Surface chemical modifications are presented for supporting primary neurons in culture. The initial substrates for culture were glass and gold. The surface modifications were based on self assembled monolayer (SAM) approaches. Glass surfaces were initially modified by silanisation with either 3-aminopropyltrimethoxysilane (APTMS) or 3-aminopropyltrimethylethoxysilane (APDES), to present amino-terminated surfaces. Gold surfaces were initially modified by thiol SAMs of either 11-amino-1-undecanethiol (AUT) or a peptide fragment of laminin (PA22-2), to present an amino- or peptide-terminated surface respectively.

The amine-terminated surfaces of both glass and gold were subject to further modification. A heterobifunctional linker, containing a polyethylene glycol (PEG) spacer, was used to couple the peptide PA22-2 to the amino-terminated surfaces.

Surface modifications were characterised using WCA, XPS and ToF-SIMS. The heterobifunctional linker bound homogeneously across the AUT SAM surface, however the linker was not distributed evenly on either of the amino silanisations of glass.

Primary neurons from dissociated embryonic rat hippocampi were cultured on the modified glass and gold surfaces. The cell viability was measured during a 3 week long culture using calcein and ethidium homodimer fluorescence. Neuronal cell cultures were viable on all the gold surface modifications. The only viable glass surface was a control surface of adsorbed poly-l-lysine (PLL) on glass. Cell viability on the AUT and the Peptide-PEG-AUT modified gold surfaces was equivalent to the PLL coated glass.

A quartz crystal microbalance was used to measure the adsorption of components from the cell culture media to the modified surfaces. The culture media was serum free, and requires a supplement for optimum culture viability. Most adsorption was observed on the AUT and peptide SAMs from the supplement, which contains proteins such as bovine albumin. The inclusion of the PEG linker between the AUT and peptide resulted in a lower mass adsorption from the media.

Both the AUT and peptide SAMs on gold supported the neuronal culture despite relatively high protein adsorption. Protein adsorption could be due to electrostatic interactions between the protein and the surface. The adsorbed protein layer is the interface upon which the neurons adhere. When attached via the PEG linker, the peptide surface had better viability, and fewer clustered neurons after 3 weeks compared to the peptide SAM without PEG. This result indicates that reducing protein adsorption upon the surface may result in more evenly distributed neurons on peptide surfaces over longer culture periods.

The presented gold surface modifications provide suitable substrates for neural cultures which can be used in existing applications for investigating neural activity, such as; multi-electrode arrays, micro-fluidics devices, and surface plasmon resonance.

## Acknowledgements

I am grateful to the many people who have encouraged and guided me throughout this research.

I am thankful to Prof. Morgan Alexander for his guidance and support. I appreciate the time for our meetings and discussions, and also the remarkably quick Email responses. His driven attitude has shown me what it takes to succeed a carrier in scientific research.

I thank Dr. Noah Russell for his support and encouragement. His multidisciplinary knowledge base has been an invaluable resource for this research. I believe I am a better scientist thanks to our discussions. A further acknowledgment is given for several of the calculations presented in this thesis.

I am grateful to Tim Smith for preparing the primary cell cultures. I thank Rod Dykeman for the thermal evaporation of gold.

Thanks to Dr. David Scurr for his help with the ToF-SIMS data acquisition. I thank Emily Smith for XPS data acquisition. I thank the following people for training on particular instruments and appreciate their time for discussions we had; Dr. Mischa Zelzer, Prof. Xinyong Chen, and Dr. Kevin Webb.

Thanks to Katharina Reusch for permission to include her cell data set for comparison.

I have been fortunate to work within two groups; the Laboratory of Biophysics and Surface Analysis (LBSA), and the Institute of Biophysics, Optical Imaging and Optical Science (iBIOS). The members of these groups have made my time in research enjoyable and I wish them all well for the future.

I am grateful to the University of Nottingham and the EPSRC for funding this project.

## Contents

---

Abstract .....	i
Acknowledgements .....	iii
Contents .....	iv
Abbreviations .....	viii
<b>I Introduction</b> .....	<b>1</b>
I-1 General Introduction.....	1
I-2 Scientific background.....	1
I-2.1 Surface modification .....	1
I-2.1.1 Organosilane self assembled monolayers.....	2
I-2.1.2 Thiol self assembled monolayers .....	6
I-2.2 Cell adhesion .....	9
I-2.2.1 Extracellular matrix .....	9
I-2.2.2 Integrin receptors.....	10
I-2.2.3 Syndecans .....	10
I-2.2.4 Cadherins .....	10
I-2.2.5 Adhesion <i>in vitro</i> .....	11
I-2.3 Surface properties influencing cell adhesion.....	11
I-2.4 Neurons.....	12
I-2.4.1 Nerve impulse.....	13
I-2.4.2 Synapses .....	14
I-2.4.3 Glia .....	15
I-2.4.4 Neural cell culture .....	15
I-2.5 Surfaces supporting neuronal cell culture .....	16
I-2.5.1 Proteins .....	17
I-2.5.2 Peptides .....	18

I-2.5.3 Other surfaces .....	19
I-3 Aim .....	20
<b>II Methods</b> .....	<b>21</b>
II-1 Surface Characterisation Techniques .....	21
II-1.1 Sessile Drop Water Contact Angle (WCA) Measurement.....	21
II-1.2 Time of Flight Secondary Ion Mass Spectrometry (ToF-SIMS) .....	23
II-1.3 X-ray Photoelectron Spectroscopy (XPS).....	24
II-2 Atomic Force Microscope (AFM) .....	26
II-3 Quartz crystal microbalance with dissipation monitoring (QCM-D) .....	27
II-4 Cell Culture .....	29
II-4.1 Light Microscopy .....	29
II-4.2 Fluorescence Microscopy.....	30
<b>III Substrate Preparation and Characterisation</b> .....	<b>31</b>
III-1 Introduction.....	31
III-2 Experimental .....	32
III-2.1 Glass Surface Modification .....	32
III-2.2 Gold Surface Preparation.....	35
III-2.3 Gold Surface Modification .....	35
III-2.4 Water Contact Angle (WCA) .....	39
III-2.5 X-ray Photoelectron Spectroscopy (XPS) .....	39
III-2.6 Time of Flight Secondary Ion Mass Spectrometry (ToF SIMS) .....	39
III-3 Results.....	40
III-3.1 Gold Adhesion Layer.....	40
III-3.2 Surface Modifications.....	41
III-3.3 Surface Wettability .....	41
III-3.4 Surface Chemistry.....	42

III-3.4.1 XPS .....	42
III-4.2 ToF-SIMS .....	45
III-5 Summary .....	54
<b>IV Response of Primary Neurons _____</b>	<b>56</b>
IV-1 Introduction .....	56
IV-2 Results .....	58
IV-2.1 Qualitative observations .....	58
IV-3 Quantitative observations .....	69
IV-4 Culture model .....	82
IV-5 Summary .....	86
<b>V Protein Adsorption _____</b>	<b>88</b>
V-1 Introduction .....	88
V-2 Experimental details .....	89
V-2.1 Quartz crystal microbalance .....	89
V-2.2 The quartz crystal sensor as a model surface .....	90
V-2.3 Adsorption of Peptide .....	91
V-2.4 Adsorption of Culture Media Components .....	91
V-3 Results .....	94
V-3.1 Peptide adsorption to gold .....	94
V-3.2 Protein adsorption from culture media .....	96
V-3.3 The effect of PEG on protein adsorption .....	100
V-4 Summary .....	100
<b>VI Discussion _____</b>	<b>102</b>
VI-1 Introduction .....	102
VI-2 Protein adsorption and cell culture .....	102

VI-3 Surface chemistry and cell adhesion .....	106
VI-3.1 Amino terminated surfaces.....	110
VI-4 Surface treatments for neuronal culture.....	111
VI-5 Neuronal culture death rate.....	111
VI-6 Current applications.....	111
VI-7 Conclusions .....	112
VI-8 Future Work.....	113
<b>References</b> .....	<b>115</b>
<b>Appendices</b> .....	<b>127</b>

## **Abbreviations**

AFM; Atomic force microscope

AM; Acetomethoxy

ANOVA; Analysis of variance

APDES; (3-aminopropyl)dimethylethoxysilane

APTMS; (3-aminopropyl)trimethoxysilane

AUT; 11-amino-1-undecanethiol

CV; Coefficient of variation

DNA; Deoxyribonucleic acid

ECM; Extracellular matrix

FBS; Foetal bovine serum

HSD; Honestly significant difference

MCP; Micro-channel plate

MEA; Multielectrode array

MPTS; 3-(Mercaptopropyl)trimethoxysilane

N-CAM; Neural cell adhesion molecule

PDL; Poly-D-lysine

PEG; Poly(ethyleneglycol)

pI; Isoelectric point

PLL; Poly-L-lysine

QCM; Quartz crystal microbalance

QCM-D; Quartz crystal microbalance with dissipation monitoring

RF; Radio frequency

SAM; Self Assembled Monolayer

SPR; Surface Plasmon Resonance

ToF-SIMS; Time of Flight Secondary Ion Mass Spectrometry

WCA; Water Contact Angle

XPS; X-ray Photoelectron Spectroscopy

# I Introduction

---

## I-1 General Introduction

The complex form and function presented by the brain makes it an interesting system to study, and the improved treatment for neurological disorders gained from knowledge of how the nervous system works make it an essential system to study. The adult human brain consists of billions of neurons. Neurons form networks of axons and dendrites which transmit electrical impulses to other cells and regions of the brain and body. There are several different types of neurons, and through the release of neurotransmitter molecules neurons have excitatory or inhibitory responses on signalling<sup>[1]</sup>. The brain is therefore a complex system, as such, studying smaller regions in isolation can be beneficial to understanding how the brain functions and processes information. To this end, cell culture techniques are being developed to grow functional networks of neurons in more accessible and defined environments. These methods typically require altering material properties to promote biocompatibility. Typically a suitable biological interface is required to promote the attachment and growth of particular cells. Understanding surface chemistry, and the modification of such surfaces is essential to developing successful interfaces for culturing neurons. These methods can then be applied to many tools and devices aimed at investigating the function of neurons, for example, electrodes and implantable devices.

## I-2 Scientific background

### I-2.1 Surface modification

The surface is defined as the interface between the bulk of the sample and its environment. Frequently, the surface chemistry is modified to achieve certain properties. Common goals include changing the surface wettability, biocompatibility, conductance, or corrosion resistance. These are desired for the final application, or for the next step in the fabrication process. Although this list is not exhaustive, its diversity is profound. As a consequence, surface modification is

widely found through scientific and commercial areas. The applications include micro-fabrication, filtration, small molecule detection and biological interfaces. Of these, biological interfaces include the cell-surface interaction, an area of interest in this study.

In this context, surface modification implies the attachment of a molecule to the surface. The molecule could adsorb onto the surface through non-covalent interactions such as ionic bonding or van der Waals forces. Also, the molecule may become physically bound to the surface through a covalent or metallic bond. Common methods for modifying surface chemistry involve wet chemistry and solid state synthesis. Wet chemistry involves solution based reactions, an example is self-assembly<sup>[2]</sup> which is discussed below. Solid state synthesis includes vacuum evaporation and chemical vapour deposition<sup>[3]</sup>, which can form monolayer films of silanes<sup>[4]</sup>.

Self assembly implies a spontaneous interaction between smaller units to form a larger product. To assemble, one or more units must be mobile. As a result, self assembly is commonly carried out in solution. The coordination of self assembly with a surface can result in a structurally orientated layer. The following sections introduce self assembled monolayers (SAMs) of organosilanes and thiols. A common goal of these processes is to modify the surface to present a specific chemical functionality at the surface.

### **I-2.1.1 Organosilane self assembled monolayers**

Two types of silane used to form SAMs are chlorosilanes and alkoxy-silanes<sup>[5]</sup>. These silanes polymerise to polysiloxanes. This is a two stage process consisting of an initial hydrolysis, followed by condensation as shown in figure I.1. Water is required to hydrolyse the silane to the reactive silanol. Self-condensation occurs between silanol molecules via the hydroxyl (OH) groups, forming the polymer. The chloro- or alkoxy-groups are convenient; preventing polymerisation during storage, and the addition of water starts the polymerisation. The amount of water added determines the extent of polymerisation<sup>[6]</sup>.

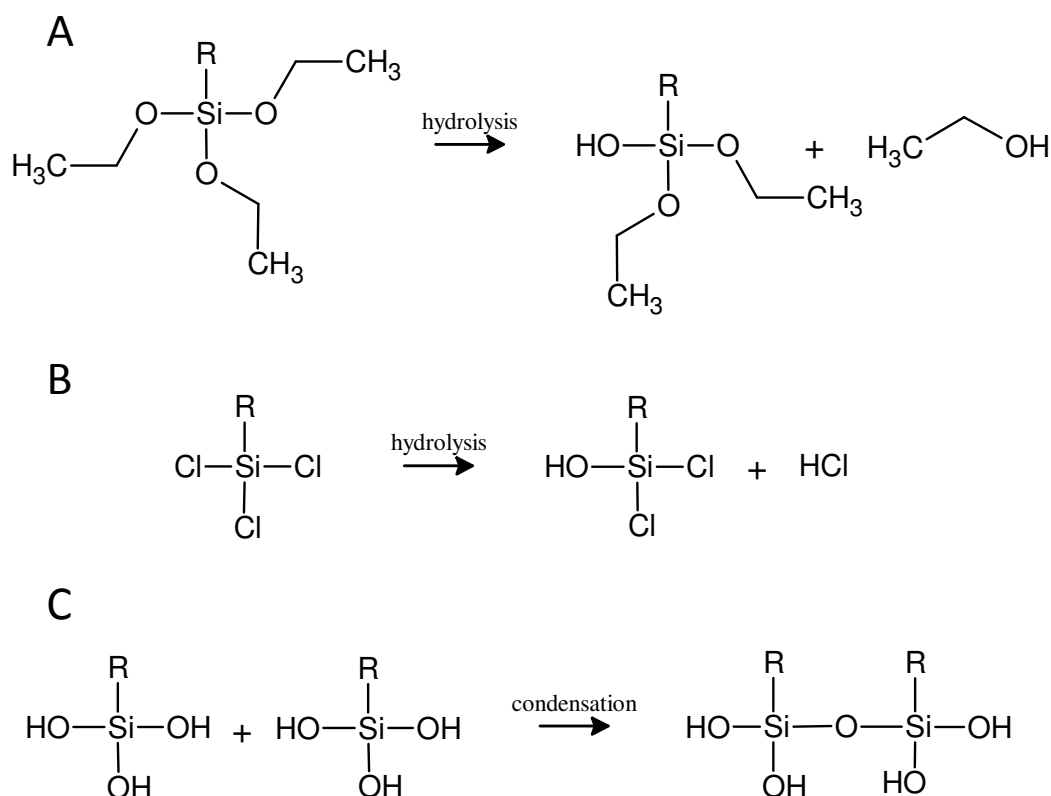


Figure I.1: Hydrolysis of an alkyl- (A) and chloro- (B) silane. Condensation between two silanols (C). Adapted from<sup>[6]</sup>.

The chemical treatment of a substrate/surface with a silane is termed silanisation. The surface must present hydroxyl groups in order for a silane to bond. Oxide surfaces will present hydroxyl groups through the chemisorption of water, which directs further physisorption of water<sup>[7]</sup>. Silicon oxides and metal oxides are commonly used substrates for silanisation<sup>[5]</sup>. Glass is also used, consisting of silicon dioxide, as well as additives such as oxides of sodium, aluminium and boron<sup>[8]</sup>. Ideally, the surface should be free of contamination, such as adventitious hydrocarbon species which adsorb from the atmosphere. Surface contamination may block silanisation and result in poor surface immobilisation. Removing contamination is commonly achieved by oxygen plasma etching or piranha etching. Oxygen plasma etching proceeds under vacuum by electron impact dissociation of oxygen to form radicals<sup>[9]</sup>. The oxygen radicals react with adsorbed organic material forming water and carbon dioxide. Oxygen radicals can also react with the substrate surface forming oxides. Piranha etching occurs in a solution of hydrogen peroxide and sulphuric acid, through the production of peroxomonosulfuric acid<sup>[10]</sup>. This

highly oxidising species will convert organic material to carbon dioxide and water. Surfaces subject to piranha etching may be oxidised and the acid can protonate the oxide forming hydroxyl groups on the surface.

Silane SAM formation is generally assumed to follow the scheme in figure I.2A. Physisorbed water directs hydrolysis to occur at the surface. The silanol then condenses with the surface and other silanol molecules, forming a covalently bound surface monolayer figure I.2B. Often, a heating step is used to remove water, thus driving the siloxane formation to completion.

In practise, the formation of well defined SAMs is difficult. Defects in packing density and polymerisation can result in untreated surface regions or multilayered structures. One possible defect is presented in figure I.2C. Inconsistent amounts of water may cause defects, inherent by the inability to restrict polymerisation to the surface only. Also, the use of functionally terminated silanes can interfere with the silanisation process. For example, terminal amino groups will hydrogen bond with surface hydroxyls<sup>[11]</sup>. The amino group can donate a proton to catalyse the direct condensation of the silane with the surface<sup>[12]</sup>, forming an amino terminated surface.

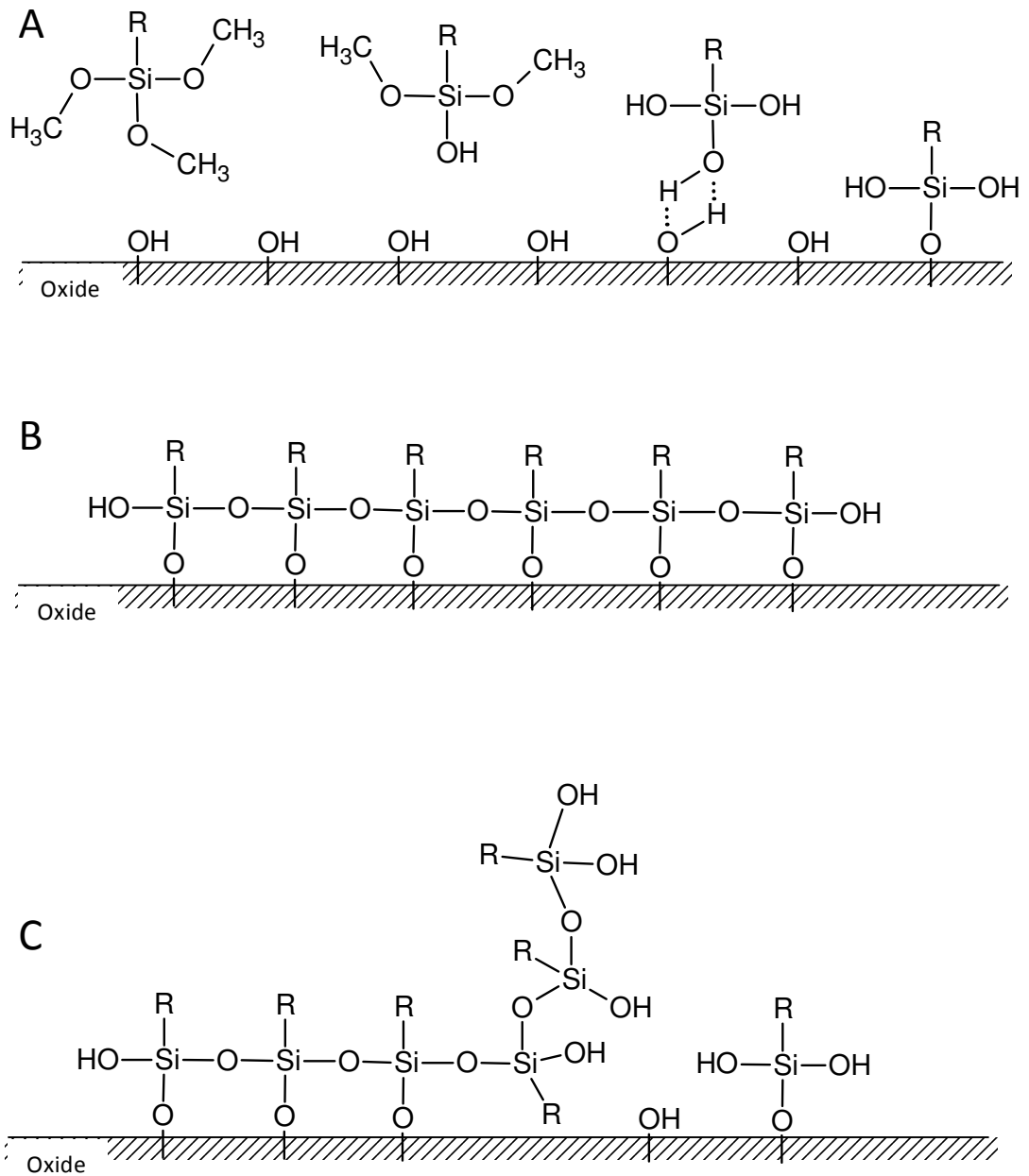


Figure I.2: Process of surface directed silanisation (A). Idealised monolayer (B). Possible defect resulting from silanisation (C)<sup>[6]</sup>.

### I-2.1.2 Thiol self assembled monolayers

Gold presents a surface which has no stable oxide under atmospheric conditions, and resists corrosion from most chemicals. Despite this noble nature, disulfides and thiols have been shown to bond with the gold surface<sup>[2]</sup>. Certain types of these molecules form orientated self assembled monolayers (SAMs). It is widely accepted that the thiol-gold SAMs are structurally more ordered than those formed by silanisation on oxide surfaces<sup>[5]</sup>, as discussed below.

The first SAMs on gold were prepared from organic disulfide molecules with 1 minute immersion times<sup>[13]</sup>. Further work demonstrated that longer immersion times (several hours) of long chain alkanethiols with gold formed well ordered SAMs<sup>[14]</sup>. An alkanethiol consists of an alkyl chain with a terminal thiol group. The opposite terminus may have a different chemistry such as an acid (COOH) or amino (NH<sub>2</sub>) group. The thiol adsorbs to the gold from solution forming a thiolate bond. Adjacent alkane chains orientate with each other via inter-molecular van der Waals forces. As a consequence, the molecules extend perpendicularly to the gold, displaying the terminal group as the new surface. This process is displayed in figure I.3.

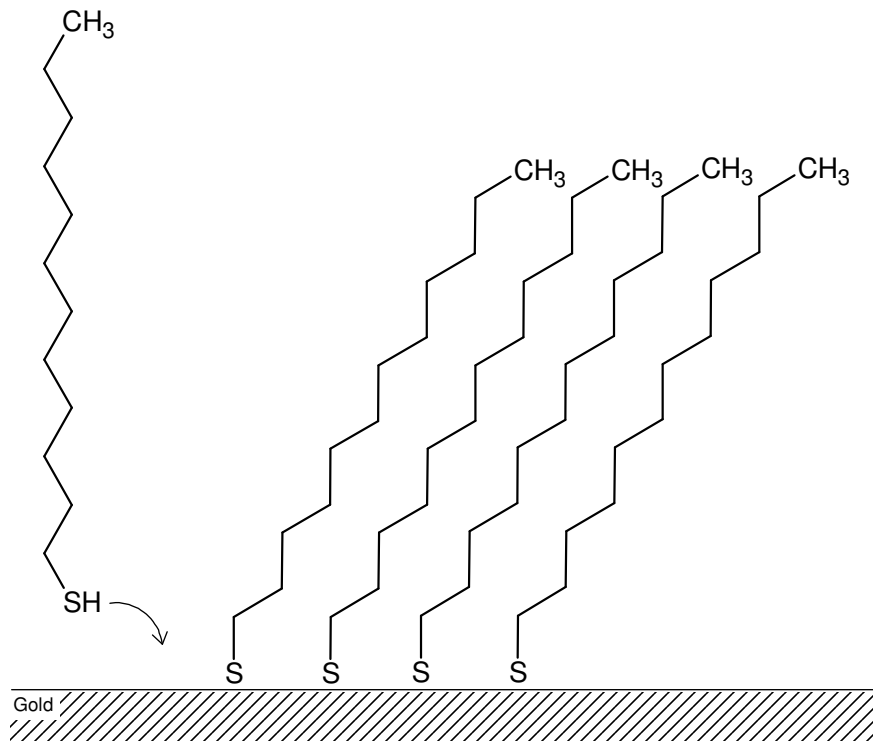
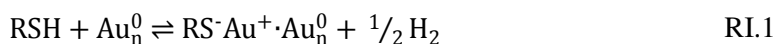


Figure I.3: Alkanethiol adsorption on gold.

It is hypothesised that formation of the gold-thiolate bond occurs through oxidative addition of the thiol bond to the gold surface. Indirect evidence for this mechanism has come from vapour phase depositions of SAMs in the absence of oxygen. Also, nitro (NO<sub>2</sub>) groups have undergone reduction to amino (NH<sub>2</sub>) groups during SAM formation. These observations support the theoretical release of hydrogen by reductive elimination<sup>[15]</sup>, as presented in reaction I.1. The bond strength is ~ 167 kJ mol<sup>-1</sup> and is sp<sup>3</sup> hybridised<sup>[16,17]</sup>.



Alkyl chains greater than 10 carbon atoms in length present more ordered monolayers in comparison to shorter chains. This is due to the increased van der Waals force between the longer chains. Long-chain alkanethiols form densely packed monolayers which are stable under ambient conditions. There are two phases to the adsorption kinetics<sup>[14]</sup>. The first phase is the chemisorption of the thiol to gold. This phase takes several minutes. During this time, the monolayer thickness increases to 80-90% (of the final thickness), and the amount of surface bound carbon saturates. The second phase is the reconfiguration of the alkyl chains into a densely packed, orientated layer. To achieve this highly orientated monolayer takes several hours.

Common substrates are thin gold films prepared by thermal evaporation or sputtering. The resulting gold surface can influence the orientation of the thiols. Gold can be formed as polycrystalline or single crystal surfaces. The unit cell (crystal) structure is face centred cubic with Miller indices of (111) or (100). Gold (111) presents the lowest surface energy, and is therefore the more thermodynamically favourable. This means that gold (111) is the main orientation at the surface<sup>[18]</sup>. Although not fully elucidated the thiol molecules are assumed to orientate in a hexagonal ( $\sqrt{3} \times \sqrt{3}R30^\circ$ ) lattice, with a distance of 0.497 nm between sulfur atoms, figure I.3. A molecular simulation indicates at least 20 molecules of 1-octadecanethiol are required to form an ordered monolayer, with extended alkyl chains<sup>[19]</sup>.

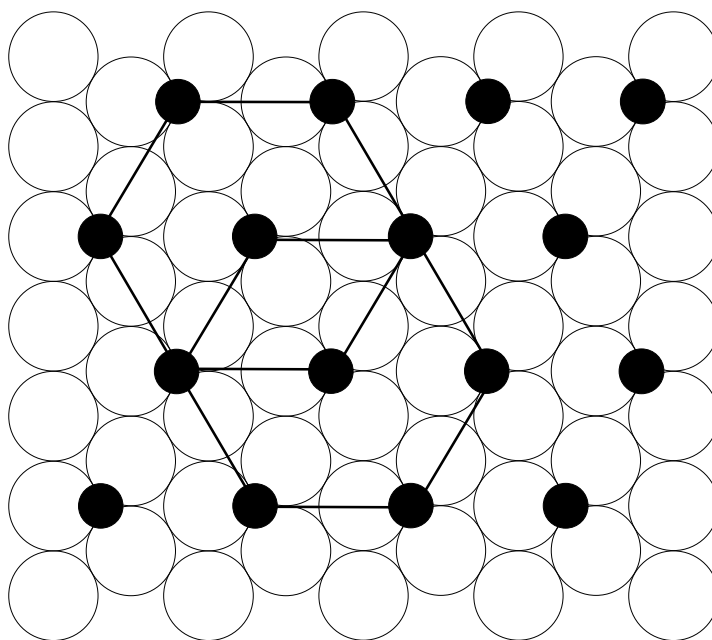


Figure I.3: Hexagonal orientation of alkane thiol bound to gold(111). Open circles are gold atoms, black circles are sulfur atoms<sup>[2]</sup>.

Although the SAM will completely cover the gold surface, some defects have been observed. Molecular vacancies (pinhole defects) occur where one or several thiolates are ‘missing’ from the surface. Domain boundaries are formed where two differently orientated thiol assemblies meet on the surface. In the case of long chain alkanethiols, the alkyl chains are supported by van der Waals forces at a  $\sim 30^\circ$  tilt from the surface normal. During the SAM formation not all regions will ‘tilt’ the same way, forming a boundary where they meet.

Alkanethiol SAMs have been shown to insulate the gold surface from ionic conduction, forming a dielectric film between the gold surface and solution<sup>[20,21]</sup>. As a result, the electric potential produced by ions moving in solution will be diminished or absent at the gold surface. This is important to consider when developing a device to detect the movement of ions in solution, such as when neurons fire action potentials as described in section I-2.4. Detecting neural activity typically requires electrodes with low impedance to improve the signal to noise ratio<sup>[22,23]</sup>. The presence of a SAM may then reduce the sensitivity of a gold electrode to recording extracellular action potentials. However, an electrode modified with an amino-terminated SAM has been used to record the impedance of a cell layer, indicating that some electrical current can cross the SAM<sup>[24]</sup>. SPR with

gold sensors has been shown to detect action potentials<sup>[25]</sup>, although alkanethiolate SAMs were not used. SPR is sensitive to changes of refractive index at the surface, which can detect binding events in the picogram range, and binding events onto alkanethiol SAMs<sup>[26]</sup>. With respect to the development of a sensor for detecting neural activity, the use of a SAM to guide neuronal cell adhesion may benefit a SPR based method over electrodes.

Depending on the final application, the preference for forming monolayer over multilayer surfaces could be inconsequential. However, a monolayer may provide a specific electrical conduction, surface energy, or rigidity: Important for electronic devices and surface force studies respectively. Monolayers also make theoretical considerations easier, such as determination of surface chemical concentration.

## **I-2.2 Cell adhesion**

Knowledge of how cells form adhesions *in vivo* is essential for understanding how cells respond on artificial bio-interfaces. This section covers general mammalian cell-cell and cell-extracellular matrix adhesion. The adhesions are mediated by specific proteins. These proteins are molecules possessing highly conserved structures which are secreted from cells, or displayed across the cell membrane as receptors. The main cell adhesion receptors are integrins, cadherins, and syndecans.

### **I-2.2.1 Extracellular matrix**

The extracellular matrix (ECM) defines the non-cellular exterior support within which a cell resides *in vivo*. Produced by cells, the ECM functions to provide mechanical support and guide cell adhesion. Recent studies indicate the ECM can display or release previously sequestered growth factors<sup>[27]</sup>. Growth factors are involved in directing cell growth, differentiation and function. Thus, the ECM is a dynamic structure important for healthy cell growth. Structurally the ECM consists of proteoglycans, collagens and elastins. Proteins secreted into the ECM that are found to influence cell adhesion include fibronectin and laminin. Adhesion between these ECM proteins and cells occurs through integrin receptors on the cell surface. As will be discussed below (section I-3.5), components of the ECM are commonly used in artificial bio-interfaces to promote cell adhesion.

### **I-2.2.2 Integrin receptors**

Integrin binding provides a strong and specific cell attachment to external surfaces. Integrins are transmembrane receptors, meaning they span across the membrane presenting internal and external domains. The receptors are heterodimeric proteins, consisting of an alpha and beta subunit. There are 24 integrin receptors<sup>[28]</sup>, with different affinities for the various ECM proteins/ligands<sup>[29]</sup>. Ligand binding promotes the receptors to migrate and cluster together<sup>[30]</sup>. Clustering leads to the localisation of intracellular signalling molecules, resulting in a cell response. Actin reorganisation for cell spreading/contraction, proliferation, and differentiation are possible results of integrin binding. Insufficient integrin binding can cause cell death, termed anoikis<sup>[31,32]</sup>. Therefore, integrin binding is important for maintaining functional and healthy cells, beyond simply anchoring the cell.

Integrin binding has been spatially controlled using nano-patterned surfaces<sup>[33]</sup>. A spacing of  $\leq 58$  nm between integrin binding sites was found to be necessary for the cell adhesion and spreading of osteoblasts and fibroblasts. This occurred despite these surfaces constricting the integrin clustering to a hexagonal pattern, which may not occur *in vivo*. None the less, results suggest the distribution of surface ligands is an important consideration for cell adhesion on artificial bio-interfaces.

### **I-2.2.3 Syndecans**

Syndecans are proteoglycans, consisting of a transmembrane protein with covalently bound carbohydrate polymers<sup>[34]</sup>. These polymers are un-branched glycosaminoglycan chains, upon which ligand binding is associated. As with integrins, syndecans can move within the cell membrane. A large number of ligands can associate with syndecans. In terms of extracellular matrix adhesions, the ligands include collagen, fibronectin and laminin. Cell-cell adhesions occur through L-selectin and N-CAM (neural cell adhesion molecule) among others. A synergistic role for syndecans involves sequestering soluble growth factors for neighbouring receptors. Also, co-operation with integrins are proposed to initiate intracellular signalling mechanisms<sup>[28]</sup>.

### **I-2.2.4 Cadherins**

Cadherins are involved in cell-cell adhesions. They require extracellular calcium ions to function, resulting in cell clusters. Members of the cadherin protein receptors

include E-cadherin (endothelial tissue), N-cadherin (neurons) and P-cadherin (placental tissue).

### **I-2.2.5 Adhesion *in vitro***

Several types of cell adhesions have been characterised *in vitro* for fibroblasts; focal complexes, focal adhesions, and fibrillar adhesions<sup>[28]</sup>. Focal complexes are temporary adhesions at the leading edge of the cell. Focal adhesions, which originate from the initial focal complexes, provide a larger anchor and stronger adhesion. Fibrillar adhesions form under the central bulk of the cell. Both focal and fibrillar adhesions involve integrin binding.

### **I-2.3 Surface properties influencing cell adhesion**

Cell adhesion to a surface will occur if the cell can attach to a surface. Therefore, the surface must have suitable properties to allow cell adhesion. This section discusses the surface properties known to influence cell adhesion.

Surface wettability has been shown to influence cell adhesion. It is generally observed that cell adhesion is more prominent on hydrophilic surfaces in comparison to hydrophobic surfaces. Gradients of wettability have been shown to influence cell adhesion. Plasma polymer gradients of allylamine and hexane display a gradient of wettability<sup>[35]</sup>: Fibroblasts preferentially adhered to the region with a 60° water contact angle, and to a lesser extent as the gradient became hydrophobic. A further study with plasma polymerised hexane revealed that primary neurons preferentially adhered to hydrophilic rather than hydrophobic regions<sup>[36]</sup>. This trend has also been observed on surfaces pre-adsorbed with cell adhesive proteins. In comparison to hydrophobic glass, hydrophilic glass resulted in increased endothelial cell adhesion when pre-adsorbed with fibronectin<sup>[37]</sup>. Similar results were observed on hydrophilic and hydrophobic acrylate polymers<sup>[38]</sup>. The trend may be attributed to different conformations of the adsorbed proteins as a result of surface wettability<sup>[39]</sup>. Specific regions of the proteins responsible for cell adhesion may become denatured on hydrophobic surfaces, resulting in reduced cell adhesion<sup>[40,41]</sup>. However, modifying surface wettability requires altering other properties which may influence cell adhesion: Such as the chemistry, roughness/topography, charge, or applied electric

field. This can make it difficult to infer cell adhesion results solely to wettability or any particular surface property, rather, all properties should be considered to provide more complete understanding.

Surface roughness has been shown to influence cell adhesion of fibroblasts<sup>[42]</sup>. Cell adhesion was preferred on hydrophilic surfaces with low roughness. Controlling surface topography provides a means to guide cellular adhesion and growth. Topography has been shown to influence the alignment of neurons in culture as reviewed<sup>[43,44]</sup>. Axons of hippocampal neurons orientated along 1  $\mu\text{m}$  wide tracks, and to a lesser extent 2  $\mu\text{m}$  wide tracks in PDMS<sup>[45]</sup>. Groove widths of 5-10  $\mu\text{m}$  in poly(methylmethacrylate) (PMMA) were also shown to guide axon outgrowth of primary neurons after a preconditioned culture with radial glia<sup>[46]</sup>.

## **I-2.4 Neurons**

Neurons are specialised cells which conduct electrical impulses to other neurons or target cells. Networks of neurons form a nervous system *in vivo*, allowing impulses to travel large distances in short times. These networks provide the interface through which an organism interacts with its environment. Responding to rapid changes internally and externally is beneficial for an organism's survival. Although the major cellular components of the brain are glia, the neurons are considered the functional units which co-ordinate the nervous system; including motor control, processing sensory information and the formation and recollection memories.

Understanding how the nervous system develops and functions allows the progression and discovery of treatments for trauma and disease. More fundamentally, the ability to study information processing and computation within neural networks may further knowledge on the biological basis for memory and consciousness<sup>[47,48]</sup>. Measuring the electrical activity of cells, termed electrophysiology, provides a way to probe the signalling of neurons. Several techniques can be used to study electrophysiology; microelectrode recordings, multi-electrode arrays (MEAs), and fluorescence imaging of voltage sensitive dyes<sup>[49]</sup>. Microelectrodes can be used in several configurations to measure extracellular or intracellular potentials, or patch clamp techniques<sup>[50,51]</sup>. Scanning ion conductance

microscopy has also been used for patch clamping ion channels of cardiac cells<sup>[52]</sup>. More recently, surface plasmon resonance (SPR) has been used to detect action potentials from explanted sciatic nerve fibres<sup>[25]</sup>, a primary culture of neurons grown on plasmonic nano-sized gold pads<sup>[53]</sup>, and from *in vivo* cortical tissue via a gold coated optical fibre<sup>[54]</sup>.

The generalised structure of a neuron is shown in figure I.4. Neurons receive incoming signals from other neurons which form synapses with the dendrites and the cell body. The impulse travels down the axon to the terminal branches, these branches can synapse with other cells.

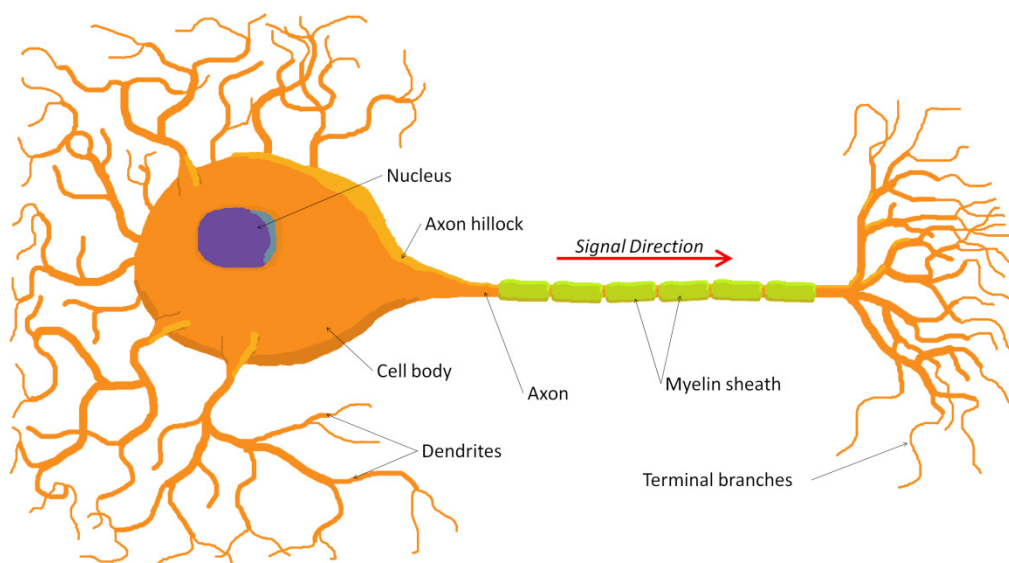


Figure I.4: Generalised structure of a neuron, adapted from<sup>[1]</sup>. The dendrites and cell body receive incoming signals which can cause the neuron to fire an impulse. The impulse travels along the axon and spreads through the terminal branches.

### I-2.4.1 Nerve impulse

Neurons conduct electrical impulses by changing the permeability of their membrane to certain ions. This is achieved by regulating voltage-gated ion channels in the plasma membrane, which open or close depending on the membrane potential. A non stimulated neuron is more negatively charged inside than outside, creating a potential across the membrane; the resting potential. The resting potential is maintained actively by sodium/potassium pumps, which requires adenosine triphosphate to pump sodium ions out, and potassium ions in. The pioneering work in this field was carried out on the squid giant axon<sup>[55]</sup>.

Stimulation causes voltage-gated ion channels to open, allowing ions to cross the membrane changing the potential. If a certain threshold potential is achieved by influx of sodium ions, an action potential will occur, initiated near the axon hillock, figure I.4. The action potential is the nerve impulse, the ‘all or nothing’ event when the membrane potential is briefly depolarised. Neighbouring voltage-gated ion channels open in response to the potential change, propagating the impulse along the neuron. Following the action potential is a refractory period (short time interval) where the membrane potential is hyperpolarised, preventing backward propagation of the impulse. An absolute refractory period exists during which time further stimulus will not cause an action potential. This results from inactivation of sodium ion channels for a short time following depolarisation.

Many neurons have myelinated axons figure I.4, consecutive regions of non conductive myelin produced by glial cells. The myelin sheath makes the signal conduction down the axon faster and more efficient than without. This is achieved by spatially restricting a high concentration of the voltage-gated sodium ion channels to the spaces between the myelin sheath, called nodes of Ranvier. As a result, the depolarisation at the previous node causes an electrotonic potential inside the axon which is able to spread to the next node and induce an action potential. This process is termed saltatory conduction.

#### **I-2.4.2 Synapses**

Synapses are the junctions between neurons and their target. Many cells can form synapses with a particular neuron and modify its activity (ability to fire action potentials), and one neuron can form synapses with different cells. These networks of processes are difficult to trace *in vivo*, but do follow an underlying structure<sup>[56]</sup>. The main types of synapse are electrical and chemical. Electrical synapses communicate the impulse directly, whereas chemical synapses can modulate the signal strength and its effect.

Electrical synapses occur where two cells are connected via channels called gap junctions. These channels allow the direct flow of ions between cells by diffusion, as a result nerve impulses travel rapidly between cells.

Chemical synapses are more common than electrical synapses in vertebrates. Chemical neurotransmitters mediate the signal between the cells. The

neurotransmitters are released when an action potential arrives at the synaptic terminal. Following diffusion across the synaptic cleft the neurotransmitters bind to specific receptors on the postsynaptic cell. The receptors are often ion channels, where ligand binding causes ions to flow into the cell and alter the membrane potential. Depending on the receptor activated, an inhibitory (hyperpolarised) or excitatory (depolarised) response can be achieved. Numerous types of neurotransmitters and receptors can be involved, implicating a complex level of control over the nerve impulse not possible with the electrical synapse alone. These factors may have implications in neuronal computation, how the networks process information<sup>[57]</sup>.

### **I-2.4.3 Glia**

Neurons are supported in their function by other cells, collectively termed glia. Glial cells provide neurons with structural support, cell guidance cues and trophic (survival) factors<sup>[58]</sup>. Although glial cells have not been shown to produce action potentials (defining them from neurons), some are excitable through changes of intracellular calcium concentrations. Astrocytes are the major glial cell type, they can form synapses between themselves and neurons, and can release and bind neurotransmitters to modify neural activity. The tripartite synapse refers to the bi-directional signalling between astrocytes and glia<sup>[59]</sup>, however there is evidence supporting the absence of this synapse in adult tissue<sup>[60]</sup>. Oligodendrocytes, another glial cell, form the myelin sheath around axons, resulting in faster signal transduction<sup>[61]</sup>.

### **I-2.4.4 Neural cell culture**

The culture of primary neurons *in vitro* results in the spontaneous formation of networks of physiologically active neurons. These networks provide models for studying neuronal signalling using electrophysiological and pharmacological tools.

Healthy cell cultures depend on several factors. A suitable media supplies the cells with essential nutrients and growth factors. In the case of a primary culture, the cells are obtained from a dissection, requiring careful isolation of live cells. Neurons are adherent cells, requiring a surface to grow upon. The surface provides an essential support for the neuron's axons and dendrites to grow along, which is required for the spontaneous formation of networks. For initial cell adhesion, it is a

requirement that the surface presents adhesion sites/molecules, without which the cells would not adhere. If no adherent substrate surface is present, the neurons can preferentially adhere to themselves, forming clusters called neurospheres<sup>[62]</sup>. Likewise, if an adherent surface does not adequately provide adhesion sites, the neurons can cluster together<sup>[63,64]</sup>.

The dissection provides a mixture of glial and neuronal cells for the culture. Cultures consisting of mostly neuron cells have been achieved<sup>[65]</sup>. Glial cells can be suppressed by adding antimetabolic agents to the culture, which kill proliferating cells (glia) allowing the non-proliferating cells, neurons, to remain the major constituents of the culture<sup>[66]</sup>. However, the lack of supporting glial cells may make the culture model less representative of the *in vivo* environment.

A commonly used commercially available media is *Neurobasal media*, which is further supplemented with *N2* or *B27* serum free supplements<sup>[67-72]</sup>. The *N2* supplement was developed for culturing a neuroblastoma cell line<sup>[73]</sup>, and *B27* was optimised for culturing primary hippocampal neurons<sup>[69]</sup>. Variations in the quality of cultures using serum containing media, such as with foetal bovine serum due to batch variability, has led to increased use of serum free media. Serum free media can contain proteins, defining it from protein free media and chemically defined media, but no serum supplement is required for cell viability<sup>[74]</sup>. Serum free media may also reduce glial proliferation<sup>[66,67]</sup>.

The cell density can also influence the morphology of the culture and activity of neurons. Cell density is controlled by adjusting the number of cells per unit volume plated onto the surface. Cultures with at least 250 cells/mm<sup>2</sup> for serum free media was required for neurons to display characteristic electrical activity<sup>[75]</sup>. At high densities, >10,000 cells/mm<sup>2</sup>, large islands of clustered cells form after 2 days<sup>[76]</sup>.

### **I-2.5 Surfaces supporting neuronal cell culture**

This section highlights surface treatments which have been used for the adherence of neural cells *in vitro*; neuronal cell cultures. Initial substrates are those commonly used in cell cultures such as glass slides, coverslips, petri dishes and tissue culture plastic. These substrates provide rigid support, are transparent for optical imaging, cheap (per unit) and can be purchased pre-sterilised for immediate use.

One of the most widely used surface treatments for neural cultures are coatings of poly(L-lysine) (PLL)<sup>[66]</sup>. The D enantiomer (optical isomer of L); PDL, is also used for culture. Generally, amino acid polymers of D enantiomers are more resistant to proteolytic degradation, as shown against trypsin cleavage<sup>[77,78]</sup>. As a result, PDL surfaces may last longer than PLL, providing better adhesion in the long term. Poly(lysine) surfaces are often used as a positive control when exploring other treatments. Dissociated cultures of embryonic rat cerebral cells have been shown to adhere to PLL and PDL coated petri dishes<sup>[79]</sup>: The cells formed networks and survived for over 14 days.

Surface treatment involves the adsorption of the poly(lysine) onto the substrate from solution. Followed by rinsing with a buffer solution or sterile water<sup>[80]</sup>, the sample may be dried before use. Covalent attachment of PDL to indium tin oxide has also supported the culture of dissociated neurons<sup>[81]</sup>. This was achieved by silanisation of the oxide surface to display amine groups, and then using glutaraldehyde to cross-link PDL amine groups with the surface bound amines.

Evidence suggests poly(lysine) promotes adhesion through electrostatic interactions between the positively charged lysine and negatively charged species on the cell<sup>[82]</sup>.

### **I-2.5.1 Proteins**

Neurons express cell adhesion receptors described in section I-3.2. These receptors are responsible for tethering the neurons to the extracellular matrix and guiding their growth. Laminin is a protein responsible for neuron adhesion *in vivo*. The protein is a heterotrimer of  $\alpha$ ,  $\beta$ , and  $\gamma$  subunits which form a cross shape. A key domain implicit of the laminin protein family is the alpha helical coiled coil domain.

Laminin displays numerous binding sites for collagen, sulphated lipids, and integrins of various cell types<sup>[29]</sup>. The  $\alpha3\beta1$ ,  $\alpha6\beta1$ ,  $\alpha7\beta1$  and  $\alpha6\beta4$  integrins have been shown to bind laminin<sup>[29]</sup>. Several regions of laminin have been implicated in the adhesion and growth of neural cells<sup>[83,84]</sup>.

Laminin mediates cell adhesion in a variety of tissues<sup>[85]</sup>. In particular, laminin was shown to promote neurite outgrowth, adhesion, and survival of neurons to greater extents than collagen and fibronectin (also ECM components)<sup>[86]</sup>. Fibronectin

is also a commonly used adhesion promoter, which has been shown to support dissociated mouse cortical neurons<sup>[87]</sup>. Adhesion occurs through binding specific integrin receptors for regions of the proteins, unlike the less specific adhesion on poly(lysine). As with poly(lysine), laminin coatings can be made by adsorption from solution<sup>[83,88]</sup>.

The conformation of these proteins is critical to their cell adhesive properties through cell receptor binding. Because the conditions for culture are biological conditions optimised for cell survival, proteins will take natural conformations. However, upon binding to a surface the protein conformation may change<sup>[39]</sup>, denaturing the cell adhesive property of the protein. The initial wettability of the surface to which the protein adsorbs has been shown to be significant. The response of fibroblasts to surfaces of adsorbed albumin and fibronectin on hydrophilic and hydrophobic plasma polymers has been explored<sup>[89]</sup>. Fibroblasts attached to a greater extent when fibronectin was adsorbed to hydrophobic plasma polymerised hexane, than hydrophilic allylamine.

A combination of poly(lysine) and laminin has also been used for neuronal cell culture<sup>[90]</sup>.

### **I-2.5.2 Peptides**

Evidence suggests that cells interact with specific peptide sequences of the cell adhesion proteins via integrin receptors<sup>[91]</sup>. The peptides can be made by enzymatic cleavage of the protein and subsequent protein fragments, or by chemical synthesis such as solid-phase peptide synthesis. When attached to a surface (covalently or otherwise) these peptides can be used to promote cell adhesion. Perhaps the most prolific of these is the arginine-glycine-aspartic acid (RGD) peptide sequence<sup>[92]</sup>, originally found in fibronectin<sup>[93]</sup>. The RGD sequence also occurs in several other ECM proteins, including collagen, vitronectin and laminin. A wide range of integrin receptors are involved in binding RGD<sup>[29]</sup>. Support for specific binding of such peptides by cells comes from several approaches: Deliberate alterations to the peptide sequence results in little or no cell adhesion; reduced adhesion is observed when soluble peptide is added during cell plating, by competing with the substrate bound peptide for receptors on the cell surface. Generally these peptides promote

adhesion to a lesser extent than the whole protein<sup>[84,94]</sup>, due to the existence of multiple adhesion sites and their conformation in the whole structure.

Several peptide fragments of laminin have been identified as adhesion promoters for neuronal cells<sup>[95]</sup>. The peptide fragments can show selectivity for different neuronal cell types<sup>[83]</sup>. The sequence RNAIAEIIKDI supported cultures of rat cerebellar neurons, the peptide was conjugated to bovine serum albumin and adsorbed to glass coverslips<sup>[96]</sup>. The sequence SRARKQAASIKVAVSADR, termed PA22-2, promoted the adhesion of PC12 cells when non-specifically adsorbed onto culture wells. However, in these initial studies the adsorption of peptide resulted in non-covalently bound surfaces, the peptides may have bound in differing configurations and with the possibility of desorbing during the culture. Integrin binding to the IKVAV sequence has been shown to involve the  $\beta$ 1 subunit<sup>[97,98]</sup>.

By adding a terminal cysteine residue to the peptide, peptide SAMs can be formed on gold through the cysteine thiol group. PA22-2 attached via the terminal cysteine on gold supported dissociated mouse hippocampal neurons<sup>[99]</sup>.

### **I-2.5.3 Other surfaces**

Surfaces presenting amine groups, analogous to poly(lysine), can promote neuronal adhesion. This has been observed for dissociated hippocampal cultures on plasma polymerised allylamine<sup>[36]</sup>, poly(allylamine)<sup>[45]</sup>, an amino-terminated SAM on gold<sup>[100]</sup>, and poly(ethylenimine)<sup>[75]</sup>.

Nerve growth factor (NGF), a protein that initiates cell survival, has been covalently linked to a poly(allylamine) coated poly(dimethylsiloxane) surface<sup>[45]</sup>: the presence of NGF resulted in faster axon formation in comparison to the poly(allylamine) coating alone.

### **I-3 Aim**

The primary aim of this thesis is to modify the chemistry of glass and gold surfaces in order to support 2D cultures of primary neurons. This will be based on silane modification of glass, and thiol modification of gold. Further, the chemical properties of the surface treatments will be analysed to help explain the cell response. Any properties found to have positive or negative influences on the cultures development and viability will provide useful input for improving future work. In order to facilitate electrophysiological recordings, the cell cultures should be viable for at least several weeks to allow the culture to develop. Successful treatments on gold surfaces would provide a platform for SPR sensors, and the recording of electrical activity within the networks by SPR.

# II Methods

---

## II-1 Surface Characterisation Techniques

A surface will interface with other solids/liquids/gases which defines it from the bulk/interior of a material. The surface will have distinct chemical and physical properties. The chemical properties include elemental and functional composition. Physical properties include topography, stiffness and surface energy. No one technique can fully characterise all properties of a surface. It is therefore necessary to use several complementary techniques to gain complete understanding of the surface. Listed below are the main techniques used in this study.

- Sessile Drop Water Contact Angle Measurement
- Time Of Flight Secondary Ion Mass Spectrometry
- X-ray Photoelectron Spectroscopy
- Atomic force microscopy

### II-1.1 Sessile Drop Water Contact Angle (WCA) Measurement

Water contact angle measurements can help determine surface energy/tension, although the influence of surface roughness must be considered<sup>[5,101]</sup>. Water is commonly used as the probe liquid because of its ease of handling and the ready availability of pure deionised water. The technique is sensitive to the top *ca.* 1 nm of the solid-liquid interface<sup>[2,102]</sup>.

A common method for measuring the WCA is to use a sessile drop<sup>[2,103]</sup>. A droplet of water is dispensed onto the surface and the angle ( $\theta$ ) between the droplet edge and the surface is recorded as shown in figure II.1. The static contact angle is taken as the angle where the three phase line (the point at which the water droplet interfaces the sample and the external environment) is in equilibrium. Once the droplet has finished spreading on the surface the base diameter is constant and the system can be considered in equilibrium. A surface's wettability can change after treatment; becoming more hydrophobic or hydrophilic.

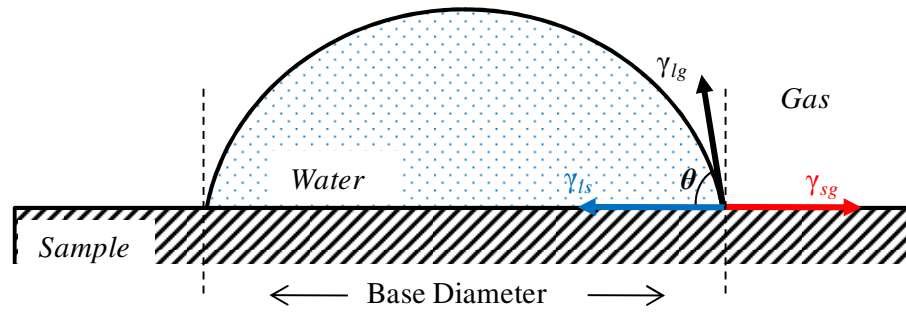


Figure II.1: Profile of a sessile drop showing  $\theta$  and the three phase line. Figure adapted from<sup>[2]</sup>.

$$\gamma_{lg} \cdot \cos \theta = \gamma_{sg} - \gamma_{sl} \quad \text{Eqn. II.1}$$

Young's equation, II.1, describes the relationship between the surface tension and the contact angle  $\theta$ <sup>[103]</sup>. Where  $\gamma_{lg}$ ,  $\gamma_{sg}$  and  $\gamma_{sl}$  are the surface tensions of the three (liquid-vapour, solid-vapour and solid-liquid) interfaces respectively.

Surface roughness will influence  $\theta$ . A surface which is homogeneously wetted by the droplet (figure II.2) can be described by Wenzel<sup>[103]</sup>. In cases where the surface is heterogeneously wetted (figure II.2), the Cassie-Baxter relation is used where the fraction by area of each known interface with the drop will influence  $\theta$ .

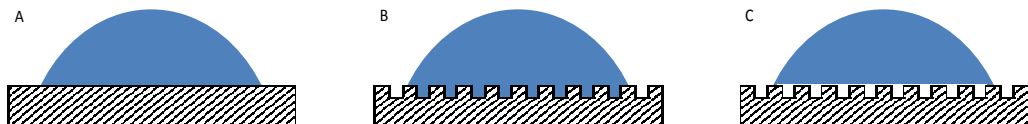


Figure II.2: Water contact angle under A) Young-Laplace, B) Wenzel, and C) Cassie-Baxter conditions.

## II-1.2 Time of Flight Secondary Ion Mass Spectrometry (ToF-SIMS)

ToF-SIMS analysis detects the chemistry of a surface in the form of a mass spectrum, although it is not readily quantifiable. The sample surface is bombarded with high energy ions to fragment and sputter compounds comprising the surface. In static SIMS where surface composition is maintained, a low primary ion beam current is used. Less than 1% of the surface is degraded, and statistically no point on the surface is bombarded more than once. Therefore only secondary ions from the native/static surface are analysed. Specifically these secondary ions originate from the uppermost 2 nm of the surface, inferring static SIMS a high surface specificity<sup>[104]</sup>.

Secondary ions are separated in a time of flight (ToF) mass analyser before detection, figure II.3. The result is a spectrum of ion intensity against mass to charge ratio. In a ToF mass analyser the secondary ions are accelerated to the same energy by an electric field before their flight time to the detector separates them by mass to charge ratio<sup>[105]</sup> defined by equation II.2. The primary ion beam is pulsed for a short time to allow ions to enter ‘flight’ simultaneously. The fragments are analysed and identified according to their mass.

$$t^2 = \frac{mL^2}{2qU_o} \propto m/q \quad \text{Eqn. II.2}$$

[Where;  $t$  is time,  $m$  is mass,  $L$  is distance of flight path,  $q$  is charge,  $U_o$  is the strength of the applied field (potential difference)].

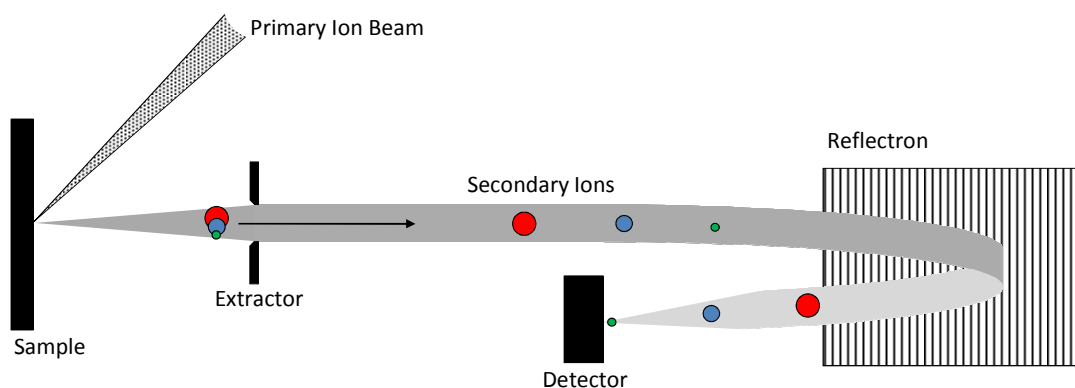


Figure II.3: Secondary ion separation in a Time of Flight mass analyser equipped with a reflectron. Lighter ions (green) travel faster than heavier ions (red). Figure adapted from<sup>[104]</sup>.

Imaging is achieved through rastering of the primary beam across the surface. The detector is a channel plate, this can be considered a 2D array of electron multipliers. An electron multiplier will amplify the signal of one ion strike by secondary emission of more electrons which under an electric field will continue to collide with the multiplier surface creating a cascade effect.

### **II-1.3 X-ray Photoelectron Spectroscopy (XPS)**

XPS yields quantitative information on the elements present on a sample surface. The technique relies on the fact that atoms hold their electrons at discrete levels/strengths characteristic to the identity and chemical state of the atoms. When X-rays are used to excite photoelectrons, this electronic structure is revealed in the energy of the photoelectrons. By knowing the X-ray energy used to cause electron emission from the surface, the energy of the resulting photoelectron and therefore the atom of origin can be identified. Only electrons excited from the top *ca.* 10 nm escape the material without undergoing an inelastic collision, as a result XPS is a surface sensitive technique.

The kinetic energy ( $E_K$ ) of a photoelectron is measured and relates to the binding energy of the electron ( $E_B$ ) by equation II.3. Where  $h\nu$  is the photon energy of the X-ray ( $h$  is the Planck constant,  $\nu$  is frequency),  $W$  is the work function determined by instrument calibration: the energy required to expel the electron into the vacuum from the Fermi level<sup>[105,106]</sup>. The binding energy defines which atomic level and which element the electron occupies. A spectrum of photoelectron counts against binding energy reveals peaks corresponding to the electron configuration of the elements present at the surface.

$$E_B = h\nu - E_K - W \quad \text{Eqn. II.3}$$

The emission of a photoelectron is shown in figure II.4. Auger electrons are also detected in XPS. Auger electrons are emitted as vacant electron orbitals (from photoelectron emission or electron stimulated emission) are filled by electron transitions from higher energy orbitals figure II.4.

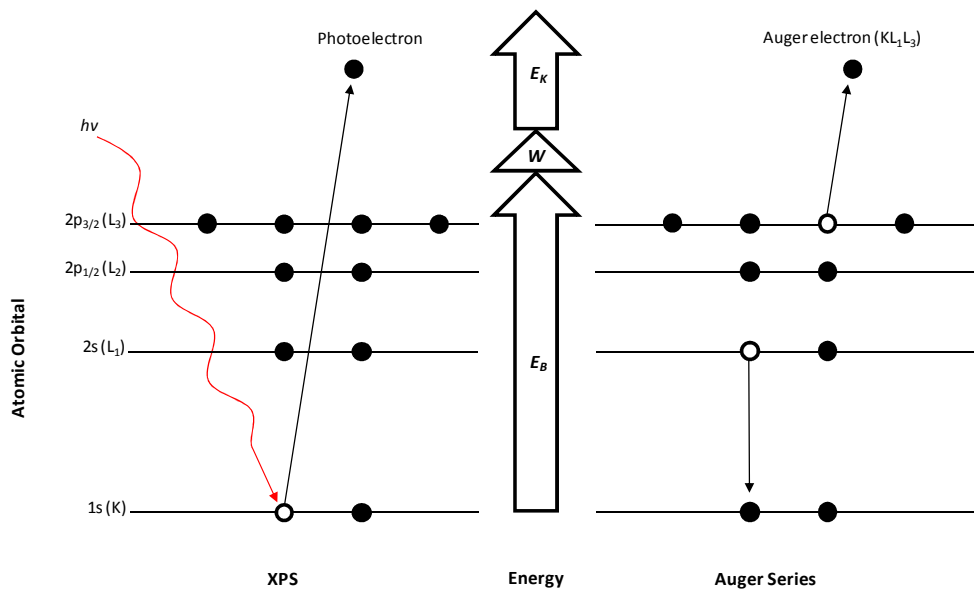


Figure II.4: Diagram showing emission of a 1s electron and a possible Auger electron as a result. Figure adapted from<sup>[104]</sup>.

A hemispherical analyser focuses photoelectrons of a given ‘pass energy’ onto the detector. Electrons are detected by an electron multiplier or channel plates. Electron multipliers work by amplification of a single electron strike by secondary emission of more electrons which under an electric field will continue to collide with the multiplier surface creating a cascade effect. A metal anode collects the electrons forming a current for the pulse counter. The micro-channel plate (MCP) detectors can be thought of as consisting of many electron multipliers arranged in a 2D format. In imaging XPS, which is not utilised in this work, a delay-line anode determines the spatial position of photoelectron impacts. This is achieved by measuring the time of arrival of the signal along the delay-lines (copper windings) from the four corners of the MCP array<sup>[107]</sup>.

## II-2 Atomic Force Microscope (AFM)

Developed to measure forces on small molecules and atoms, the AFM uses a sharp tip to interact with a surface via a cantilever (spring)<sup>[108]</sup>. By measuring the deflection of the cantilever the tip-sample force can be measured. Measurable forces include attractive, repulsive, magnetic, electrostatic and van der Waals. Topographical images at the nanometre scale can be obtained by raster scanning the tip across the surface.

The probe is manipulated through piezoelectric translators for fine control. Cantilever deflection is commonly measured optically with a resolution of 0.01 nm<sup>[109]</sup>. This optical lever technique, figure II.5, records the motion of a laser reflection from the back of the cantilever using photodiodes. Images can be obtained using contact mode or tapping mode. In contact mode, the tip remains in contact with the surface throughout the raster scan. As a result, the absolute spatial resolution is determined by the tip radius (5-10 nm). In tapping mode the tip intermittently contacts the surface. The tapping is achieved using a piezo-oscillator, which drives the cantilever near its resonant frequency. The root mean square amplitude of the oscillation can be converted to height to give topographical images.

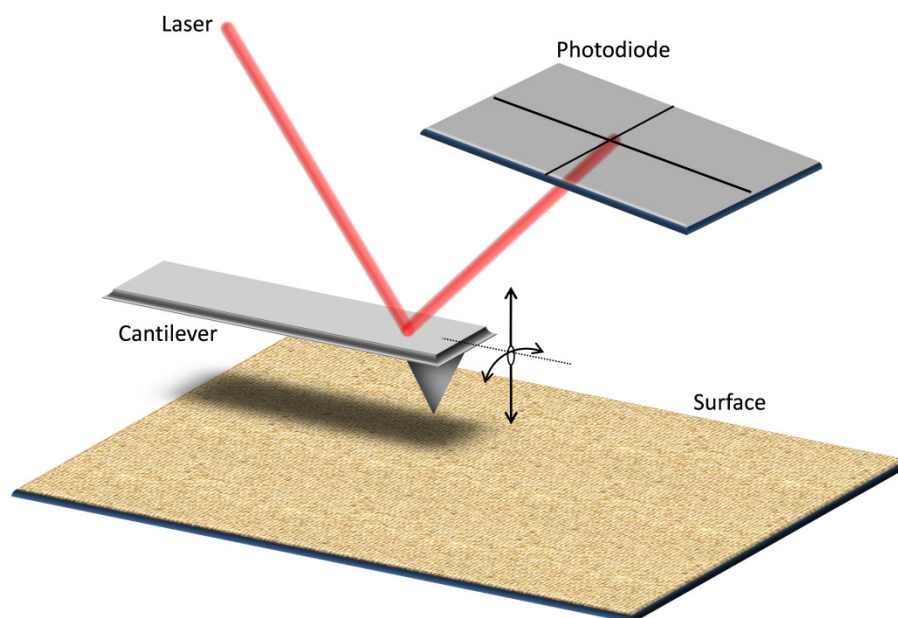


Figure II.5: Optical lever setup for AFM. A photodiode detects the laser reflection spatially. Arrows depict directional motions of the cantilever as a result of surface-tip forces and surface topography.

## II-3 Quartz crystal microbalance with dissipation monitoring (QCM-D)

The QCM-D is a sensitive mass balance that works on the principle of a dampening action resulting when components adsorb onto a vibrating quartz crystal figure II.6. This is described by the Sauerbrey equation, II.4. The piezoelectric properties of quartz allow mechanical vibrations to occur in response to applied voltages. Therefore by applying different voltages the fundamental and harmonic resonances can be achieved.

The dissipation can be measured by removing the applied voltage: The decay of the crystals resonance frequency is measured as the crystal relaxes. This provides information on the rigidity of the film and its coupling to the sensor. A soft elastic film will dampen vibrations through friction and viscosity<sup>[110]</sup>.

$$\Delta m = \frac{-\Delta f \cdot Dq \cdot Vq}{2 \cdot f_{und}^2 \cdot n} \quad \text{Eqn. II.4}$$

[Where;  $\Delta m$  is mass change,  $\Delta f$  is change in frequency (Hz),  $Dq$  is the density of quartz ( $2.648 \times 10^9$  ng/cm<sup>3</sup>),  $Vq$  is the speed of sound in quartz ( $334$  m/s<sup>-1</sup>),  $f_{und}$  is the fundamental frequency of the quartz sensor (5 MHz), and  $n$  is overtone number (1, 3, 5 or 7)].

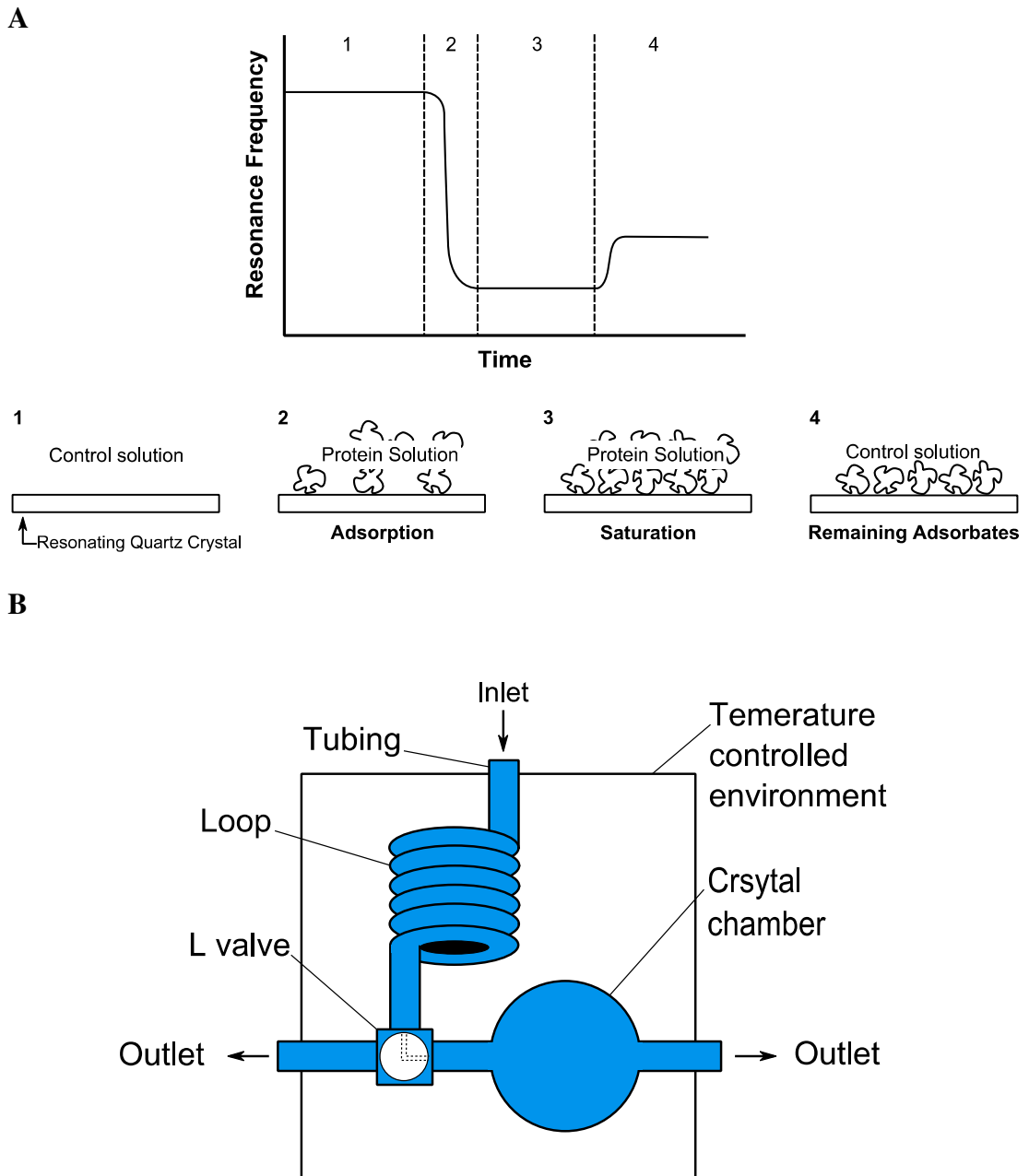


Figure II.6: A) The frequency response curve of a QCM crystal to protein adsorption from solution. The 4 stages are represented diagrammatically: The frequency is stabilised with a control solution (1); addition of a protein solution causes a frequency decrease, indicating protein adsorption to the crystal (2); the protein adsorption will saturate over time (3); rinsing with the control solution removes weakly adsorbed protein (4). B) Simplified schematic of the QCM instrument, the L valve allows the test solution to be changed without influencing the crystal chamber environment.

## II-4 Cell Culture

Primary cultures of dissociated embryonic rat hippocampal neurons were prepared and cultured at low density in serum free media.

Hippocampi were explanted from rat embryos at day E18-E19 of gestation and dissociated enzymatically in 2 ml of HEPES-buffered Hanks balanced salt solution (HBSS), containing 200  $\mu$ l (1% wt/vol) Trypsin and 20  $\mu$ l (0.5% wt/vol) DNase, for 20 minutes at 37°C. To inactivate the trypsin, Eagle's Basal Medium (BME) containing foetal bovine serum (FBS) was used to wash the hippocampi. Further dissociation was then achieved by gently triturating with a fire polished glass Pasteur pipette in the presence of DNase. The dissociated cell suspension was then centrifuged for 5 minutes at 1200 rpm. The resultant pellet of cells was re-suspended in the serum free *Neurobasal* media containing *B27* supplement and 0.5 mM glutamine.

Coverslips were separately placed in 6 well tissue culture plates. Each coverslip was plated with 75,000 dissociated cells in 300  $\mu$ l media, and incubated for 30 minutes at 37°C to allow cell adhesion to occur. The wells were then flooded with *Neurobasal/B27* media to a total volume of 2 ml. The media was replaced after the first 24 hours with fresh media, and then maintained every 4 days by replacing half of the media with fresh media. The cultures were maintained at 37°C in a humidified 5% CO<sub>2</sub> atmosphere.

### II-4.1 Light Microscopy

Phase contrast images of the cultures were captured with a Nikon eclipse Ti inverted microscope.

Under normal bright field microscopy, transparent specimens such as biological cells are poorly resolved. The advent of the phase contrast microscope allowed transparent specimens to be imaged with better contrast<sup>[111,112]</sup>. The technique achieves a higher contrast image by converting changes in the phase of light (introduced by the specimen) into changes of amplitude. A phase ring positioned in the microscope condenser forms a ring of parallel light, which illuminates the specimen. This light becomes focused on a matching phase ring located in the objective lens, where the phase becomes shifted by a quarter wavelength, and the

intensity is attenuated. However, some light is scattered and phase shifted by the specimen. This scattered light is also collected by the objective lens, but over a larger area than the light collected by the phase ring. As a result, a large phase difference between non-scattered and scattered light causes interference as they recombine (a change of amplitude), forming a high-contrast image.

## **II-4.2 Fluorescence Microscopy**

Fluorescence microscopy was carried out on a Nikon eclipse Ti inverted microscope. A live/dead cell viability assay with ethidium homodimer-1 (EthD-1) and calcein AM was used. EthD-1 has excitation and emission wavelengths of 528 nm and 617 nm respectively in the presence of DNA. The fluorescence of EthD-1 is enhanced by intercalating into DNA, however, EthD-1 cannot cross the membranes of live cells. EthD-1 can penetrate disrupted membranes indicative of dead cells thus labelling them<sup>[113]</sup>. Calcein has excitation and emission wavelengths of 495 nm and 515 nm respectively. Calcein AM, an acetoxymethyl ester of calcein, is cell permeable and weakly fluorescent. Once inside a cell, native enzyme esterase activity cleaves off an acetoxymethyl group to form calcein. Thus, calcein can fluoresce in live cells. To carry out the assay, sample coverslips were incubated at 37°C with 4 µM EthD-1 and 8 µM calcein AM for 30 minutes. The coverslips were then immersed in fresh media and imaged immediately.

# III Substrate Preparation and Characterisation

---

## III-1 Introduction

To support the survival of neurons in cell culture the substrate surface should be compatible with cell adhesion and growth. The substrates used were 19 mm diameter glass cover slips with and without a gold coating. We investigated the chemical modification of both the glass and gold, both of which have benefits for use in cell culture. Firstly, both glass and gold are resistant to corrosion in biological media making them suitable for long term cultures. Several methods are available to modify the chemistry of their surfaces<sup>[2]</sup>. Lastly, adhered cells can be observed via a light microscope (if the gold film is transparent), which is essential for monitoring culture progress. This chapter deals with the surface chemical modifications taken from the literature and their comprehensive characterisation. This was achieved using ToF-SIMS, XPS and WCA as described in chapter II. This characterisation of the surface chemistry is necessary to interpret the neuronal cell culture results which are presented in chapter IV.

To support the adhesion and growth of the neuronal cell culture, the peptide fragment of laminin PA22-2 is used. The amino acid sequence of PA22-2 is CSRARKQAASIKVAVSADR, which has been shown to promote adhesion of neurons<sup>[114]</sup>. Although, the smaller sequence of IKVAV has also proved effective for supporting neuronal cultures<sup>[115]</sup>, the terminal cysteine residue of the longer peptide provides a thiol group which will be exploited for the surface modification. Surfaces with exposed PEG chains have been shown to reduce non-specific protein adsorption<sup>[116,117]</sup>. A PEG linker will be used to tether the peptide to the surface, with the aim of reducing non-specific adsorption from the media during cell culture. Reduced protein adsorption may improve the cell adherence resulting in cultures with good surface coverage, as discussed in chapter 4.

## **III-2 Experimental**

### **III-2.1 Glass Surface Modification**

#### **Pre-treatment**

To remove particulates from the surface introduced during packaging, the as received cover slips were sonicated for 10 minutes in 10% (v/v) 'decon 90' detergent in deionised water. The detergent was rinsed off using copious amounts of deionised water. Cover slips were dried using a nitrogen stream.

#### **Oxygen Plasma**

Surfaces exposed to atmospheric conditions will adsorb volatile hydrocarbon species. The removal of adventitious hydrocarbon exposes the underlying substrate surface, such as hydroxyl groups required for silanisation. Highly reactive oxygen radicals oxidise organic material to carbon dioxide and water. The radicals are produced by electron impact dissociation as a result of the plasma.

Pre-treated cover slips were placed in a RF plasma barrel etcher. Oxygen plasma treatment was carried out at 0.2 mbar, at 60 W for 10 minutes. These cover slips were used for silanisation or treatment with poly-L-lysine.

#### **Silanisation**

The principles of silanisation are described in I.3. Three silanes were used to modify the surface of glass; (3-mercaptopropyl)trimethoxysilane (MPTS), (3-aminopropyl)trimethoxysilane (APTMS), and (3-aminopropyl)dimethylethoxysilane (APDES). Their structures are presented in figure III.3. MPTS was used as a layer to increase adhesion of gold to glass. APTMS and APDES were expected to provide amino terminated surfaces. Surface models resulting from APTMS, APDES and MPTS silanisation are shown in figure III.1. The methods used to modify the surfaces are described below, APTMS and APDES treatments followed the same protocol.

*(3-mercaptopropyl)trimethoxysilane (MPTS) treatment*

Glass cover slips were subjected to the following procedure, adapted from<sup>[118]</sup>;

- Rinsed with propan-2-ol.
- Immersed in a 50:1:1 solution of propan-2-ol : MPTS : deionised water at 80°C for 10 minutes.
- Rinsed with propan-2-ol and dried under nitrogen stream.
- Placed in an oven at 100°C for 10 minutes.
- The above procedure was repeated for a total of three times.
- Stored at 40°C until used.

*3-Aminopropyltrimethoxysilane (APTMS) / 3-aminopropyldimethylethoxysilane (APDES) treatment*

Glass cover slips were;

- Rinsed with anhydrous toluene.
- Immersed in a 1% (v/v) silane in anhydrous toluene for 1 hour. The use of anhydrous toluene is intended to confine the hydrolysis of the silane to the surface. This is because water molecules will be present at the surface, as a result of adsorption of water vapour from the atmosphere.
- Rinsed consecutively with anhydrous toluene, ethanol and distilled water.
- Placed in an oven at 100°C for 1 hour.

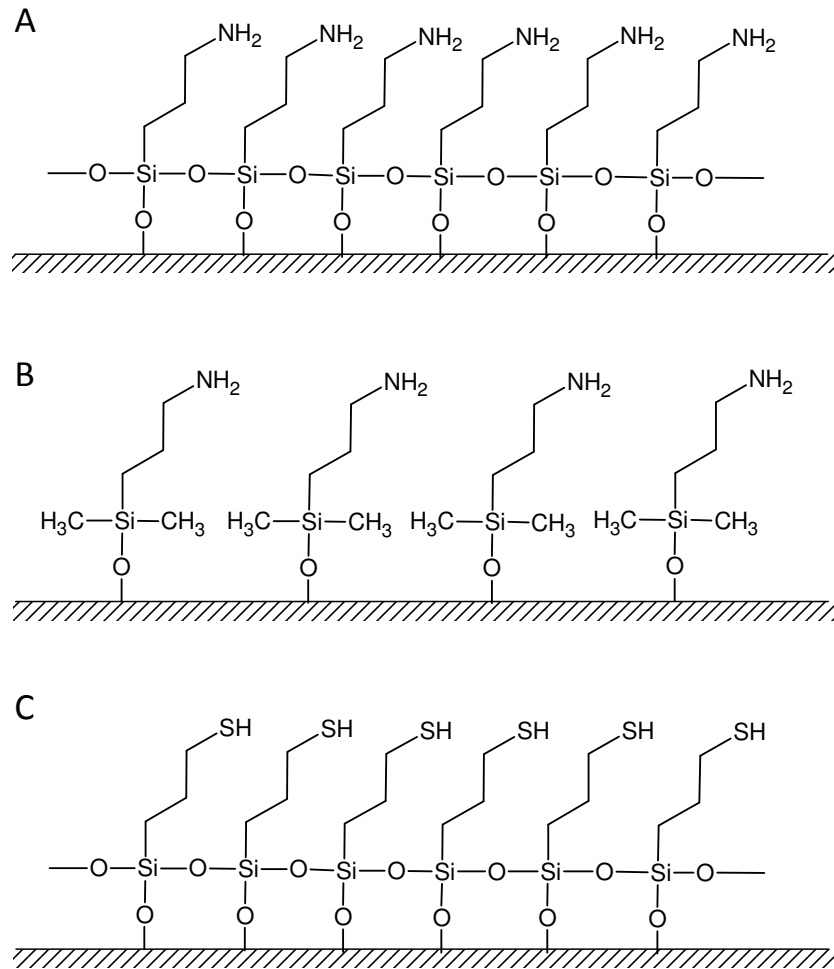


Figure III.1: Model surface representation of APTMS (A), APDES (B), and MPTS (C) silanisation.

### Poly-L-lysine (PLL) Adsorption

The structure of poly-L-lysine (PLL) is shown in figure III.3. This is thought to adsorb to the glass surface via electrostatic interaction between the  $\text{NH}_3^+$  and the negative surface charge of glass<sup>[119]</sup>.

#### *PLL treatment*

Glass cover slips were;

- Rinsed with deionised water.
- Immersed in PLL solution for 5 minutes.
- Rinsed with deionised water, and dried under nitrogen stream.

### **III-2.2 Gold Surface Preparation**

Gold is not reactive with glass, and does not readily form stable oxides. This means an adhesion layer is required, forming a sandwich layer which can bond between the glass and gold. Metals such as chromium and titanium can form stable oxides with glass and metallic bonds with gold, thus making them useful adhesion layers. However, a metal adhesion layer can compromise the performance of SPR sensors, which is a potential application for this work. To avoid using a metal adhesion layer, the use of a silane adhesion layer was considered. The silanisation of glass with MPTS is expected to present thiol groups which would bond to gold<sup>[118,120]</sup>.

Gold coated cover slips were prepared by thermal metal evaporation in a bell jar. The sample chamber was under vacuum,  $10^{-5}$  mbar. A liquid nitrogen cold trap was used to prevent contamination of the samples by diffusion pump oil vacuum back streaming. A current was passed through a tungsten filament containing gold causing evaporation. The evaporated gold condensed on all surfaces in 'line of sight' of the filament. A uniform thickness of 50 nm gold was coated onto the cover slips. This was achieved by monitoring the deposition with a quartz crystal microbalance positioned the same distance from the filament as the cover slips.

### **III-2.3 Gold Surface Modification**

Freshly evaporated gold has a high surface energy, which can promote adsorption of adventitious hydrocarbons. Oxygen plasma treatment was expected to remove adventitious hydrocarbon. Oxygen plasma treatment was carried out at 0.2 mbar, at 60 W for 5 minutes in a RF plasma barrel etcher. These samples were used immediately for the subsequent surface modifications.

#### **Self Assembled Monolayers of Thiols**

The principles of thiol SAM formation are described in I.3. Two molecules were used, 11-amino-1-undecanethiol (AUT) and the peptide PA22-2 (their structures are shown in figure III.3). Both molecules contain a terminal thiol group, which is expected to bind to gold. The AUT is expected to present amino groups on the gold surface.

### *11-amino-1-undecanethiol (AUT) treatment*

Gold cover slips were;

- Rinsed with ethanol.
- Immersed in a solution of 1 mM AUT in ethanol for at least 18 hours.
- Rinsed with ethanol.
- Rinsed with deionised water and dried under nitrogen stream.

### *Peptide fragment of laminin, NH<sub>2</sub>-CSRARKQAASIKVAVSADR-COOH (PA22-2) treatment*

Gold cover slips were;

- Rinsed with deionised water.
- Immersed in a solution of 0.1 mM peptide in PBS for at least 18 hours.
- Rinsed with deionised water and dried under nitrogen stream.

### **Poly-L-lysine (PLL) Adsorption**

It is expected that PLL will adsorb to gold via electrostatic interaction between positively charged lysine residues and the negatively charged surface of gold<sup>[121]</sup>.

### *Poly-L-lysine (PLL) treatment*

Gold cover slips were;

- Rinsed with deionised water.
- Immersed in PLL for 5 minutes.
- Rinsed with deionised water, and dried under nitrogen stream.

### **Peptide Coupling to Amino Terminated Surfaces**

The APTMS and APDES silanisation, and AUT SAM present free amino groups on glass and gold respectively. A heterobifunctional linker, alpha-Maleinimido-omega-carboxysuccinimidyl polyethylene glycol ester, was used to attach the peptide to the amino terminated surfaces. The reaction scheme is presented in figure III.2. A nucleophilic substitution from the surface amine to the succinimidyl ester forms an amide bond, joining the linker to the surface. Subsequent addition of a thiol causes nucleophilic addition on the maleimide group, forming a thioether bond. The polyethylene glycol (PEG) chain has a molecular weight of ~5000 Da, with a length of ~50 nm. Using the linker, peptide attachment to the APTMS, APDES and AUT

was attempted by the following treatment. The resulting samples are termed APTMS-PEG-Peptide, APDES-PEG-Peptide and AUT-PEG-Peptide.

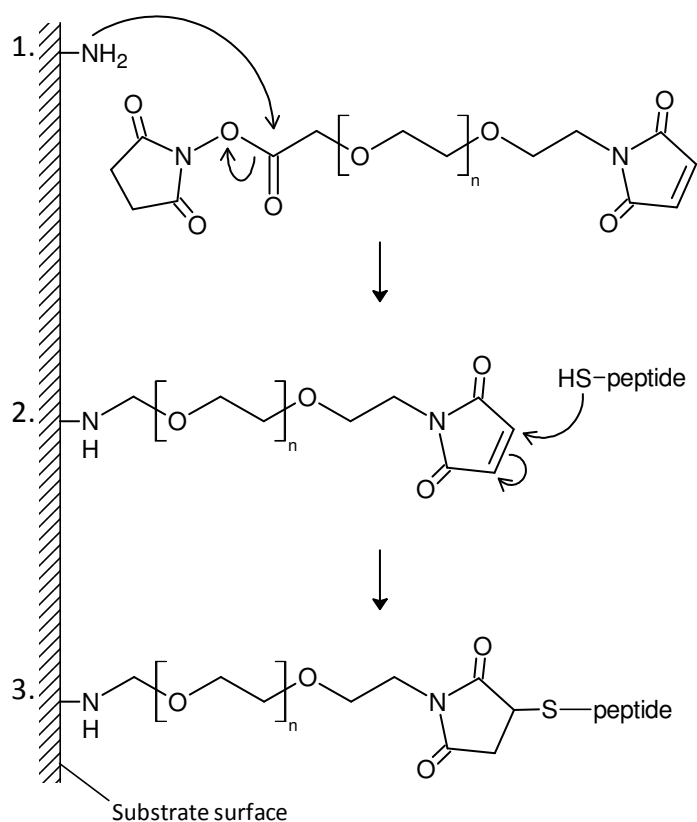


Figure III.2: Reaction scheme of alpha-Maleinimido-omega-carboxysuccinimidyl ester polyethylene glycol with an amine surface (1), and then a peptides thiol (2). Covalently linking the peptide to the surface (3).

#### *PEG linker treatment*

APTMS-glass, APDES-glass and AUT-gold samples were;

- Immersed in a 1 mM alpha-Maleinimido-omega-carboxysuccinimidyl ester polyethylene glycol solution in dimethylformamide (DMF) for 2 hours.
- Rinsed with DMF, and dried under nitrogen.

#### *Peptide PA22-2 treatment of maleimide terminated surface*

Amino-PEG-maleimide terminated surfaces were;

- Immersed in a 0.1 mM peptide solution in PBS at  $5^\circ\text{C}$  for 3 hours.
- Rinsed with deionised water, and dried under nitrogen.

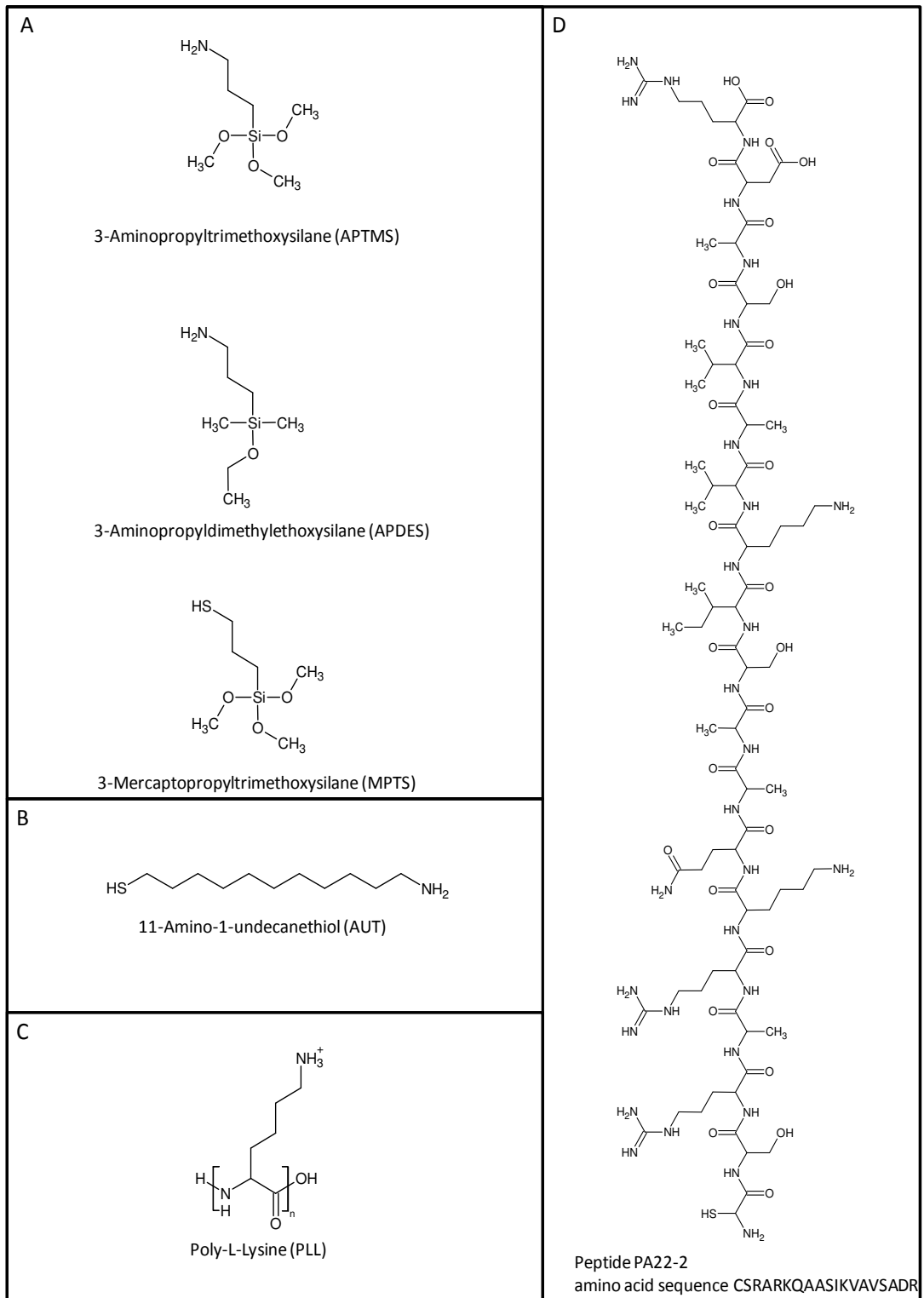


Figure III.3: Chemical structures of the silanes (A), thiol (B), poly-l-lysine (C), and peptide (D) used for surface modification.

### **III-2.4 Water Contact Angle (WCA)**

Static water contact angles were recorded on a CAM 200, KSV instruments. A 10  $\mu$ l droplet of deionised (18.2 M $\Omega$ -cm) was lowered to contact the surface and the needle withdrawn. Video frames were captured every second for 10 seconds. The droplet profiles were fitted using the Young-Laplace method. The left and right contact angles were averaged to give the WCA and extrapolated to time 0 to account for evaporation.

### **III-2.5 X-ray Photoelectron Spectroscopy (XPS)**

XPS was carried out using a Kratos AXIS ULTRA with a mono-chromated Al  $K\alpha$  X-ray source (1486.6 eV) operated at 15 mA emission current and 10 kV anode potential. Spectra were analysed using casaXPS software. Atomic compositions for samples were determined from a linear background. Chosen peak areas were divided by the relative sensitivity factor and the transmission as determined through calibration of the instrument. The resultant value when taken as a ratio of the total for all identified peaks is the final atomic composition.

### **III-2.6 Time of Flight Secondary Ion Mass Spectrometry (ToF SIMS)**

ToF-SIMS was carried using a TOF-SIMS IV from ION-TOF GmbH. Spectra were obtained using a Bi<sup>+3</sup> primary ion source operated in high current bunched mode, with a pulse width of 10.2 ns. On the glass samples only, a flood gun was used to prevent charging of the surface by showering the surface with low energy electrons.

Initial ion intensities were corrected for shot noise and then normalised by the spectrum total ion intensity for comparison.

### III-3 Results

#### III-3.1 Gold Adhesion Layer

The silane (3-mercaptopropyl)trimethoxysilane (MPTS) was used to promote gold adhesion to the glass cover slips. ToF-SIMS analysis indicates the presence of sulphur, evidence that MPTS is present on the glass surface, table III.1 and figure III.4. The resulting gold coated substrates proved resistant to gold delamination from the glass on handling.

Ion (mass)	Normalised Ion Intensity ( $\times 10^5$ )	
	Oxygen Plasma Etched Glass	MPTS Coated Glass
$O^-$ (15.995)	18268	11968
$OH^-$ (17.003)	12164	8534
$S^-$ (31.970)	62	3499
$SH^-$ (32.981)	128	4038

Table III.1: ToF-SIMS ion intensities of negative sulphur and thiol ions on oxygen plasma etched glass and after MPTS silanisation.

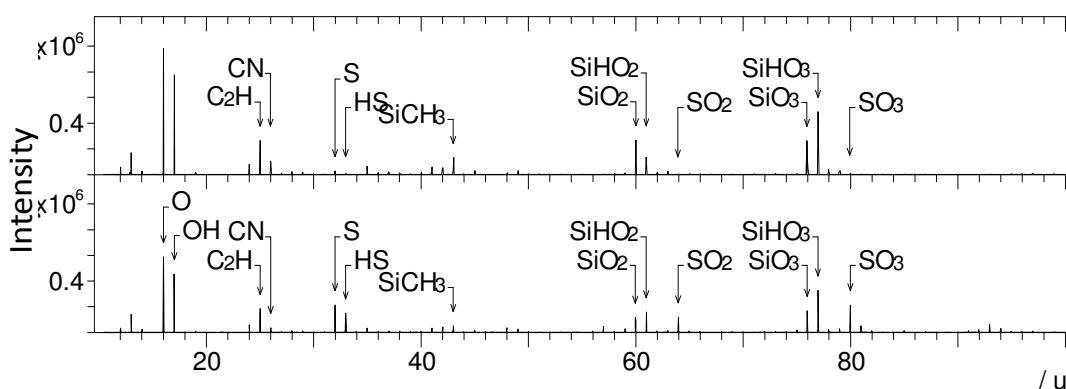


Figure III.4: Negative ion mode ToF-SIMS spectra. Oxygen plasma etched glass (top) and MPTS treated glass (bottom).

### III-3.2 Surface Modifications

Several surface treatments of glass and gold were explored to investigate their suitability to promote cell adhesion, summarised in table III.2. The steps taken to prepare the surfaces are presented in section III.2. For clarity, x-PEG-Peptide refers to the intended amine termination with subsequent modifications by the succinimidyl-PEG-maleimide linker, and then the peptide.

<b>Treatments on GLASS</b>	<b>Treatments on GOLD</b>
Poly-L-lysine	Poly-L-lysine
3-Aminopropyltrimethoxysilane (APDES)	11-amino-1-undecanethiol (AUT)
3-Aminopropyltrimethoxysilane (APTMS)	Peptide
APDES-PEG-Peptide	AUT-PEG-Peptide
APTMS-PEG-Peptide	

Table III.2: Summary of surfaces investigated.

### III-3.3 Surface Wettability

Changes of surface chemical composition can result in changes in wettability. WCA measurements from glass and gold surface treatments were obtained using a sessile drop approach and are presented in table III.3.

<b>Glass Surface Treatment</b>	<b>Static water contact angle (°)</b>
Oxygen plasma etched	<10
PLL	31 ±2
APDES	67 ±2
APDES-PEG-Peptide	62 ±6
APTMS	35 ±4
APTMS-PEG-Peptide	59 ±7
<b>Gold Surface Treatment</b>	
Oxygen plasma etched	<10
PLL	34 ±4
Peptide	57 ±5
AUT	41 ±5
AUT-PEG-Peptide	61 ±6

Table III.3: Sessile drop water contact angles of glass and gold surface treatments

A very low water contact angle is observed after oxygen plasma treatment for both glass and gold surfaces. This indicates that the oxygen plasma treatment has removed hydrophobic organic matter that has adsorbed to the surface. Gold should

be completely wetted, but this is difficult to achieve practically because of volatile organic contamination adsorbed on most surfaces from the ambient atmosphere. Apart from the glass-APDES treatment which presents the highest WCA, the amine terminated surfaces of PLL, APTMS and AUT present a range of WCA's from 31° to 41°. Therefore, these surface treatments appear to present more polar groups than the APDES. This is the first sign that the APDES treatment may not have been efficient or complete, and as a result did not display the polar amine functionalities as intended. These results will be discussed further below in the light of XPS and ToF-SIMS results.

### **III-3.4 Surface Chemistry**

#### **III-3.4.1 XPS**

To compare the elemental composition of the surface after surface treatment, XPS was carried out. The main focus will be comparing the amounts of N, O and C across the samples to help determine how successful the surface treatments were.

##### **Glass Surface Treatments**

Wide scan XPS spectra are shown for comparison in appendix 1. The elemental composition of the treated glass surfaces are shown in table III.4. Glass is composed of silicate oxides of other elements. This is confirmed by the high amounts of oxygen and silicon on all of the glass surfaces. The observation of boron suggests that this is a borosilicate glass. The presence of carbon indicates some advantageous contamination from volatile carbonaceous species.

Notably, the PLL, APDES, and APDES-PEG-Peptide treatments show elemental compositions similar to the oxygen plasma etched glass. The ToF-SIMS results will further confirm if these treatments were successful.

APTMS treatment shows increased amounts of carbon, and nitrogen in comparison to the oxygen plasma treatment (control). An APTMS treatment that was the only carbon and nitrogen included in the XPS analysis would have a C:N ratio of approximately 3:1, the observed ratio is 4:1. The discrepancy could be from

advantageous hydrocarbon contamination increasing the ratio of carbon. The amount of oxygen detected has decreased after treatment by approximately half, suggesting the oxygen signal from the glass is being attenuated by the over layer.

APTMS-PEG-Peptide treatment shows increased oxygen compared to the APTMS alone, but the other detected elements have similar percentages. The PEG and peptide components contain oxygen which may account for the observed value over that of APTMS alone. However, the amount of oxygen is less than the control, indicating the treatment has attenuated the oxygen signal from the glass substrate.

Glass Treatment	Atomic Composition (%)				
	C	O	N	Si	B
Oxygen plasma etched	9.6	60	1.5	22	3.3
PLL	8.5 ± 0.4	61 ± 3	0.77 ± 0.4	23 ± 0.8	3.0 ± 3
APDES	6.7 ± 0.08	61 ± 0.3	1.3 ± 0.04	24 ± 0.8	3.3 ± 0.5
APDES-PEG-Peptide	8.4 ± 0.7	60 ± 0.6	1.8 ± 0.1	23 ± 0.3	2.6 ± 0.06
APTMS	35 ± 0.6	33 ± 0.5	8.7 ± 0.3	18 ± 0.1	1.4 ± 0.1
APTMS-PEG-Peptide	36 ± 2	41 ± 0.8	6.4 ± 0.4	15 ± 0.3	1.4 ± 2
	Zn	Ti	K	Na	Cl
Oxygen plasma etched	0.68	0.74	1.8	0.52	-
PLL	0.60 ± 0.04	0.90 ± 0.1	2.0 ± 0.2	0.68 ± 0.3	-
APDES	0.56 ± 0.007	0.77 ± 0.02	2.0 ± 0.2	0.39 ± 0.1	-
APDES-PEG-Peptide	0.48 ± 0.2	0.79 ± 0.004	1.4 ± 0.07	1.1 ± 0.02	-
APTMS	0.24 ± 0.09	0.22 ± 0.07	0.76 ± 0.09	0.071 ± 0.4	3.2 ± 0.05
APTMS-PEG-Peptide	0.03 ± 0.002	0.13 ± 0.03	0.40 ± 0.07	0.05 ± 0.06	0.28 ± 0.2

Table III.4: Relative atomic composition of treated glass surfaces. Mean and standard deviation from two different regions.

## Gold Surface Treatments

The atomic compositions for the treated gold surfaces are presented in table III.5, the spectra are shown for comparison in appendix 1. The most abundant elements on the gold surfaces are gold and carbon. As with the glass, carbonaceous contamination is attributed to volatile species in the atmosphere. Also, consequences of the PLL treatment are not readily apparent from these elemental composition results.

Gold Treatment	Atomic Composition (%)				
	C	O	N	Au	S
Oxygen plasma etched	38 ± 0.2	8.3 ± 0.8	4.1 ± 0.8	50 ± 0.2	-
PLL	33 ± 4	9.3 ± 0.4	5.0 ± 1	52 ± 5	-
Peptide	40 ± 3	13 ± 0.8	10 ± 0.1	37 ± 2	-
AUT	59 ± 0.5	2.6 ± 0.5	5.1 ± 0.6	31 ± 0.3	2.4 ± 0.3
AUT-PEG-Peptide	57 ± 3	8.0 ± 0.7	4.1 ± 1	29 ± 4	2.3 ± 0.6

Table III.5: Relative atomic composition of treated gold surfaces. Mean and standard deviation from two different regions.

When directly bound to gold, the XPS analysis of the peptide surface contains more oxygen and nitrogen compared to the control. This increase is attributed to the peptides –HN-CO- backbone structure. This treatment has also attenuated the signal from the underlying gold, indicating the significant peptide coverage of the surface.

The XPS analysis of the AUT-gold surface indicates more carbon and a decreased oxygen and gold signal in comparison to the control resulting from substrate signal attenuation by the over layer. Although the amount of nitrogen does not differ from the control, the observed C:N ratio of 11.6:1 is close to the expected ratio of 11:1. With the observed sulphur, these results indicate the presence of AUT on the gold. The observed ratio for N:S is 2:1, the expected ratio is 1:1. The difference could be due to the addition of nitrogen contamination present on the oxygen plasma treated gold.

AUT-PEG-Peptide surface treatment resulted in increased oxygen on the gold surface, compared to the AUT-gold. This is attributed to the high oxygen content of the PEG chain, and the presence of oxygen in the peptide. Attenuation of the gold signal also indicates an over layer has formed.

### III-4.2 ToF-SIMS

The identification of components on the surfaces using fragments of their molecular structure is possible using ToF-SIMS. With prior knowledge of the expected surface composition, it is possible to search for ion fragments native to specific surface treatments. For example, amino acids can be identified by certain characteristic ion fragments<sup>[122]</sup>. Although several amino acids can contribute to the same fragment ion, some fragments are more specific. One of these fragments,  $C_2H_6NO^+$ , is most specific to serine. As serine is present in the peptide, identification of  $C_2H_6NO^+$  will be useful for discerning between the peptide and PLL (peptide polymer) treatments. The PEG polymer consists of the  $-[OC_2H_4]-$  repeating unit shown in figure III.2. Major ions dominating PEG spectra are  $C_2H_5O^+$  and  $C_2H_5O_2^-$ , which have very little contribution from peptide fragments. Identification of these ions will be used to help determine successful surface modification. Ion images were used to determine surface homogeneity, these are displayed in full in appendices 16-19, from these selected images are shown through this thesis.

## Glass Surface Treatments

Normalised ion intensities of selected fragments from ToF-SIMS analysis of treated glass surfaces are listed in table III.6. Spectra are shown in appendices 2-7.

Ions +	Normalised Ion Intensity ( $\times 10^5$ )					
	Oxygen Plasma etched	PLL	APDES	APTMS	APDES- PEG- Peptide	APTMS- PEG- Peptide
<b>CH<sub>3</sub></b>	497	392	558	648	596	1636
<b>NH<sub>3</sub></b>	7	67	60	126	46	32
<b>C<sub>2</sub>H<sub>2</sub></b>	214	185	219	306	184	209
<b>C<sub>3</sub>H<sub>3</sub></b>	1278	2072	1664	2544	1329	1486
<b>SiOH</b>	1350	1189	2406	2192	1234	1182
<b>C<sub>2</sub>H<sub>5</sub>O</b>	836	510	424	113	1586	11146
<b>C<sub>2</sub>H<sub>6</sub>NO</b>	21	17	24	10	214	42
<b>C<sub>5</sub>H<sub>10</sub>N</b>	66	1590	65	54	621	114
–						
<b>O</b>	17312	13354	16778	5225	10278	5729
<b>OH</b>	12416	9997	10598	4157	7101	5399
<b>CN</b>	1817	5445	2892	14690	8583	5679
<b>Si</b>	286	245	388	232	199	112
<b>SiC</b>	22	21	35	24	20	11
<b>CNO</b>	1191	2980	995	1216	5762	2889
<b>SiO</b>	34	32	115	84	58	39
<b>C<sub>3</sub>N</b>	97	190	104	693	306	380
<b>SiC<sub>2</sub></b>	16	13	20	31	14	14
<b>SiO<sub>2</sub></b>	3732	2990	4161	1624	2169	1298
<b>C<sub>2</sub>H<sub>5</sub>O<sub>2</sub></b>	7	5	4	7	26	159
<b>Si<sub>2</sub>HO<sub>2</sub></b>	5	4	10	44	9	12

Table III.6: Positive and Negative ion intensities from treated glass surfaces. Normalised by total ion count.

The PLL treatment has a large  $C_5H_{10}N^+$  (attributed to lysine) intensity in comparison to all other treatments. Less specific peptide fragments including  $NH_3^+$ ,  $CN^-$  and  $CNO^-$  have higher intensities on PLL than the control. These observations are seen on both the glass and gold PLL treatments. In contrast to the XPS results, which did not detect PLL through the nitrogen signal, the presence of the  $C_5H_{10}N^+$  ion from ToF-SIMS highlights the instruments greater sensitivity for detecting thin films. The low WCAs of  $31^\circ$  and  $34^\circ$  on the PLL may suggest the underlying hydrophilic surface was detected by the water probe, indicating the adsorbed layer is

thin. The distribution of the ion fragments attributed to PLL show that the surface coverage of PLL on both glass and gold surfaces is homogeneous, figure III.5.

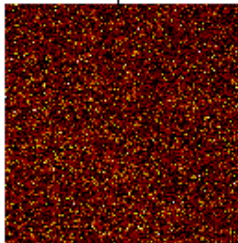
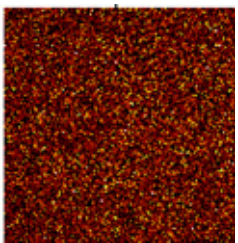
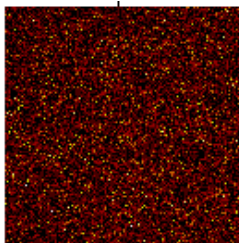
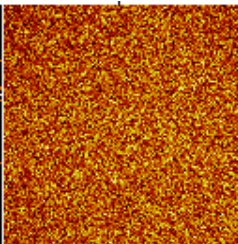
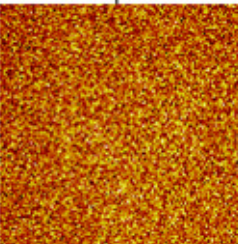
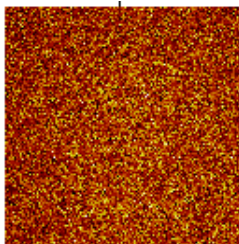
Surface	Ion Images		
	$C_5H_{10}N^+$	$CN^-$	$CNO^-$
PLL-Glass			
PLL-Gold			

Figure III.5: ToF-SIMS ion images of PLL treated glass and gold. Images are 500×500  $\mu\text{m}$ .

Silanisation with APDES and APTMS resulted in a small increase in alkyl fragments of  $CH_3^+$  and  $C_3H_3^+$ . These could come from the alkyl chain of the silanes. Intensities of  $CN^-$  and  $C_3N^-$  attributed to each silanes terminal amine group are higher on APTMS. Along with the increased nitrogen on APTMS observed by XPS, and the more polar surface of APTMS from the water contact angle results. This evidence indicates more amine groups are present on the APTMS surface than the APDES. Also, attenuation of the  $O^-$  and  $OH^-$  intensity on APTMS, which is not observed for APDES, indicates higher surface coverage of APTMS. Surface coverage of both APDES and APTMS treatments appears homogeneous, as shown by the distribution of  $CN^-$  in figure III.6.

The APTMS/APDES-PEG-Peptide treatments show increased  $C_2H_5O^+$  (attributed to PEG) intensity above all other treatments. Apart from the initial silane used, either APTMS or APDES, the conditions for the binding of the PEG linker and peptide were identical, as described in section III-2.1.

The PEG linker is expected to bind to exposed amino groups on the surface following silanisation. The previous observations that APTMS silanisation has more nitrogen than APDES silanisation, indicates APTMS treatment presents more amino groups for the succinimidyl function of the PEG linker to react with. Explaining why the  $C_2H_5O^+$  intensity is seven times greater on the APTMS-PEG-Peptide than the APDES equivalent, table III.6. There is a heterogeneous distribution of PEG on both APTMS-PEG-Peptide and the APDES equivalent, shown in figure III.6.

Surface	Ion Images					
	$CN^-$	$CNO^-$	$C_2H_5O_2^-$	$C_2H_5O^+$	$C_2H_6NO^+$	$C_5H_{10}N^+$
APDES						
APTMS						
APDES- PEG- Peptide						
APTMS -PEG- Peptide						

Figure III.6: ToF-SIMS ion images of APDES and APTMS silanised surfaces, and subsequent PEG and Peptide treatments on glass. Images are  $500 \times 500 \mu m$ .

It is apparent from the ToF-SIMS ion images that APDES/APTMS-PEG-Peptide treatments have formed heterogeneous surface modifications. The only difference between treatments was the initial silane used. It is important to note that the equivalent modification on AUT-gold has resulted in uniform ion images of the PEG and peptide fragments, figure III.8, suggesting the reaction of the PEG linker was successful. Apart from the initial SAM formation of AUT on gold, the conditions for the PEG linker and peptide binding were identical and in parallel to those on the APDES/APTMS silanised glass. This implies that the condition of the initial amine surface determines the success of the surface modification. However, several factors should be considered to explain the heterogeneity. Firstly, although the APDES and APTMS silanes show uniform coverage, the amine groups required for binding the

PEG linker may not be available to react. This could be due to hydrogen bonding of the amine with the surface hydroxyl groups in combination with the inherent variability in how the silane molecules can polymerise with themselves and the surface<sup>[6]</sup>. As a result, some amine groups may become 'blocked' within the silane layer, which may account for non-uniform binding of the PEG linker. Secondly, the intensity of ions detected by ToF-SIMS is influenced by topography, which can result in artefacts present in the ion images<sup>[123]</sup>. The PEG linker is a long polymer, ~5000 Da and ~50 nm long. Clustering of the PEG linker molecules at binding sites on the surface may contribute to topographical changes across the surface. A further study with AFM may confirm this, but has not been done.

Both APTMS/APDES-PEG-Peptide treatments show the presence of the peptide, indicated by the  $C_2H_6NO^+$  ion (attributed to serine). The peptide was expected to bind to the PEG linker through reaction with the linkers terminal maleimide group. Evidence for this reaction is shown from ion images of the APTMS-PEG-Peptide: Ions attributed to the peptide ( $CNO^-$ ,  $C_2H_6NO^+$  and  $C_5H_{10}N^+$ ) follow the same spatial distribution as the PEG ions, figure III.6.

The intensities of  $C_5H_{10}N^+$ ,  $CNO^-$  and  $CN^-$  indicate more peptide is present on the APDES-PEG-Peptide surface and that the peptide is has a more homogeneous coverage than the APTMS equivalent. This is a surprising result considering that the  $C_2H_5O^+$  intensity indicates more PEG linker was present on the APTMS, which should in turn provide more peptide binding sites. To help explain this, the ToF-SIMS ion images of the PEG ions which reveal some heterogeneity are compared in figure III.7. On the APDES-PEG-Peptide sample, regions of PEG ions are small, ~25  $\mu m$  in diameter. Between these small regions the PEG ion intensity is almost zero, figure III.7B. Therefore, the PEG linker has only bound in small regions to the underlying APDES silane. It is apparent that APDES silanisation has not presented enough amino groups for the PEG linker to bind uniformly. These results indicate the APDES-PEG-Peptide surface is actually peptide adsorbed upon the APDES silanisation, and has not worked as intended. This is supported by the lower nitrogen content and more hydrophobic surface of APDES in comparison to APTMS. The PEG fragment ion  $C_2H_5O^+$  shows wide islands of high intensity on the APTMS-PEG-Peptide sample. Between these islands the PEG ion intensity is approximately three times less than the brighter regions, shown by the line scan and histogram in

figure III.7B and C. Therefore, the PEG linker has bound across the entire APTMS surface, but appears to vary in concentration across the surface.

The difference in peptide intensity between APDES-PEG-Peptide and APTMS-PEG-Peptide samples could be explained in terms of physisorption. That is, more peptide adsorbs to the APDES surface than binds to the APTMS-PEG linker surface. This possibility is supported by the distribution of peptide ion fragments  $\text{CNO}^-$ ,  $\text{C}_2\text{H}_6\text{NO}^+$  and  $\text{C}_5\text{H}_{10}\text{N}^+$ . These ions have very little intensity outside of the higher intensity PEG region on APTMS-PEG-Peptide samples. However, peptide ions display homogenous coverage on the APDES-PEG-Peptide surface, indicating an adsorbed layer. This adsorbed peptide layer is too thin to be detected by XPS, explaining why ADPES-PEG-Peptide did not differ widely from the control in terms of elemental composition.

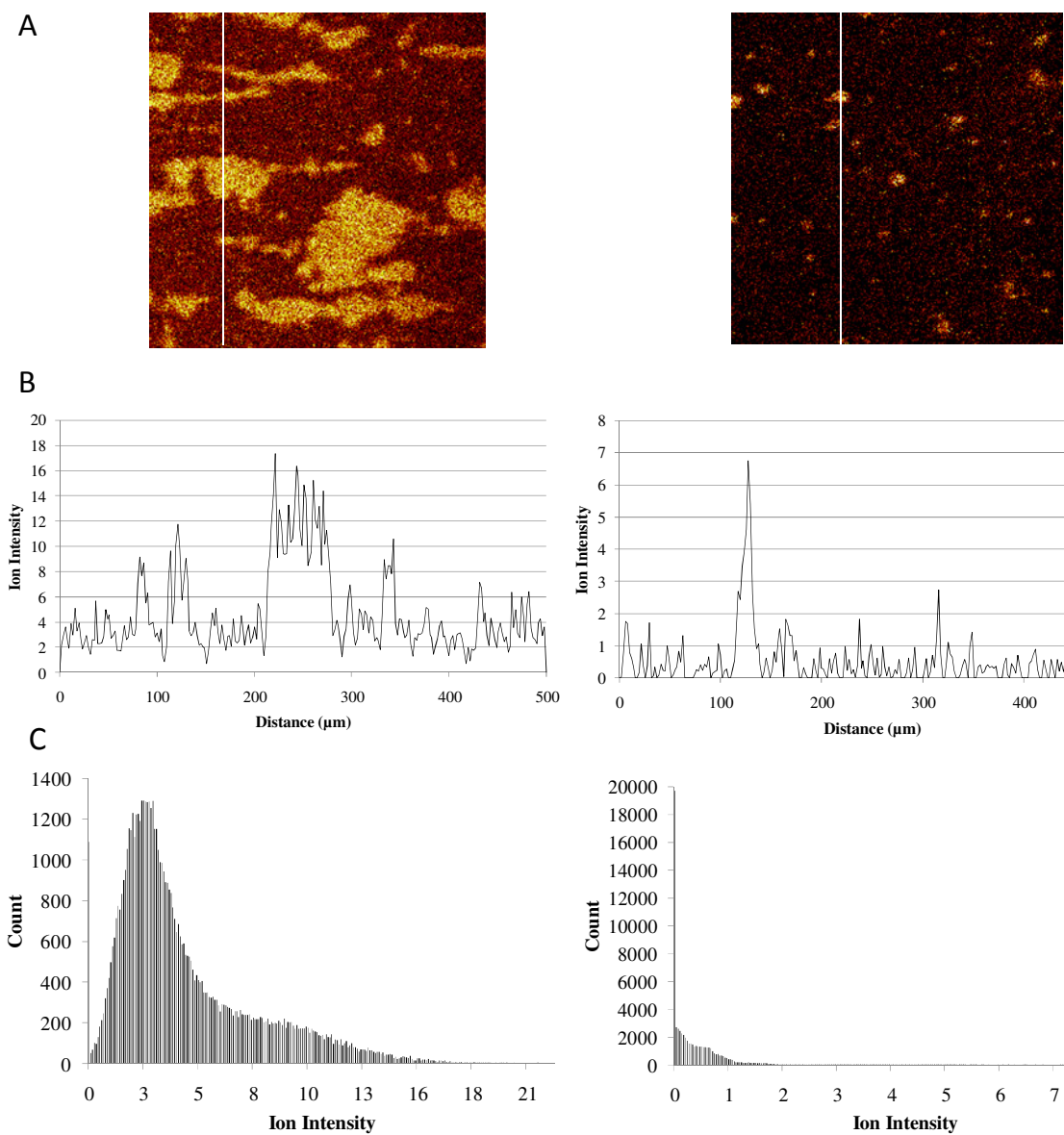


Figure III.7: Comparison of  $C_2H_5O^+$  (PEG) ion intensity on APTMS-PEG-Peptide (left) and APDES-PEG-Peptide (right) ToF-SIMS ion images,  $500 \times 500 \mu m$  (A). White lines indicate line profiles (B). Image intensity histogram (C).

## Gold Surface Treatments

ToF-SIMS results for gold are shown in table III.7. Spectra were collected with the same parameters as the glass samples except the flood gun was not required because the gold samples are conductive. The spectra are presented in appendices 8-15. All treatments appear to attenuate the Au<sup>+</sup> and Au<sup>-</sup> intensity in comparison to controls. This observation implies each treatment has coated the gold surface. As seen on glass, PLL adsorption to gold is indicated by the strong C<sub>5</sub>H<sub>10</sub>N<sup>+</sup> ion intensity. PLL-gold also presents the highest NH<sub>3</sub><sup>+</sup> intensity. The distribution of these ions indicates that PLL has a uniform coverage on gold, appendix 17.

Ions +	Normalised Ion Intensity ( $\times 10^5$ )				
	Oxygen Plasma etched	PLL	AUT	Peptide	AUT- PEG- Peptide
CH <sub>3</sub>	218	231	226	201	490
NH <sub>3</sub>	5	191	82	41	28
C <sub>2</sub> H <sub>2</sub>	92	82	70	61	67
C <sub>3</sub> H <sub>3</sub>	705	1294	1517	582	911
CHS	150	50	335	20	174
C <sub>2</sub> H <sub>5</sub> O	311	408	453	163	6536
C <sub>2</sub> H <sub>6</sub> NO	19	18	19	870	196
C <sub>5</sub> H <sub>10</sub> N	107	6468	425	2287	638
Au	199	170	99	78	63
-					
O	1453	958	742	1416	931
OH	1270	706	1109	1149	987
CN	4939	6900	4105	8783	5528
S	92	38	306	12	155
CNO	2182	4299	935	7701	3265
CS	9	5	5	1	3
C <sub>3</sub> N	170	190	151	246	261
CSO	165	48	46	4	10
C <sub>2</sub> H <sub>5</sub> O <sub>2</sub>	13	6	12	15	182
SO <sub>3</sub>	214	80	5215	487	3648
Au	4363	2708	3770	617	2805
AuS	79	48	630	22	379

Table III.7: Positive and Negative ion intensities from treated gold surfaces. Normalised by total by total ion count.

AUT modification of gold presents higher intensities of  $\text{NH}_3^+$ ,  $\text{CHS}^+$ , and  $\text{C}_3\text{H}_3^+$  ions in comparison to the control. These are attributed to the amine, thiol and alkyl chain of AUT respectively. The increased alkyl contribution is supported by the increase of carbon detected by XPS over that of the control, table III.5. A good indication that the thiol had bound to gold is the observed  $\text{AuS}^-$  ion. However, the presence of  $\text{SO}_3^-$  indicates some of the thiol was oxidised, forming a sulfonate<sup>[124]</sup>. Sulfonates do not bind to gold and would be displaced from the surface by thiol adsorption. In this case the sulfonate has not been completely removed during the rinsing stage of sample preparation, or was formed subsequently. The ion images indicate that AUT has formed a homogeneous surface coverage, figure III.8.

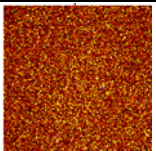
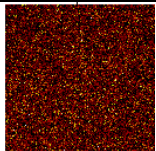
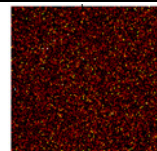
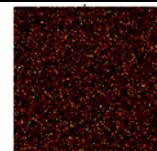
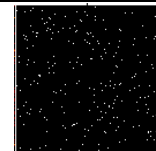
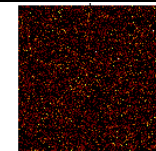
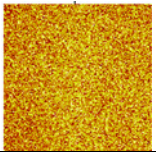
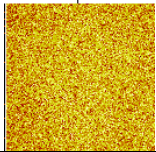
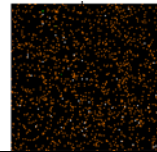
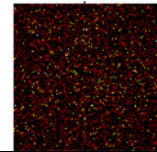
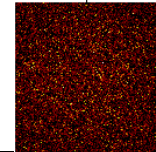
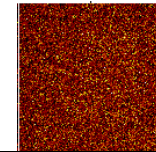
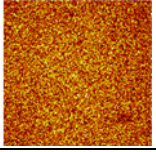
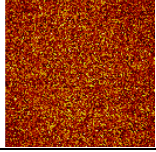
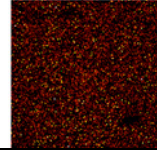
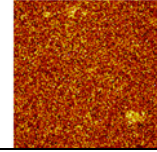
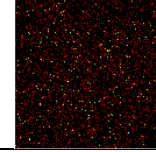
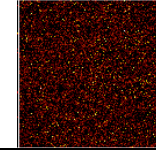
Surface	Ion Images					
	$\text{CN}^-$	$\text{CNO}^-$	$\text{AuS}^-$	$\text{C}_2\text{H}_5\text{O}^+$	$\text{C}_2\text{H}_6\text{NO}^+$	$\text{C}_5\text{H}_{10}\text{N}^+$
AUT						
Peptide						
AUT-PEG-Peptide						

Figure III.8: ToF-SIMS ion images of AUT, Peptide and AUT-PEG-Peptide surfaces on gold. Images are 500×500  $\mu\text{m}$ .

Peptide treated gold, expected to bind via the cysteine thiol, presented a surface with more nitrogen and oxygen when compared to the controls from XPS. The ToF-SIMS results show that  $\text{O}^-$  and  $\text{OH}^-$  ion intensities do not differ from the control. However, the  $\text{CNO}^-$  ions have three and a half times more counts than the control, which are attributed to the peptide bonds. This surface also presents the highest intensity of the  $\text{C}_2\text{H}_6\text{NO}^+$  ion attributed to serine. The ion images for serine and lysine ions show a uniform intensity. Therefore, the peptide-gold surface is homogeneous.

Analysis of the AUT-PEG-Peptide surface reveals the AuS<sup>-</sup> ion, from the initial AUT binding gold. Compared with AUT alone, the AuS<sup>-</sup> ion intensity is lower because of attenuation by the PEG linker and subsequent peptide layer above. The C<sub>2</sub>H<sub>5</sub>O<sup>+</sup> ion of the PEG chain has fourteen times more counts than any other surface, confirming the presence of PEG. Compared to the control, counts for the serine ion fragment are ten times higher, and that of lysine is six times higher. These results indicate the AUT-PEG-Peptide treatment was successful. In comparison with peptide-gold, the serine and lysine fragment intensities are four times lower on the AUT-PEG-Peptide surface. Therefore, AUT-PEG-Peptide presents less peptide than the peptide-gold surface. Although this result appears to be supported by the higher oxygen and nitrogen on peptide-gold from XPS analysis, the contribution of the AUT and PEG components unbalance the elemental ratios. Finally, in contrast to the heterogeneous PEG distribution on the APTMS-PEG-Peptide surface on glass. The AUT-PEG-Peptide ion images have a more homogeneous coverage of C<sub>2</sub>H<sub>5</sub>O<sup>+</sup> (PEG), figure III.8. The small lighter region is a defect in the gold film and is present in the total ion image, appendix 16.

### **III-5 Summary**

To determine the success of chemical modifications of glass and gold surfaces they have been investigated by water contact angle, X-ray photoelectron spectroscopy, and time of flight secondary ion mass spectrometry. The modifications were intended to functionalise the surfaces with amine groups, or to bind a peptide fragment of laminin.

Five glass surfaces were prepared; two via silanisation with amine terminated alkoxysilanes (APTMS and APDES); two by binding the peptide to the APTMS and APDES surface via a maleimide-PEG-succinimidyl linker; and one final surface of adsorbed PLL. Silanisation with APTMS and APDES were intended to functionalise the glass surface with amine groups, these amine groups would be required in order to bind the PEG linker, which subsequently binds the peptide. Both XPS and ToF-SIMS show the APTMS treated surface has more nitrogen, and amine associated fragments than ADPES. As a consequence more PEG-linker has bound to the APTMS surface over APDES, but both surfaces have a patchy distribution of

PEG. The heterogeneous distribution of PEG could be a result of non uniform silanisation of the glass surface. The peptide has bound to the PEG-linker on APTMS, following the underlying heterogeneous distribution of PEG. In contrast to the peptide binding on APTMS-PEG-Peptide, because less PEG linker bound to the APDES surface, the peptide seems to have homogeneously adsorbed over the APDES surface. Therefore, neither silanisation attempt has introduced enough amine content to result in a homogeneous coverage of PEG linker, and subsequent peptide. However, when APTMS was used, there are regions of APTMS-PEG-Peptide. The PLL adsorbed layer is homogenous, as determined from ToF-SIMS, indicating PLL has successfully physisorbed onto the glass.

Four gold surfaces were prepared; one via adsorption of an amino terminated alkyl-thiol (AUT); one via direct adsorption of the peptide; one by binding the peptide to the AUT surface via a maleimide-PEG-succinimidyl linker; and a final surface of adsorbed PLL. The AUT has bound to gold indicated by the presence of AuS ion fragments with ToF-SIMS. Identification of amino acid ion fragments indicates the presence of peptide when adsorbed to gold, and also when bound by the PEG linker. In contrast to the glass surfaces, all the gold modifications result in a homogeneous distribution of characteristic ion fragments chosen to represent each modification. Therefore, the modification with AUT was successful; both peptide modifications have been successful; and the PLL successfully adsorbed to gold. These results also indicate that for the methods chosen in this study, thiol modification of gold has provided a more reliable surface functionalisation than silanisation of glass.

# IV Response of Primary Neurons

---

## IV-1 Introduction

This chapter presents the ability of each surface to support a low density neuron cell culture. Primary cultures of neurons dissociated from embryonic rat hippocampi were used, as described in chapter II. Poly-L-lysine (PLL) is commonly used to support cultures of neurons on a variety of surfaces, therefore PLL surface treatments have been included for comparison.

Initially cultured neurons settle from a cell suspension and adhere to the surface. If the conditions are favourable, processes grow out from the cells within 24 hours. The term ‘processes’ refers to the long, thin projections of membrane from the cell body. One of the processes forms the axon, while the rest form dendrites. These processes grow along the surface, eventually reaching target cells where synapses develop between the axons and dendrites, figure IV.1. Neurons in mature networks spontaneously begin firing action potentials.

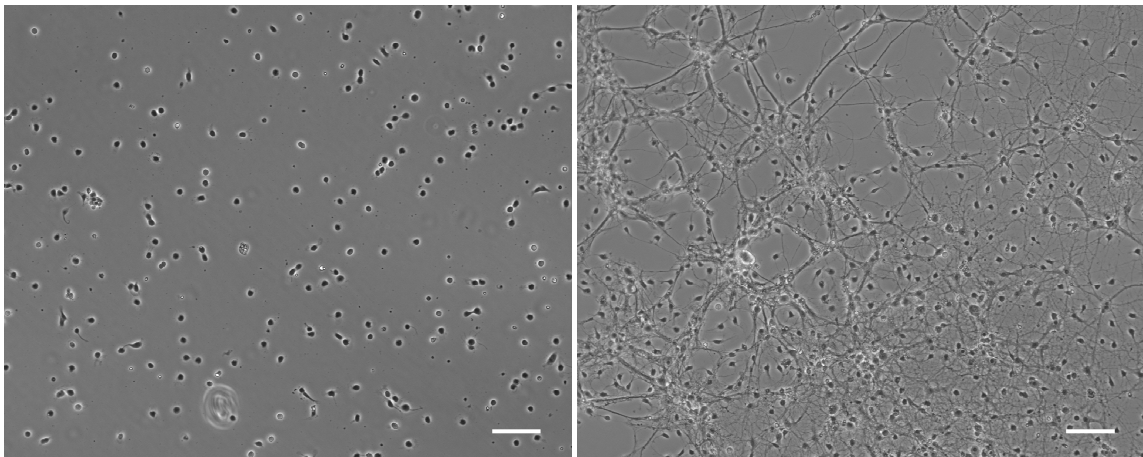


Figure IV.1: Phase contrast images of embryonic rat hippocampal neurons cultured on PLL coated glass. After initial plating, the neurons have few processes (left). Axons and dendrites then develop, spread over the surface and form synapses with other cells. A resulting network at 14 days *in vitro* is shown (right). Scale bar is 100  $\mu\text{m}$ .

The formation of homogenous networks with evenly spaced cells occurs spontaneously when the properties of the surface/substrate as well as culture conditions are favourable to support the neural network. However, it has been shown that cultures of higher densities,  $> 10,000 \text{ cells/mm}^2$ , initially form homogenous

networks which then collapse to form large clusters approximately  $\sim 250 \mu\text{m}$  long after 2 days culture<sup>[76]</sup>. At lower cell densities the process is different; tight clusters of cells form when the cells prefer to adhere to themselves rather than the surface<sup>[63]</sup>. Example images of cell clusters and processes are shown in figure IV.2. Clustered groups of cells are unfavourable for imaging applications which aim to monitor properties of individual cells, such as with SPR imaging. Clustering requires higher resolution images and refocusing to distinguish between cells, which is difficult on the timescale of action potentials. A typical action potential lasts a few milliseconds, consisting of several phases described in section I-3.4. Thus, a large bandwidth, typically 10 KHz, is required to record the shape and detail of each action potential. In order to image these properties, it would be beneficial for all cells to be in focus and distinguishable from each other.

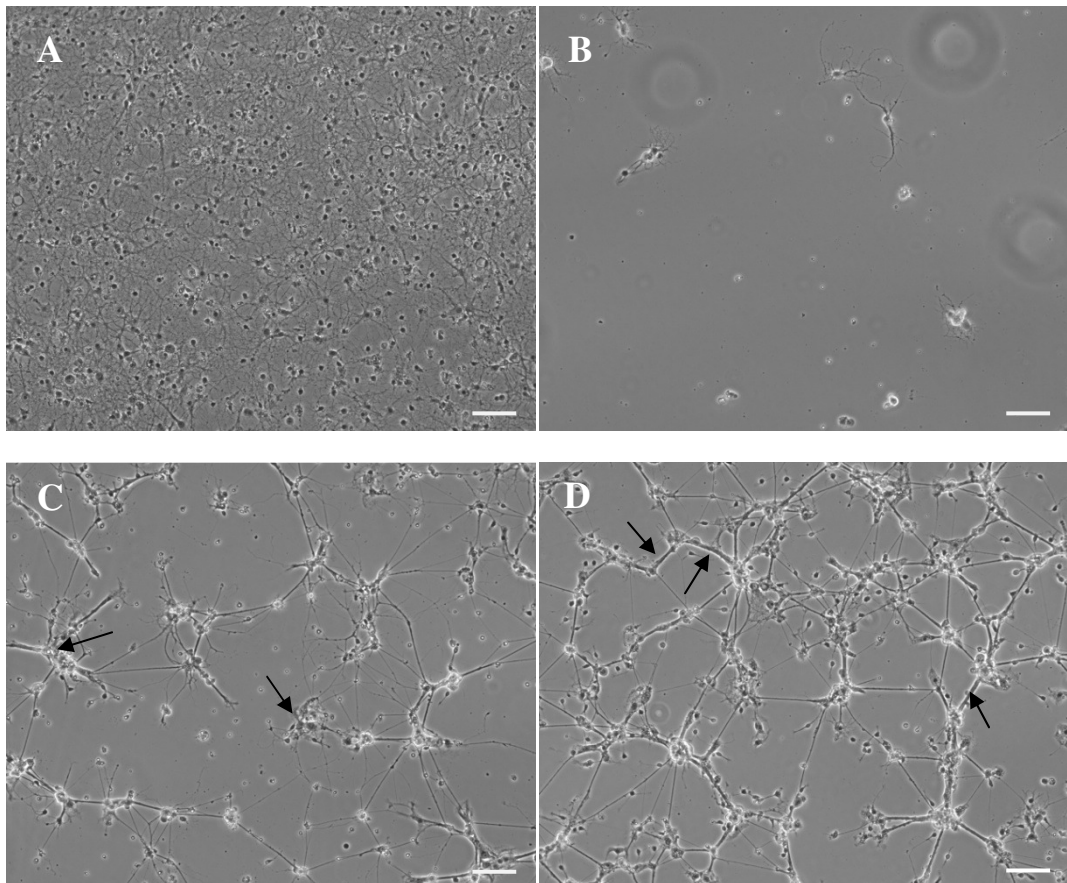


Figure IV.2: Example observations from phase contrast images of neural cultures at 14 days *in vitro*. A) High surface coverage of separated cells, with fine processes and little cell clustering. B) Low surface coverage with few cells. C) Low surface coverage with clusters of cells indicated by arrows. D) Clusters of processes form thick structures indicated by arrows. Scale bar is  $100 \mu\text{m}$ .

## IV-2 Results

### IV-2.1 Qualitative observations

Representative images from calcein fluorescence from days 7 and 21 show the morphology of the living cells on the variety of glass and gold surface treatments, figure IV.3. Desirable cultures in this study would show evenly distributed single cells with evenly distributed axons and dendrites forming between them. Cultures displaying non-continuous or patchy growth, and/or clustering of cells or processes, indicate the surface is not able to support the culture optimally. These qualitative observations have been summarised in table IV.1.

Treatment	Surface coverage	Separated cells	Clusters of cells	Clusters of processes
<i>Glass Surface</i>				
PLL	<u>High</u>	<u>High</u>	<u>Low</u>	<u>Low</u>
APDMES	Very low	Very low	High	n/a
APDMES-PEG-Peptide	Very low	Very low	High	n/a
APTMS	Low	Low	High	High
APTMS-PEG-Peptide	Very low	Very low	<u>Low</u>	n/a
<i>Gold Surface</i>				
PLL	Low	Low	High	High
Peptide	Medium	Low	High	Medium
AUT	<u>High</u>	<u>High</u>	<u>Low</u>	<u>Low</u>
AUT-PEG-Peptide	<u>High</u>	<u>High</u>	<u>Low</u>	<u>Low</u>

Table IV.1: Qualitative observations of neural cultures at day 21. The underlined responses are considered indicative of a suitable culture environment; a high surface coverage of non-clustered cells and processes.

The cell response was poor on all treated glass surfaces except PLL. On PLL surfaces cells have a high survival rate, and tend to distribute uniformly across the surface throughout the 21 days culture. Cell processes also spread uniformly over the PLL-glass surface. Initially the APTMS surface showed good cell coverage but by day 21 the cells had formed small clusters and their processes had gathered into fascicules (bundles of processes), figure IV.3. Cell adhesion and survival was very low on all other glass surfaces (APDMES, APDMES-PEG-Peptide, APTMS-PEG-Peptide); on these surfaces the few surviving cells tended to cluster together.

On all gold surfaces neuronal cultures exhibited a high survival rate and uniform coverage, which was in contrast to the glass surfaces. Initially the cells did not

cluster and their processes spread uniformly over the surfaces. However, clustering of cells was seen on the PLL and Peptide (without PEG) surfaces by day 21. The AUT and AUT-PEG-Peptide surfaces continued to support uniformly distributed networks, with no significant clustering of either the cells or their processes, until week 3 of the culture. The cell response to AUT and AUT-PEG-Peptide treated surfaces was qualitatively comparable to the PLL-glass control.

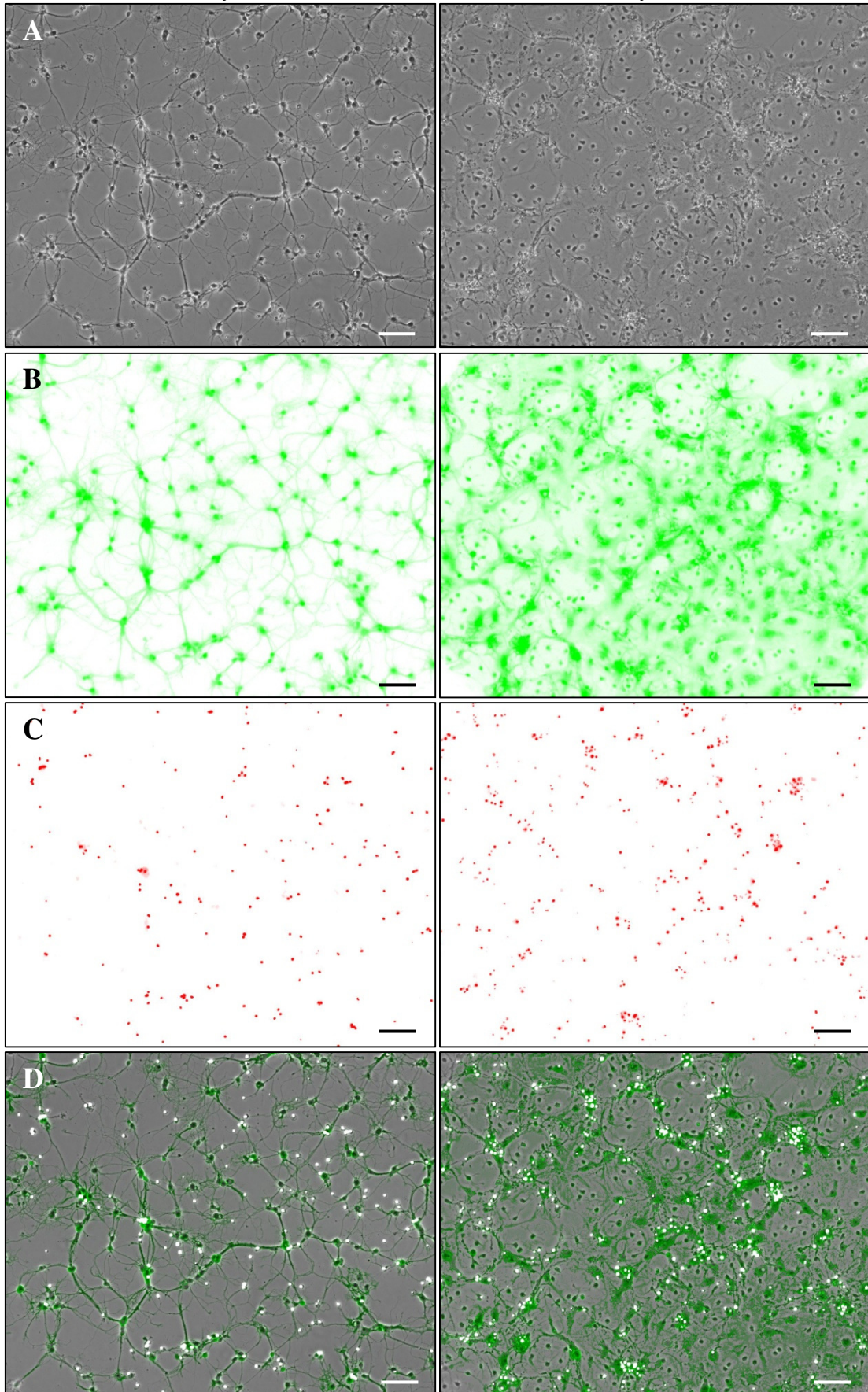
---

Figure IV.3: Representative images at day 0 and 21 for all surface treatments. A) Phase contrast images are unmodified. B) Live images, from calcein fluorescence, were processed as follows for clarity; converted to 8 bit grayscale, colour inverted, colourised green, contrast enhanced. C) Dead images, from ethidium homodimer fluorescence, were processed for clarity as with the live images, except colourised red. The dead cells were made white for the overlay by further processing; made binary, dilated once, and inverted. D) Image overlays of the phase contrast, processed live and dead images. Scale bar is 100  $\mu\text{m}$ .

Glass: PLL

Day 7

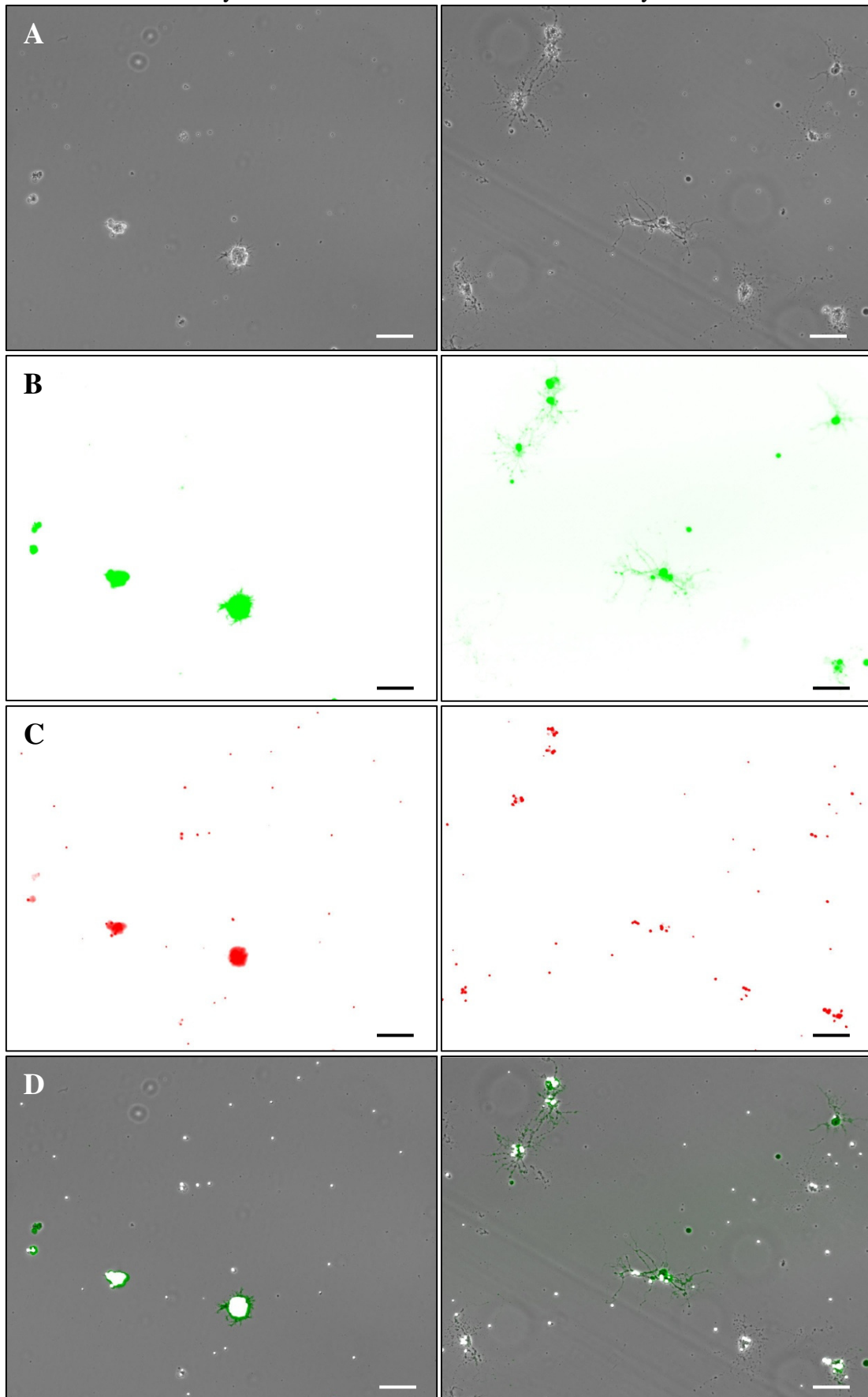
Day 21



Glass: APDES

Day 7

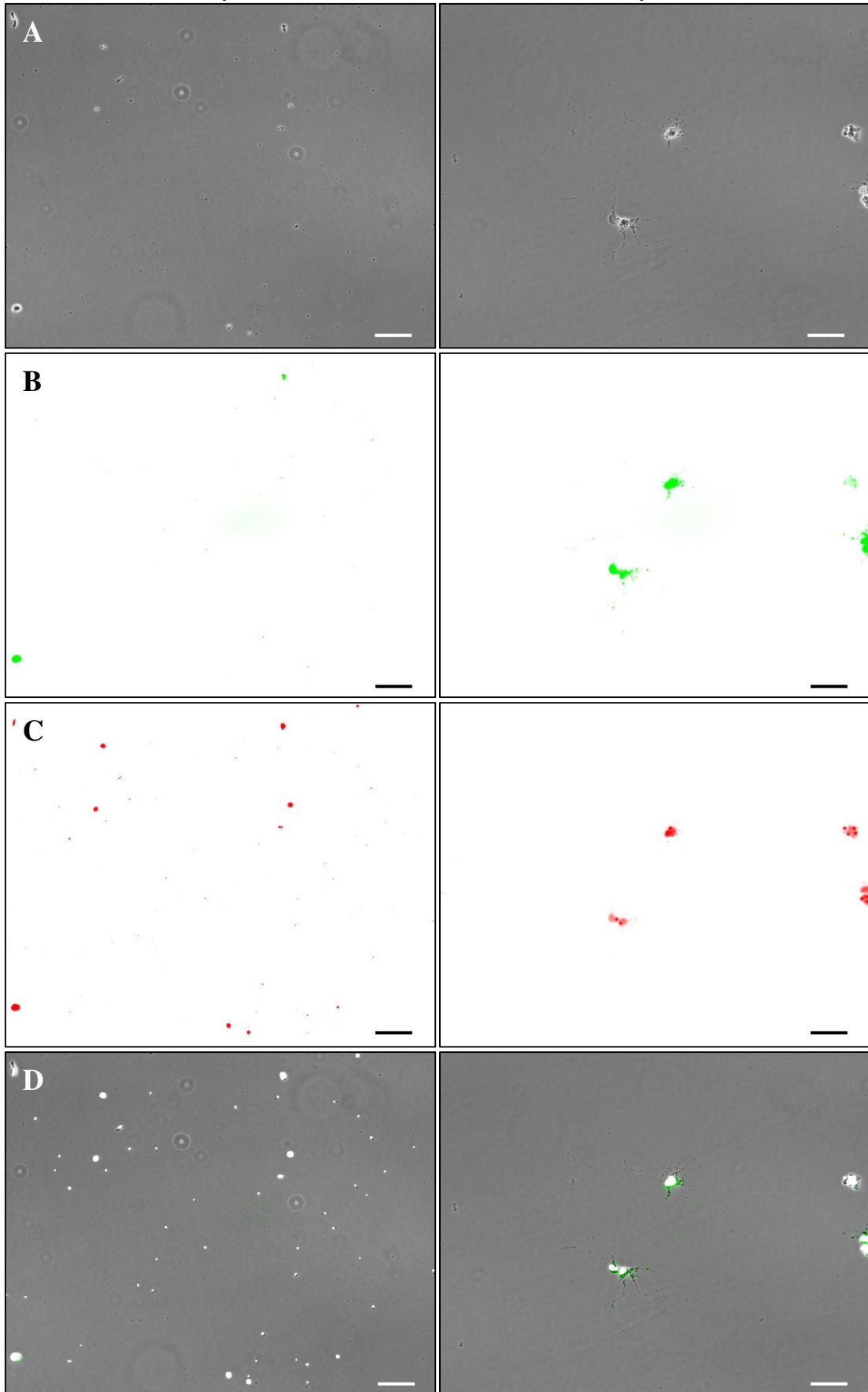
Day 21



Glass: APDES-PEG-Peptide

Day 7

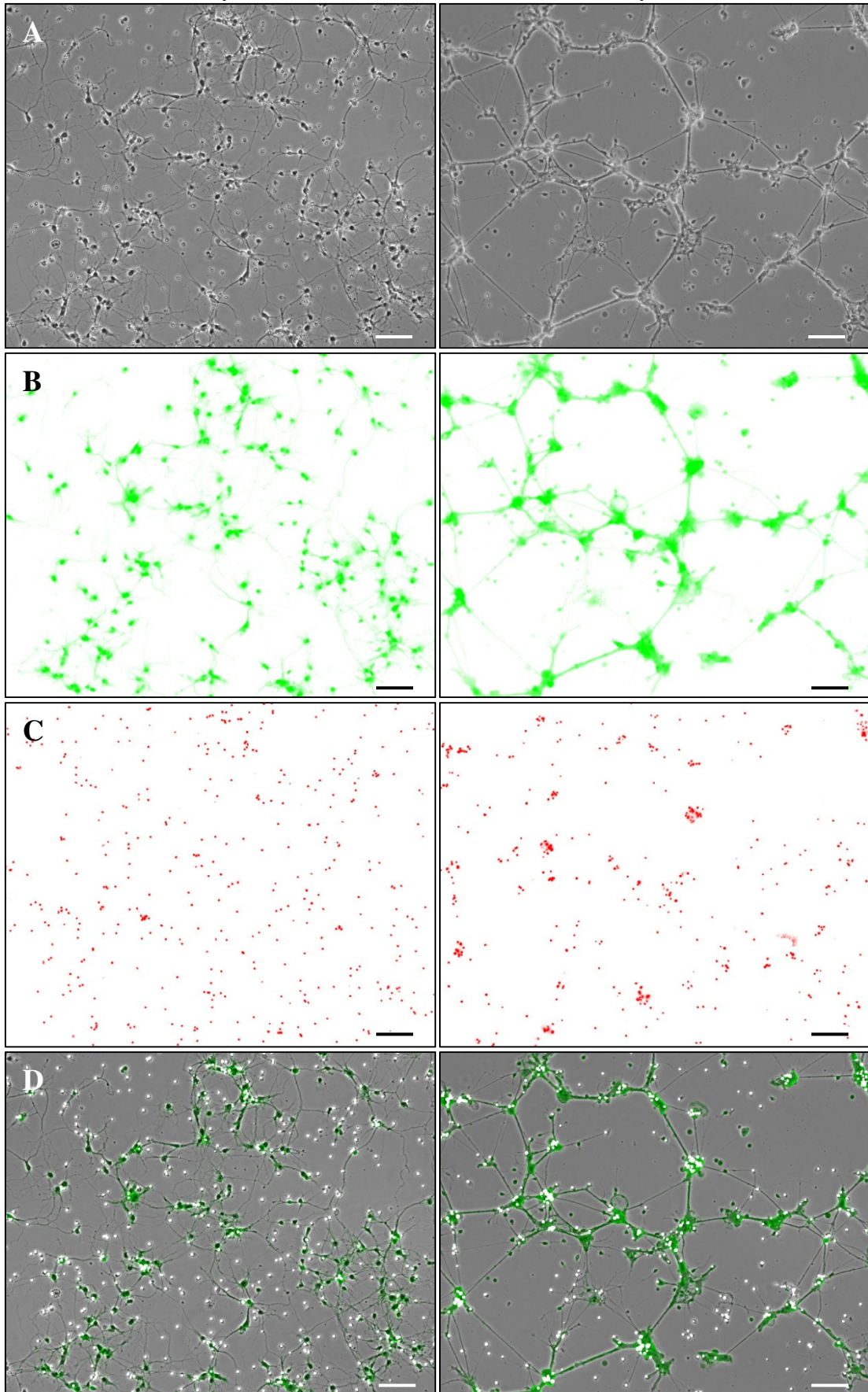
Day 21



Glass: APTMS

Day 7

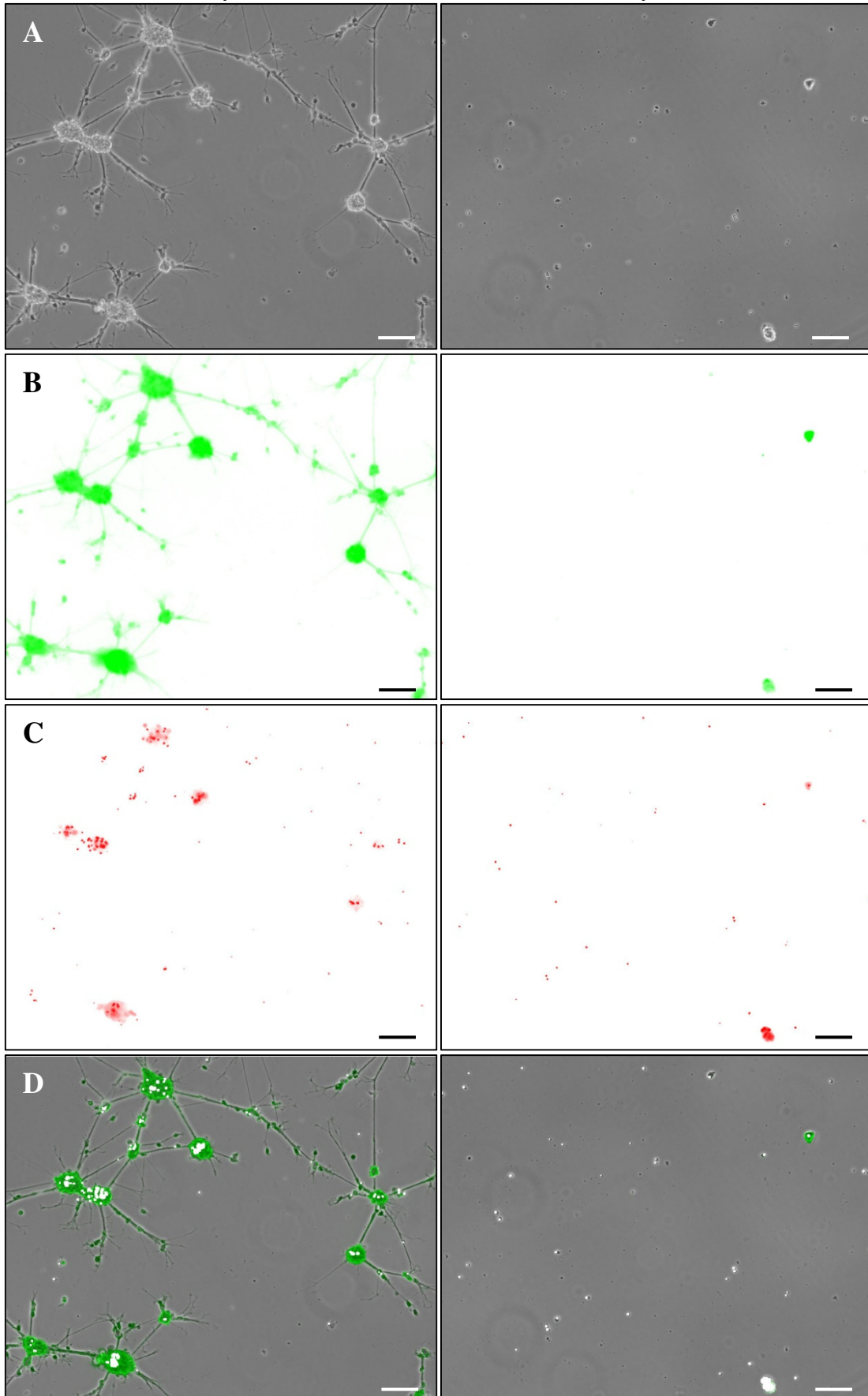
Day 21



Glass – APTMS-PEG-Peptide

Day 7

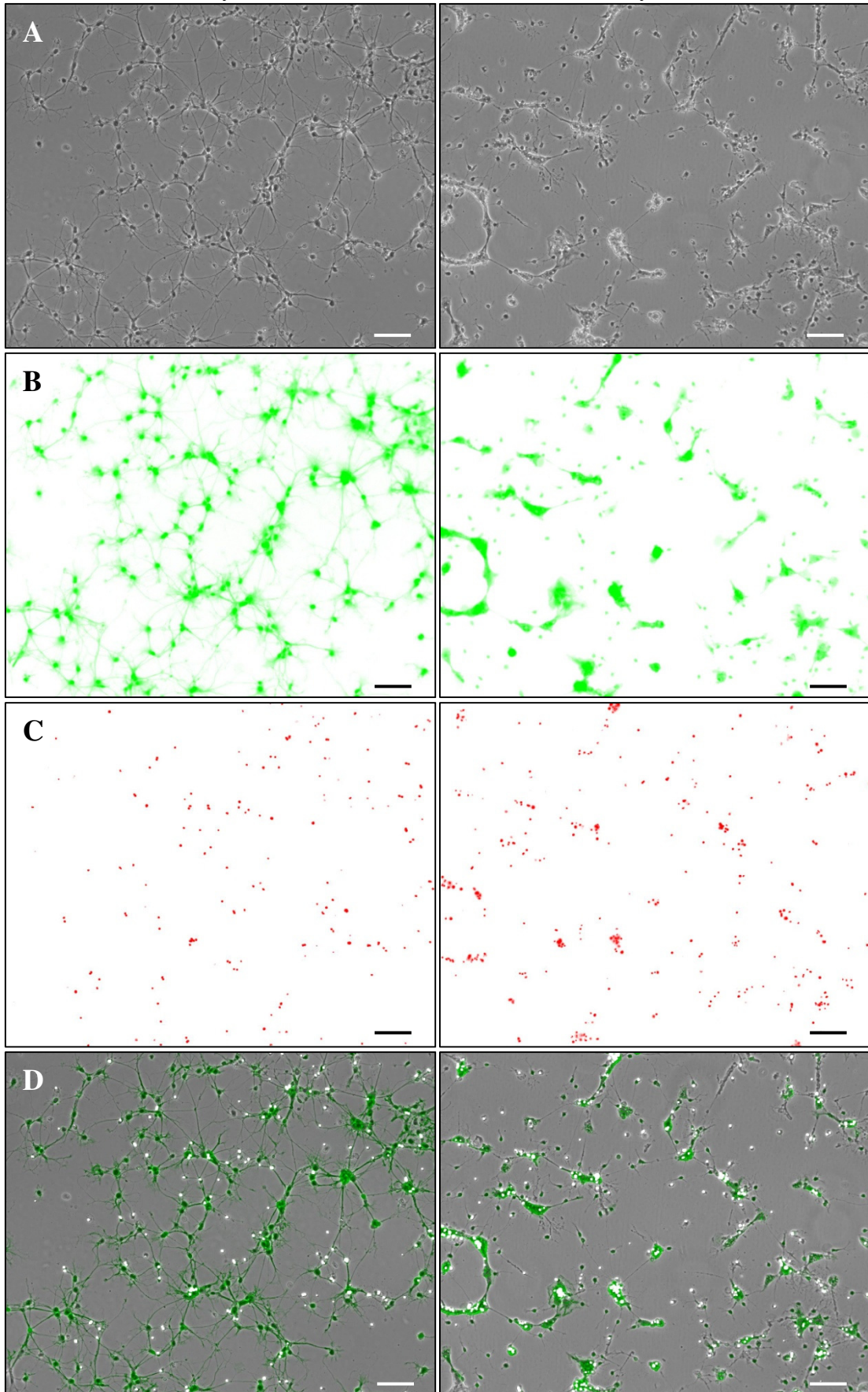
Day 21



Gold - PLL

Day 7

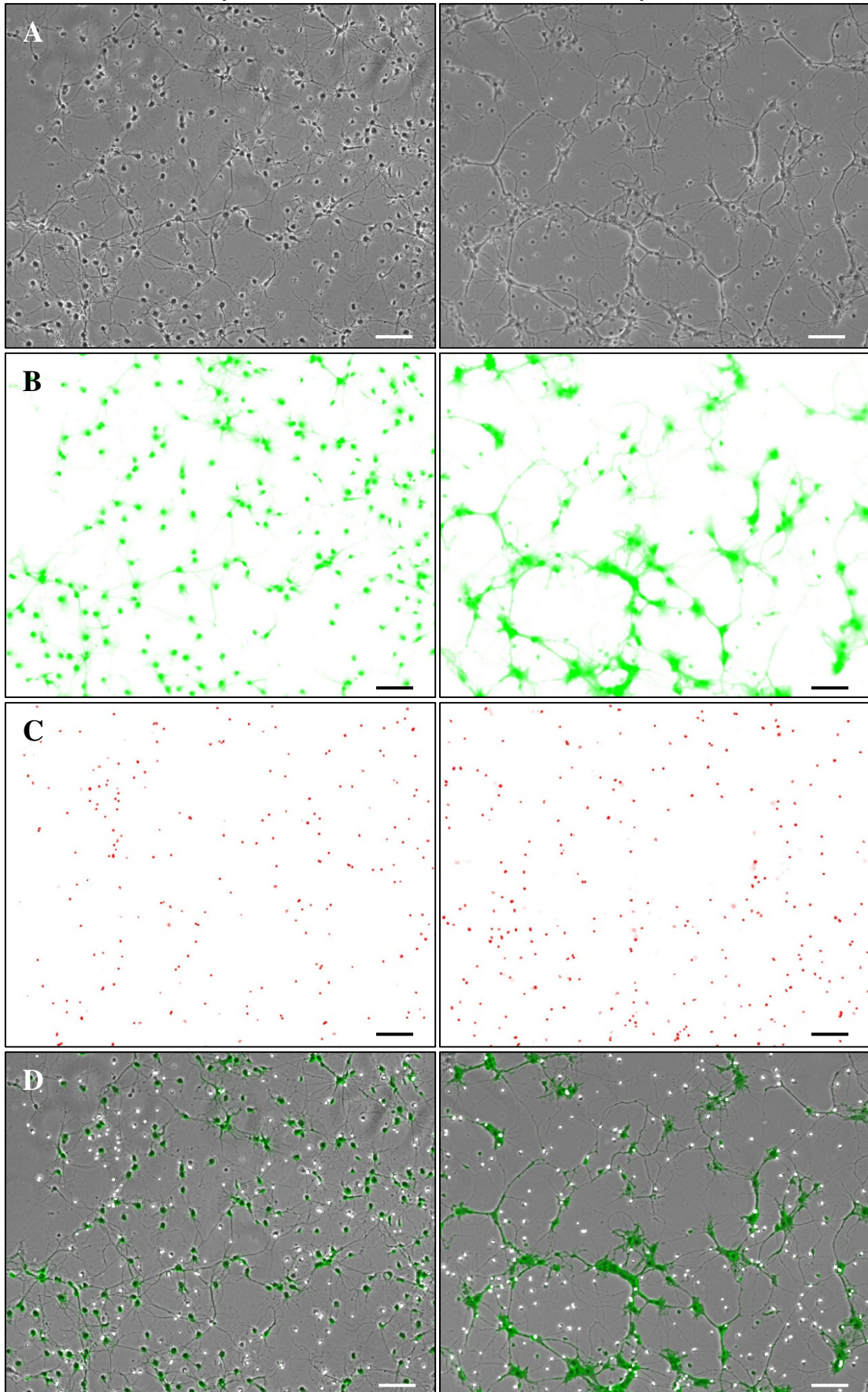
Day 21



Gold – Peptide

Day 7

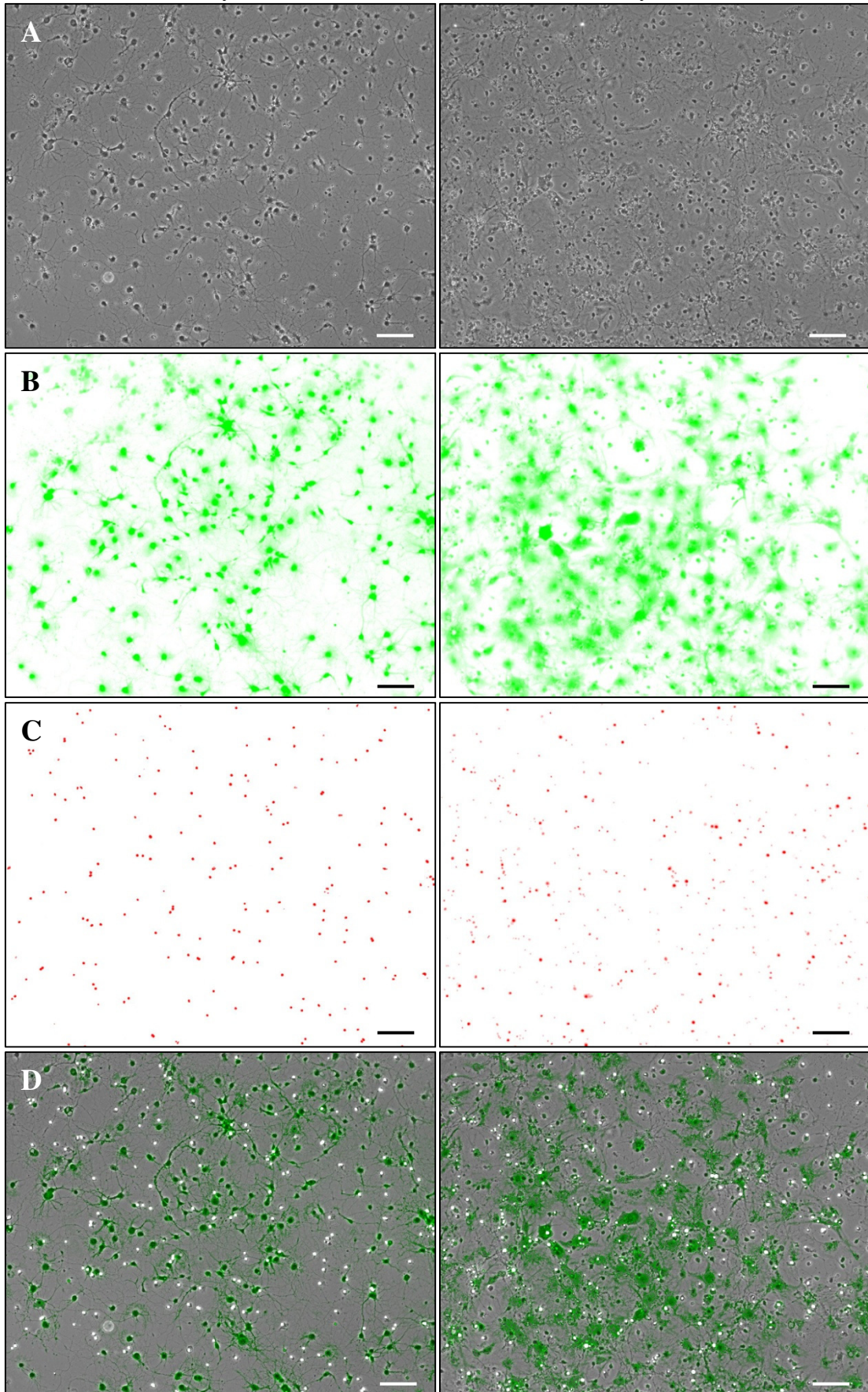
Day 21



Gold – AUT

Day 7

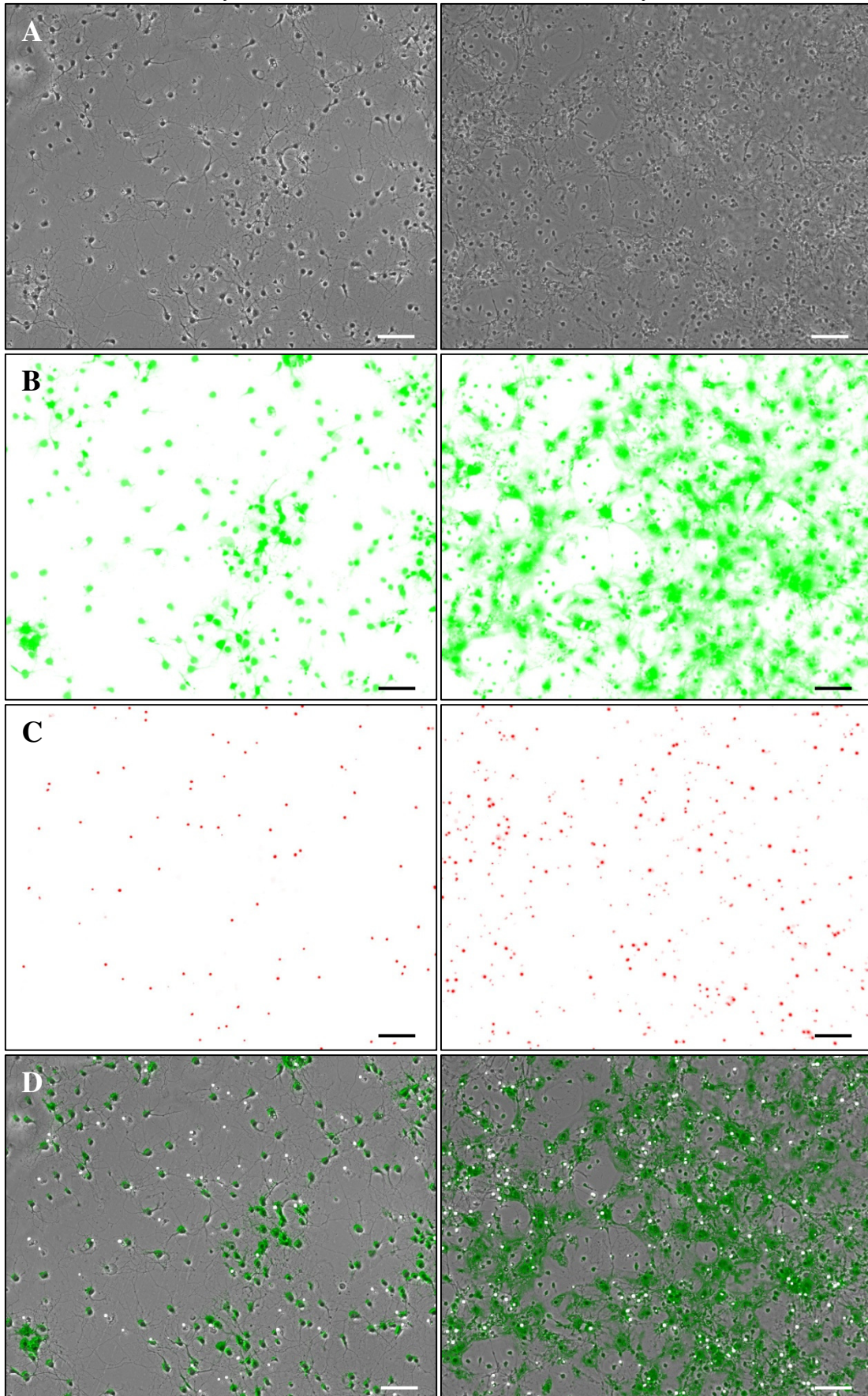
Day 21



Gold – AUT-PEG-Peptide

Day 7

Day 21



### **IV-3 Quantitative observations**

To obtain a quantified response of cell growth between surfaces the cells were stained with calcein and ethidium fluorescent dyes, figure IV.3. Live cells were marked by their ability to uptake and cleave calcein AM to calcein which then fluoresces green. While dead cells present no barrier to ethidium homodimer which binds to DNA and fluoresces red. The counting procedure was performed manually because as the culture matures a dense network of processes cover the surface. This makes reliable counting by an automated or semi-automated program difficult. However, by alternating between phase contrast and fluorescent images, manual counting gives accurate results with an estimated error rate of less than 7 % based on repeatability of results. On surfaces where cells have clustered (APDMES, APDMES-PEG-Peptide and APTMS-PEG-Peptide on glass) reliable counting of cells was not possible. The results would be unreliable for comparison with other surfaces and have therefore been omitted from quantitative analysis. The counts for live and dead cells are shown in figure IV.4.

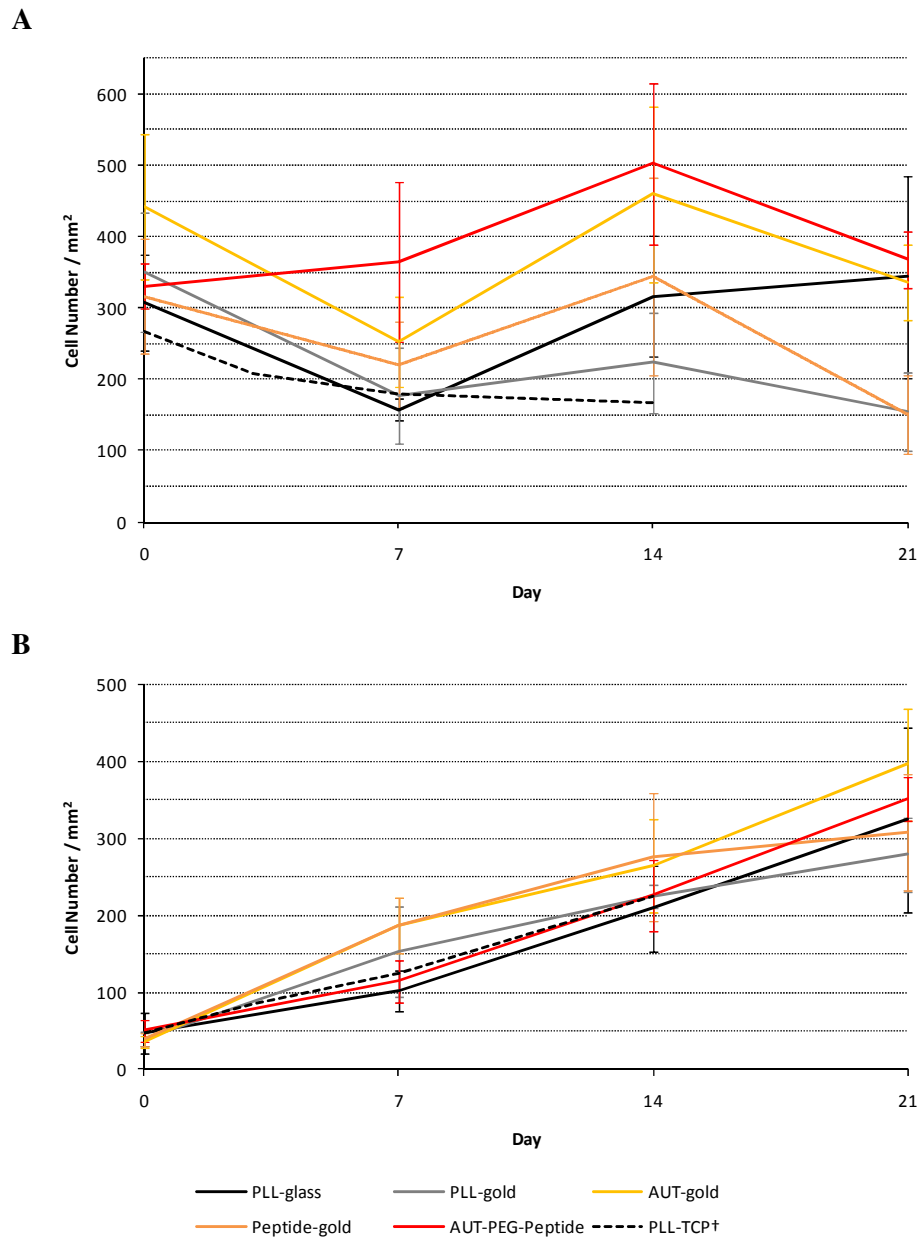


Figure IV.4: Average Live(A) and Dead(B) cell counts. Error bars are standard deviation (n=6 at day 0, n=9 at days 7-21). <sup>†</sup>Unpublished data from separate culture preparation, used with permission (Acknowledgement: Katharina Reusch).

The average number of living cells varies considerably with surface and time, as seen in figure IV.4A. After 21 days culture the highest numbers of live cells are observed on Peptide-PEG-gold, AUT-gold, and PLL-glass surfaces. Fewer live cells are observed on PLL-gold and Peptide-gold surfaces at 21 days culture. An ANOVA test shows that the mean live cell numbers are significantly different between surface treatments at day 21;  $F(4, 40) = 17.18, P < 0.001$ . A Tukey HSD post hoc means comparison indicates that the mean live cell numbers on PLL-gold and Peptide-gold

are equal, and these are significantly different from the remaining surfaces ( $P < 0.01$ ).

The Pearson correlation coefficient was calculated to determine if there was correlation between the average number of live and dead cells. The number of live cells at each time point may correlate with the change of dead cell numbers (death rate) over the following time period, 1 week. The least squares approach was used to determine the linear regression of average cell number against time for live and dead cells. The results are presented in table IV.2.

Surface	Pearson Correlation Coefficient Av. Cell Number		Linear regression ( $R^2$ ) Av. Cell Number v Time	
	Live v Dead <sup>(a)</sup>	Live v Death Rate <sup>(b)</sup>	Live	Dead
PLL-glass	0.52	-0.34	0.17	0.98
PLL-gold	-0.86	0.84	0.63	0.97
AUT-gold	-0.27	0.94	0.02	0.99
Peptide-gold	-0.44	-0.19	0.29	0.92
AUT-PEG-Peptide	0.36	0.79	0.18	0.98
PLL-TCP	-0.85	-0.76	0.77	0.99

Table IV.2: Correlation and Regression analysis of average cell number. <sup>(a)</sup> Correlation between live and dead cells at each time point. <sup>(b)</sup> Correlation between the average number of live cells at  $T_n$  and the change of dead cell numbers (death rate) between  $T_n$  and  $T_{n+1}$ .

The correlation between average live and dead cell numbers varies for the different surface modifications. A strong negative correlation was found on the PLL-gold and PLL-TCP surfaces. A small negative correlation was found for the Peptide-gold and AUT-gold surfaces. A negative correlation indicates that as the live cell numbers increase the dead cell numbers decrease, and vice versa. In contrast to the negative correlation, the PLL-glass and AUT-PEG-Peptide surfaces have a positive correlation. A positive correlation indicates that both live and dead cell numbers either increase or decrease together.

The variation in live v dead correlations across different surfaces could be due to the observed trends of live and dead cells over time. Live cell numbers show a linear trend on PLL-gold and PLL-TCP surfaces, which have declining live cell numbers

over the culture. The remaining live cell counts appear to show no linear trend with time, and no other trend is apparent figure IV.4. In contrast to the live cells, the number of dead cells shows a strong linear trend with time; all surfaces show a linear increase in dead cells during the culture. Thus, the strong negative correlation between live and dead cells on PLL-gold and PLL-TCP surfaces is explained by the declining number of live cells, and increasing number of dead cells.

The live cell numbers correlate positively with the death rate on PLL-gold, AUT-gold and AUT-PEG-Peptide surfaces. The positive correlation indicates that the number of live cells and the death rate either increase or decrease together. A negative correlation was found on PLL-TCP surface, and to a lesser extent on PLL-glass and Peptide-gold surfaces. The negative correlation indicates that as live cell numbers increase the death rate decreases, and vice versa.

To test how consistent the cell coverage was for individual surface modifications, the coefficient of variation (CV) has been shown for live and dead cell counts, figure IV.5. The CV is appropriate for comparing the variation when sample means differ.

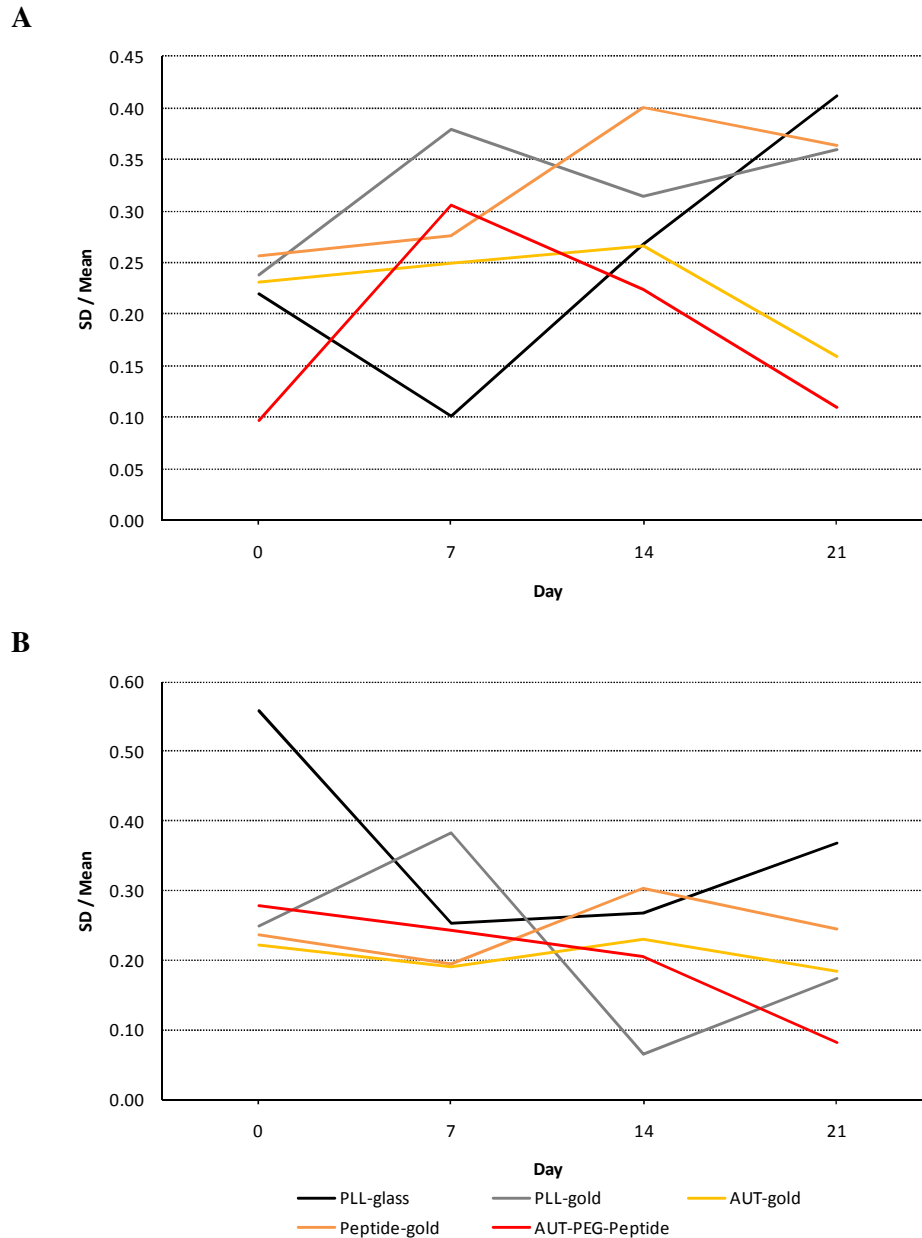


Figure IV.5: Coefficient of variation for Live(A) and Dead(B) cell counts. Standard deviation divided by mean describes the coefficient of variation (CV).

On day 0 the number of live cells fluctuate the least on the Peptide-PEG-gold surface, in comparison to the other samples. The PLL-glass, PLL-gold, AUT-gold and Peptide-gold surfaces show similar variations of live cell counts on day 0.

The live cell coverage varies the most on the PLL-gold and Peptide-gold surfaces, which show high variations compared to other treatments, over the culture time period.

The variation of live cell number on PLL-glass increases after the first week, and presents the highest variation of all surface treatments at day 21. Indicating that at day 21, the cell coverage varied the most on the PLL-glass surfaces.

In comparison with the other surface treatments, the AUT-gold surface shows more constant variations in live cell numbers over time. Both AUT-gold and Peptide-PEG-gold show lower variations in live cell numbers at day 21, in comparison to the other treatments. Therefore, the AUT-gold and Peptide-PEG-gold surfaces have the most consistent cell coverage at day 21.

In general, the coverage of dead cells is most inconsistent on the PLL-glass surface. The number of dead cells varies most on the PLL-glass surface, and the magnitude of this variation is highest on day 0.

The Peptide-gold surface displays less consistent dead cell coverage over the first week, and a more consistent coverage over the second and third weeks.

The AUT-gold, Peptide-gold, and Peptide-PEG-gold surfaces show a more consistent coverage of dead cells over the culture time period. The Peptide-PEG-gold surface shows the least variation of dead cell numbers at day 21.

A proportion of the cells will die during culture preparation due to physical stresses during the dissection. These dead/dying cells will be present in the cell suspension plated onto the surfaces. The average number of dead cells is the same for all surfaces at time zero;  $F(5, 24) = 0.77$ ,  $P = 0.58$ . This would be expected if the surfaces did not cause significant cell death before counting on day 0 (4 hours after plating), and also implies the cells were evenly distributed in the suspension. However, the live cell counts do show variation from 300 to 450 cells/mm<sup>2</sup> at day 0, figure IV.4. Assuming an even distribution in suspension, an average count of 219 cells/mm<sup>2</sup> is expected.

The cells were plated by placing a droplet of media of volume,  $V$ , onto round substrates of diameter,  $D$ . Due to water surface tension the height of the droplet,  $z$ , varies with the radius,  $r$ , across the substrate. The relationship between droplet height and radius,  $z(r)$  is dependent on the wettability of the substrate surface, which can be described by the WCA,  $\Phi$ , figure IV.6.

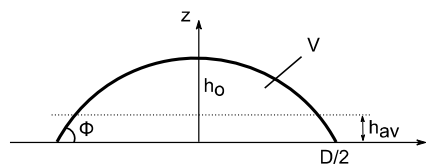


Figure IV.6: Droplet of WCA  $\Phi$ , with central height of  $h_0$ , average height of  $h_{av}$  and a volume of  $V$ . Figure used with permission (Acknowledgement: Dr Noah Russell) .

Assuming the cells are initially evenly distributed within the droplet, as they settle from suspension, the cell density at the surface will depend on the droplet height. The variation in cell density across the surface will therefore be dependent on the WCA.

The heterogeneity in cell density on a surface,  $H$ , can be defined by the ratio of the height of the droplet in the centre,  $h_0$ , to its mean height,  $h_{av}$ . Assuming a spherical droplet,  $H$  can be described by the WCA, equation IV.1.

$$H = 3 - \frac{3}{\cos \phi + 2} \quad \text{Eqn IV.1}$$

The heterogeneity of the cell density on the surface varies with water contact angle, described by equation IV.1, from 2 times the average cell density to 1.5 times the average cell density between 0° and 90° WCA, figure IV.7.

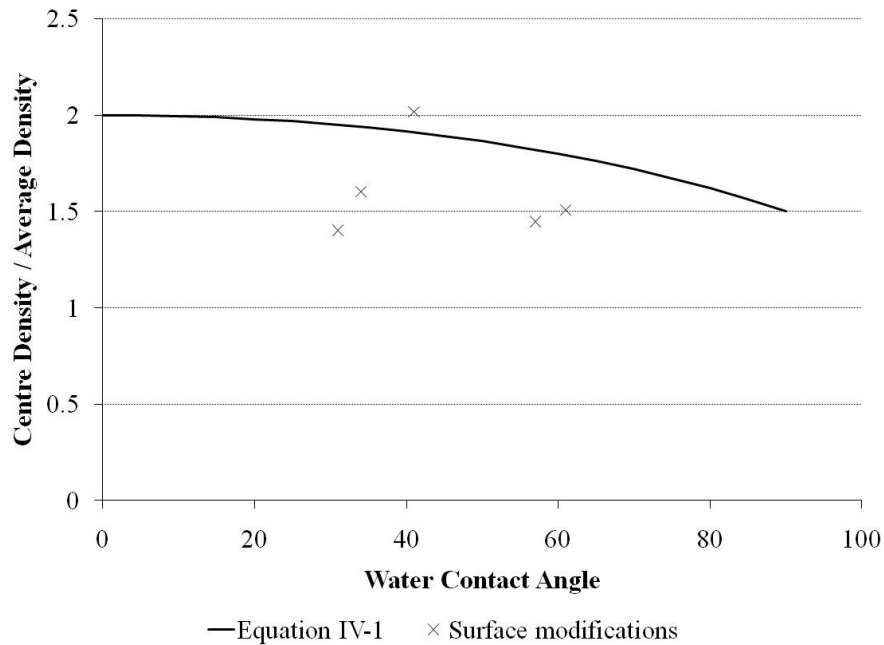


Figure IV.7: Heterogeneity of cell density as a function of water contact angle. Live cell counts for the surfaces were divided by the predicted 219 cells/mm<sup>2</sup> and plotted against their WCA.

The majority of surfaces have lower ratios of heterogeneity than that predicted by equation IV.1, figure IV.7. This ratio, predicted by the model, applies to the centre of the droplet. Although the cell counting was sampled from the central region of the surface, it was not exactly from the centre of the substrate. This would cause a reduced ratio in comparison to the predicted value.

Several other factors may affect the cell distribution. Following plating, cells were given 30 minutes to ‘settle’ before the wells were flooded with media. Loosely bound cells could be displaced. The variation across surfaces could then be due to cells having different affinities for each surface. Dead cells in suspension will adhere to the surface by adsorption. However, dead cells are unlikely to spread on any surface by forming adhesion domains with receptors, and rearrangement of their internal structures. Therefore, little variation in dead cell numbers would be expected

between different surfaces. In comparison, live cells can adhere and spread to differing extents depending on the surface properties. The possibility of cell displacement from the surface may explain the variation between samples, and may also account further towards the lower than predicted ratios of heterogeneity.

To determine if cell division may account for the above average live cell numbers, time lapse images were taken following the addition of media 30 minutes after plating the cells. Images were taken at 20 minute intervals for 5 hours, on PLL coated glass coverslips, figure IV.8. The difference in cell numbers after 5 hours indicates that the cultures are not proliferating fast enough to explain the above average cell numbers at time 0.

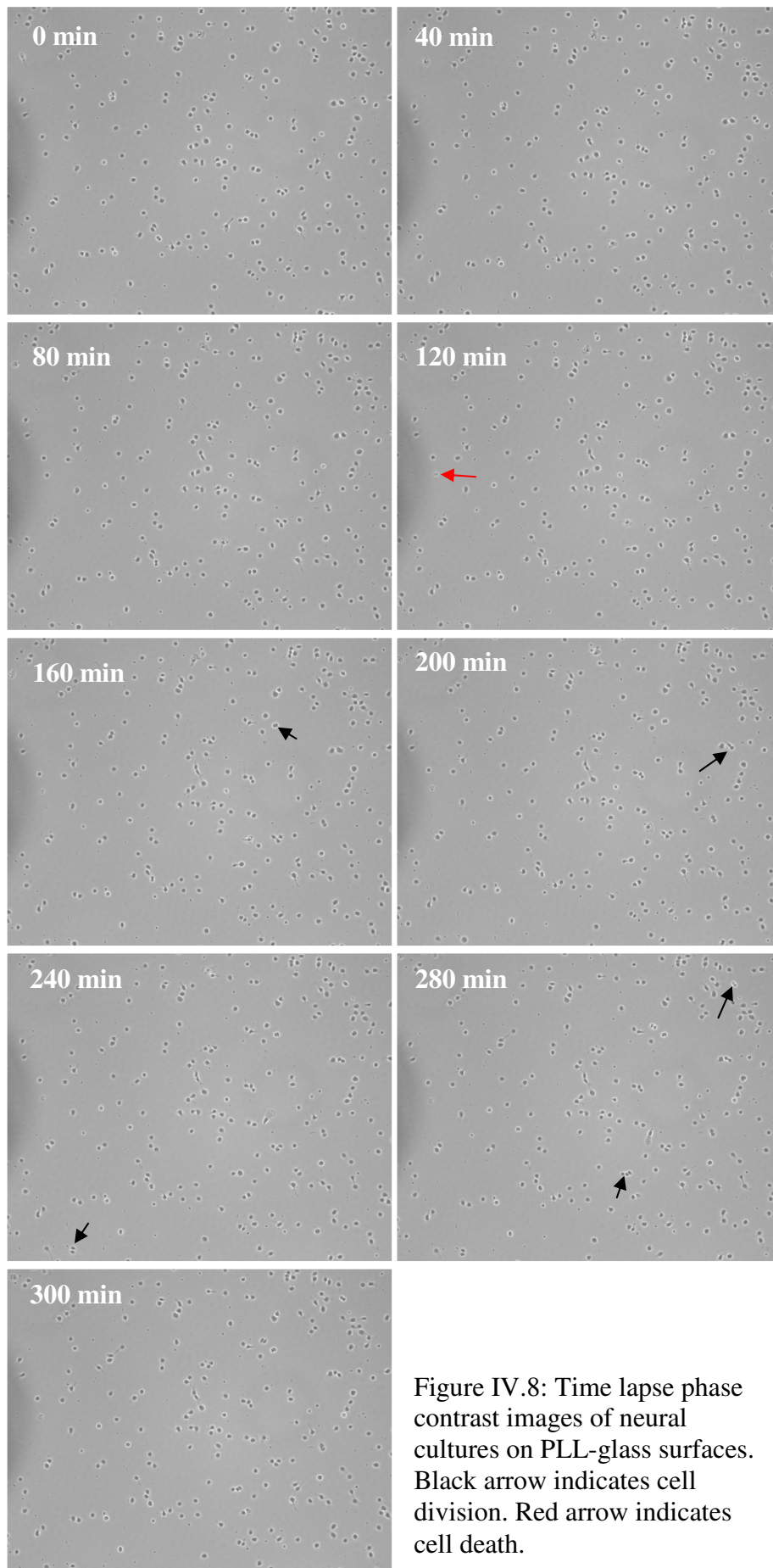


Figure IV.8: Time lapse phase contrast images of neural cultures on PLL-glass surfaces. Black arrow indicates cell division. Red arrow indicates cell death.

The most striking result in the data is that the average dead cell count follows a strong positive regression with time, which is not observed for the live counts, table IV.2. Furthermore, this trend is comparable across all surfaces, figure IV.4B. Linear regression shows an average death rate of 14 cells/mm<sup>2</sup>/day. It is noted that this data was collected from one cell culture preparation. To test the reproducibility of these data a separate data set has been included for comparison, for cells grown on PLL treated tissue culture plastic; with acknowledgment to Katharina Reusch for permission to include this data. This data was collected from another preparation where the culture conditions were identical, but the cell counting was automated. The resulting average number of dead cells shows the same magnitude and positive regression as with the presented surfaces.

The death rate, found by dividing the average change in number of dead cells by the number of days *in vitro* is shown in figure IV.9. Surface treatments of PLL-gold and Peptide-gold present decreasing death rates over the culture period. The death rate increases on the PLL-glass and Peptide-PEG-gold surfaces over week 2 and week 3. On the AUT-gold surface, the death rate decreases over week 2 and then increases over week 3. The significantly lower live cell numbers observed on PLL-gold and Peptide-gold surfaces shown in figure IV.4A, could account for a reduced death rate because fewer live cells are available to contribute to the pool of dead cells.

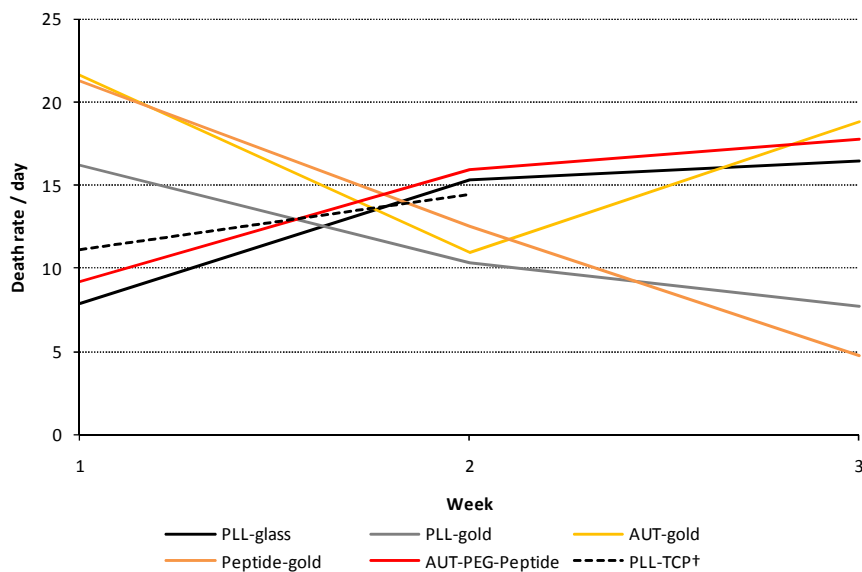


Figure IV.9: Average change in number of dead cells divided by the number of days *in vitro* for the presented surfaces. †Acknowledgment to Katharina Reusch for permission to include her data from tissue culture plastic.

A repeated measures ANOVA was conducted on the dataset to determine if cell numbers varied across different surfaces over time. Strictly speaking, the dataset does not follow a repeated measure of the same sample across time because the samples were not viable following staining. However, it is reasonable to assume that counts at each time point are not fully independent from the previous time (for each separate surface). This is because the culture would develop with time. Therefore, a repeated measures ANOVA is appropriate because it will account for a correlation over time, if present.

Test comparing numbers of;	F value	Significance
Live cells v surface	18.157	< 0.001
Live cells v day	12.150	< 0.001
Surface*day (interaction)	3.511	< 0.001
Dead cells v surface	3.296	0.027
Dead cells v day	177.543	< 0.001
Surface*day (interaction)	2.108	0.026

Table IV.3: Repeated measures ANOVA, (df=6).

The results of the ANOVA are displayed in table IV.3. This analysis confirms statistically the observation that the live cell counts differ significantly with surface treatment ( $F = 18.157$ ,  $P < 0.001$ ) and across time ( $F = 12.15$ ,  $P < 0.001$ ). The surface-time interaction term is also significant ( $F = 3.511$ ,  $P < 0.001$ ). Therefore the surfaces effect live cell numbers differently over time. The dead cells show a very significant time trend ( $F = 177.543$ ,  $P < 0.001$ ), with a slight but significant dependence on surface treatment ( $F = 3.296$ ,  $P = 0.027$ ) and a small interaction effect ( $F = 2.108$ ,  $P = 0.026$ ).

Although the surfaces show significant differences between dead cell counts, the apparent death rate (14 cells/mm<sup>2</sup>/day) is independent of surface or live cell numbers, figure IV.4B. The trend implies that dead cell counts accumulate over time, i.e. dead cells are not readily removed from the culture. Removal of dead cells by phagocytosis is unlikely to occur in adherent cultures<sup>[125]</sup>, therefore dead cells would not be removed as they are *in vivo*. Each dead cell count will have a contribution from previous weeks; however, this does not explain the strong regression observed in the data.

## IV-4 Culture model

Dissociated cultures of primary hippocampal neurons have been shown to include neurons, glial cells (incl. astrocytes), and neural progenitors<sup>[72,126]</sup>. In particular the progenitor cells can become neurons by differentiating, neurogenesis<sup>[72,127]</sup>. Neurons are considered non proliferative, whereas glia can divide and proliferate<sup>[128]</sup>. Neural progenitors can divide, but can also differentiate into neural or glial cell types.

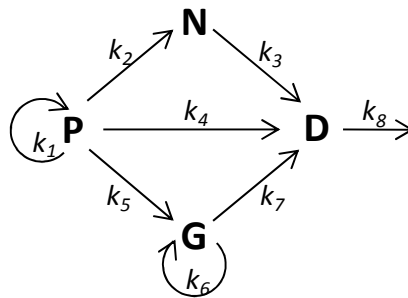


Figure IV.10: Cell culture model. Populations of Neural progenitor (P), Neuron (N), and Glial (G) cells contribute to dead cells (D). Rate constants ( $k$ ) for proliferation, differentiation and death are shown.

The proliferation of some mammalian cell types in culture may not follow an exponential trend<sup>[129]</sup>. However, an initial phase of exponential growth can be expected, and has been observed for the pheochromocytoma cell line, PC12<sup>[130]</sup> an immortalised neural cell line. The probability a live cell dies over a certain time period would be constant. The increased number of dead cells during any time period may then be expected to be proportionate to the number of live cells in the culture. Thus, fluctuations in the number of live cells would be expected to influence the numbers of dead cells. A positive correlation between the number of live cells and the death rate was found on the PLL-gold, AUT-gold and AUT-PEG-Peptide surfaces. Suggesting that as the number of live cells increases, so does the death rate. However, when considering all surfaces, there is no trend to the number of live cells with time. The magnitude of live cell numbers also varies with surface and time. In contrast, the numbers of dead cells appears consistent for all surfaces in terms of magnitude and rate of change. This lack of correlation between live and dead cell counts is unexpected. Forming a mathematical model of the cell culture may help explain these results. A complex culture model is presented in figure IV.10, depicting rate constants for proliferation, progenitor differentiation and death rate.

To test the cell culture model in figure IV.10 is beyond the scope of this study, requiring methods to identify the live and dead cell types, and many data points to follow the progress of the culture.

A simplified model is proposed in figure IV.11. The model makes the following assumptions: Live cells can replicate or die; the probability of cell death is always constant, and independent of other cells; the probability of replication is also constant; and dead cells don't leave the surface,  $k_3=0$ <sup>[125]</sup>.

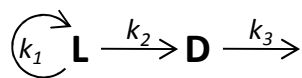


Figure IV.11: Simplified cell culture model. Live cells (L) can proliferate at rate  $k_1$  or die at rate  $k_2$  becoming dead cells (D). Dead cells may leave the surface at rate  $k_3$ .

Following the above assumptions; the number of dying cells is proportional to the number of live cells for a short time interval. This relationship is described by two coupled ordinary differential equations (ODEs); the rate of change of live cells is given by equation IV.2, and the death rate by equation IV.3. This implies that the death rate is a constant fraction of live cell number.

$$\frac{dL}{dt} = (k_1 - k_2)L \quad \text{Eqn IV.2}$$

$$\frac{dD}{dt} = k_2L \quad \text{Eqn IV.3}$$

The live and dead cell populations based on the above assumptions can be determined through the solutions to the ODEs, equations IV.4 and IV.5. The model predicts that both live and dead populations should follow exponential trends. However, the data contradicts this, figure IV.4; live cells show no clear trend, and dead cells show a linear trend on all surfaces.

$$L = L_0 e^{(k_1 - k_2)t} \quad \text{Eqn IV.4}$$

$$D = \frac{k_2}{(k_1 - k_2)} L_0 (e^{(k_1 - k_2)t} - 1) + D_0 \quad \text{Eqn IV.5}$$

From the above model, equation IV.3 in particular, there are two possible ways to achieve a linear death rate: if  $L$  was constant, or if  $k_2$  is inversely proportional to  $L$ . The viability results show that  $L$  was not constant figure IV.4, which could therefore indicate that death rate varies inversely with the population size of live cells. The models assumptions; live cells die independently of other cells with a constant probability, and replicate with a constant probability, are then incorrect. In order for the death rate to be inversely proportional to the number of live cells, implies the live population influence the death rate possibly through a soluble survival factor. The fact that the dead cell numbers follow a similar trend on all surfaces indicates that the biological mechanism of the soluble factor is robust, and relatively simple to initiate.

The above evidence indicating that the death rate is inversely proportional to the live cell population has not been reported before. However, taking into account the roles of cell signalling, growth factors and culture density does provide support for the observation. Changing the cell density changes the amount of direct cell-cell interaction and also the concentration of soluble factors released by the cells, both of which correlate positively with density. Changing the cell density has been shown to have a parabolic effect on cell viability, reducing the viability at low and high densities, indicating an optimum depending on the culture<sup>[131]</sup>. Further, the electrical activity of neurons has been shown to be reduced at low densities, indicated by a lack of synchronised bursting activity below 250 cells/mm<sup>2</sup><sup>[75]</sup>. Most cells require growth factors for survival and proper function. Neurotrophic factors are growth factors involved in neuron survival<sup>[132,133]</sup>. Conditioned media is media collected

from a living culture, and thus contains neurotrophic factors secreted by the cells. Media can be 'conditioned' with one cell type, and then used to culture a different cell type. In comparison to non-conditioned media, increased survival rates of neurons are recorded using conditioned media<sup>[134,135]</sup>, which are attributed to the presence of neurotrophic factors. One study found increased concentrations of glutamine in conditioned media from cortical neurons, and that cell viability was comparable between non-conditioned media supplemented with glutamine and the conditioned media<sup>[136]</sup>. Neurotrophins are soluble peptides secreted by neuronal cells which are required for the survival of neurons. Several neurotrophins have been identified: nerve-growth factor, brain-derived neurotrophic factor, and neurotrophin-3, -4/5 and -6/7<sup>[128]</sup>. These factors can influence the differentiation of progenitor cells into neurons<sup>[137]</sup>. Differentiation has also been directed by influence of the surface-bound factors<sup>[115]</sup>. These studies imply the role of signalling and cell density, either directly or through soluble factors, on cell viability.

It is important to consider aspects of the cell signalling and apoptosis mechanisms which could dictate the above hypothesis. Apoptosis is the common mechanism of cell death *in vitro*<sup>[125,138]</sup>, as opposed to autophagy and necrosis. Apoptosis is programmed cell death initiated by internal or external cues. Internal triggers would include damaged DNA and malfunctioning proteins. External triggers would include ligand binding of 'death signals' or lack of neurotrophic factors received from neighbouring cells. Apoptosis is characterised morphologically by the condensation and fragmentation of chromatin, rounding of the cell, and blebbing of the plasma membrane. Apoptosis acts to prevent rupturing of the plasma membrane which could release harmful factors into the cellular environment. Anti-apoptotic signalling can occur through neurotrophin binding of Trk receptors of neurons, resulting in survival<sup>[128]</sup>.

It is proposed that the live population of cells influences the death rate through a combination of apoptotic and neurotrophic factors. Although no effort has been made to identify these factors.

To test the hypothesis that the population of live cells secrete a soluble survival factor which influences the death rate requires further investigation. The soluble factor may have a critical concentration at which the cells survival is optimal.

Assuming the soluble factor is excreted by each cell at a constant rate, and that it will dilute in the media. Cell viability studies varying the cell density (within a constant volume of media) would determine if the death rate varied with size of the population. A deviation of the death rate at higher or lower densities would imply a concentration dependant factor, such as a growth factor. If the observed death rate was constant at all cell densities, dilution of a constantly secreted factor is not supported, because at low densities the secreted factor should be below a critical concentration. A supporting experiment whereby the cell culture volume is varied (with a constant cell density) would yield equivalent results: Again, a constant death rate for all volumes would accept the null hypothesis. More sampling points for viability counts over a longer time (than studied here) is required for confirmation of the trend in death rate. Confirmation of a soluble factor could be supported by regular media changes. Adding fresh media would dilute a soluble factor, adding conditioned media (media previously used for neuronal culture) would be a control. Observed differences in death rate may be attributed to soluble factors. If such experiments as above implied a soluble factor was involved, the identification of the molecule would be beneficial.

## **IV-5 Summary**

The various surface modifications of glass and gold were investigated for their ability to support primary cultures of embryonic rat hippocampal neurons. Cell viability was determined from calcein and ethidium homodimer fluorescence.

All of the gold surface modifications supported the neural culture for at least 21 days. The cultures showed a high coverage of live cells which formed processes. The highest live cell numbers were observed on the AUT and AUT-PEG-Peptide surfaces, these were comparable to the PLL-glass control surface at day 21. The peptide and PLL modified gold surfaces showed lower live cell numbers at day 21 in comparison to the PLL control. The cells on the peptide and PLL modified gold became clustered over the period of the culture, resulting in a patchy distribution of clustered cells and clustered processes. The high coefficient of variation for live cells at day 21 on peptide and PLL modified gold also indicates the cell coverage varied across these samples, due to the patchy distribution of clustered cells.

The only glass modification to support the culture was the control PLL surface. The APTMS and APTMS-PEG-Peptide surfaces had initial cell adhesion, but the cultures became clustered and uncountable after the first week. The APDES and APDES-PEG-Peptide surfaces had very few living cells, which were clustered together.

The surfaces that did support viable neural cultures had an apparent linear trend in the dead cell numbers. The trend was similar for all surfaces regardless of the live cell numbers. Through the use of a mathematical model to describe the culture, the linear trend in dead cells could be explained if the death rate varied inversely with the size of the live cell population. That is, a larger population of live cells will have a lower death rate. This relationship implies that the live cell population is secreting a soluble survival factor which influences the death rate of the culture.

# V Protein Adsorption

---

## V-1 Introduction

The response of the primary neuron culture on several surfaces has been discussed in chapter IV. To gain some information that may help explain the cell response results requires consideration of the mechanisms of cell attachment (chapter I), and also the surface chemistry (chapter III). It is important to note that the surface will be exposed to the components of the culture media before the cell settles on the surface. These soluble factors include proteins, amino acids and vitamins which are required to maintain the viability of the cells. They will adsorb to the surface in a way dependant on their chemistry and that of the surface, mainly via ionic and van der Waals forces. Small molecules and ions are likely to be displaced as the cell receptor proteins sense the surface. Larger proteins can adsorb irreversibly to the surface, with extended van der Waals forces and hydrophobic/hydrophilic interactions<sup>[139]</sup>. Protein adsorption from culture media has been shown to mask pre-defined surface chemistry and influence cell attachment: Selective attachment of mature and progenitor endothelial cells to peptide surfaces was observed under serum free conditions, but not with serum (2% FBS)<sup>[140]</sup>; human fibroblast adhesion and spreading on fibronectin was prevented by adsorbing bovine serum albumin onto the fibronectin<sup>[141]</sup>. This chapter investigates the adsorption of proteins, and how this could influence the cell response.

## **V-2 Experimental details**

### **V-2.1 Quartz crystal microbalance**

A quartz crystal microbalance (*Qsense* D300) was used to measure the adsorption of components to a surface. The QCM technique is described in chapter II. Briefly, a test solution was washed over a resonating quartz crystal. The resulting adsorption and desorption at the crystal-solution interface was observed as a decrease or increase in resonance frequency respectively. The resonance frequency was converted to mass using the Sauerbrey equation II.4, and the resulting change in mass determined.

In order to re-use QCM sensors, they were immersed in a piranha etch solution for 5 minutes. The piranha solution consisted of a 3:1 mixture of sulphuric acid and hydrogen peroxide. The solution will oxidise organic material, forming carbon dioxide and water, thus removing contamination from the sensor surface. The QCM sensors were then rinsed with copious amounts of deionised water and then dried under a nitrogen stream. The QCM sensors were further subjected to oxygen plasma etching (0.2 mbar and 60 W for 5 minutes in a RF plasma barrel etcher) before each experiment or surface treatment. This was to keep conditions constant with the surface modifications presented in chapter III.

## V-2.2 The quartz crystal sensor as a model surface

The *Qsense* gold coated crystal sensor required by the QCM was used to model the surface of the gold coated cover slip. To infer the results of adsorption/desorption to the cover slip, it is important that the gold surface topography and area are similar.

Atomic force microscopy (AFM) was used to image and compare the surface topography of the QCM sensor to a gold coated cover slip. Tapping mode AFM was carried out in ambient conditions with a silicon nitride cantilever. The results are shown in Figure V.1. Both images show granular structure, consistent with thermally evaporated gold and a polycrystalline structure<sup>[18]</sup>. The average roughness was 1.29 nm for the sensor, and 0.53 nm for the cover slip. The dimensions of possible adsorbing species such as proteins can be *ca.* 5-15 nm, which are unlikely to be influenced by the difference in roughness. With respect to the AUT SAM, the length of the AUT molecule is similar to the difference in roughness  $\sim 1$  nm. Therefore, AUT SAM maybe more disordered on the rougher QCM sensor. However, surfaces with the peptide ( $\sim 4$  nm long) and the PEG ( $\sim 50$  nm long) modifications would be less influenced by the change in roughness which is overcome by their length. These observations show the sensor surface is a suitable model for the cover slips.

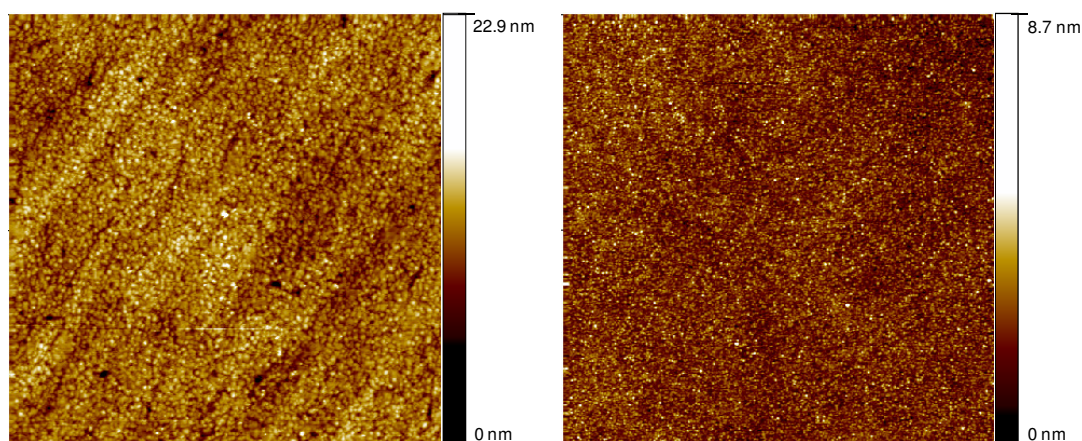


Figure V.1: Comparative height images of a  $5 \times 5 \mu\text{m}^2$  area on a gold coated QCM sensor (left) and gold coated cover slip (right). Colour scale is height nm.

### **V-2.3 Adsorption of Peptide**

QCM sensors were oxygen plasma etched; 0.2 mbar and 60 W for 5 minutes in a RF plasma barrel etcher. These samples were rinsed with deionised water, dried under a nitrogen stream, and then used for the peptide adsorption experiment.

Phosphate buffered saline (PBS) was used as the deposition solution for the peptide (0.1mM) on gold samples in the QCM, analogous to the process used to functionalise cover slips (Chapter III). The QCM resonance frequency was stabilised against PBS buffer before the addition of the peptide solution. Once the frequency was stable the peptide solution was flowed over the crystal. The dynamic adsorption process was allowed time to equilibrate, determined by a stable resonance frequency. Finally, a rinsing step with PBS buffer removes non-specifically adsorbed peptide.

### **V-2.4 Adsorption of Culture Media Components**

The gold QCM sensors were subjected to the same treatments as the gold substrates described in chapter III to form the surfaces of 11-amino-1-undecanethiol SAM (AUT-gold), the peptide SAM (Peptide-gold), and finally the peptide linked to AUT via a PEG chain (AUT-PEG-Peptide gold). The treatment steps are reproduced below.

QCM sensors were oxygen plasma etched; 0.2 mbar and 60 W for 5 minutes in a RF plasma barrel etcher. These samples were used immediately for the subsequent surface modifications.

#### *11-amino-1-undecanethiol (AUT) treatment*

QCM sensors were;

- Rinsed with ethanol.
- Immersed in a solution of 1 mM AUT in ethanol for at least 18 hours.
- Rinsed with ethanol.
- Rinsed with deionised water and dried under nitrogen stream.

*Peptide fragment of laminin, NH<sub>2</sub>-CSRARKQAASIKVAVSADR-COOH (PA22-2) treatment*

QCM sensors were;

- Rinsed with deionised water.
- Immersed in a solution of 0.1 mM peptide in PBS for at least 18 hours.
- Rinsed with deionised water and dried under nitrogen stream.

*AUT-PEG-Peptide modification*

QCM sensors pre-treated with AUT were;

- Immersed in a 1 mM alpha-Maleinimido-omega-carboxysuccinimidyl ester polyethylene glycol solution in dimethylformamide (DMF) for 2 hours.
- Rinsed with DMF, and dried under nitrogen.
- Immersed in a 0.1 mM peptide solution in PBS at 5°C for 3 hours.
- Rinsed with deionised water, and dried under nitrogen.

Adsorption from the media was determined on these surfaces. The cell culture media was *Neurobasal* media with a *B27* supplement, the components are listed in table V.1. PBS was used to stabilise the QCM before addition of the media, and afterwards to remove weakly adsorbed molecules.

<u><i>Neurobasal Media</i></u>	Concentration		<u><i>B27 Supplement</i></u>
	mg/litre	$\mu$ M	
<u><i>Inorganic salts</i></u>			<u><i>Proteins</i></u>
CaCl <sub>2</sub> (anhydrous)	200	1800	Albumin (bovine)
Fe(NO <sub>3</sub> ) <sub>3</sub> .9H <sub>2</sub> O	0.1	0.2	Catalase
KCl	400	5360	Insulin
MgCl <sub>2</sub> (anhydrous)	77.3	812	Superoxide dismutase
NaCl	3000	51300	Transferrin
NaHCO <sub>3</sub>	2200	26000	
NaH <sub>2</sub> PO <sub>4</sub> .H <sub>2</sub> O	125	900	<u><i>Other components</i></u>
<u><i>Other components</i></u>			Biotin
D-glucose	4500	25000	Retinyl acetate
Phenol red	8.1	23	L-carnitine
HEPES	2600	10000	Corticosterone
Sodium pyruvate	25	230	Ethanolamine
<u><i>Amino acids</i></u>			Galactose
L-alanine	2.0	20	Glutathione
L-arginine.HCl	84	400	Thyronine
L-asparagine.H <sub>2</sub> O	0.83	5	Linoleic acid
L-cysteine	1.21	10	Linolenic acid
L-glutamine	73.5	500	Progesterone
L-glutamate	3.7	25	Putrescine
Glycine	30	400	Selenium
L-histidine.HCl.H <sub>2</sub> O	42	200	Tocopherol
L-isoleucine	105	800	Tocopherol acetate
L-leucine	105	800	
L-lysine.HCl	146	5	
L-methionine	30	200	
L-phenylalanine	66	400	
L-proline	7.76	67	
L-serine	42	400	
L-threonine	95	800	
L-tryptophan	16	80	
L-tyrosine	72	400	
L-valine	94	800	
<u><i>Vitamins</i></u>			
D-Ca pantothenate	4	8	
Choline chloride	4	28	
Folic acid	4	8	
i-Inositol	7.2	40	
Niacinamide	4	30	
Pyridoxal.HCl	4	20	
Riboflavin	0.4	1	
Thiamine.HCl	4	10	
Vitamin B12	0.34	0.2	

Table V.1: Components of the *Neurobasal media* and *B27* supplement, adapted from<sup>[69]</sup>

## V-3 Results

### V-3.1 Peptide adsorption to gold

The coverage of the peptide PA22-2 on gold has been determined to be uniform with ToF-SIMS, chapter III. To estimate the peptide density requires that the mass adsorbed to the surface is known. This can be measured with the QCM as the surface is assembled in the instrument. The frequency response and Sauerbrey mass gain due to the peptide adsorption are presented in appendix 20.

The resulting mass change upon exposure to a 0.1 mM concentration of PA22-2 in PBS was  $379 \pm 33$  ng/cm<sup>2</sup>. Given the peptides molecular mass (2017.34 amu), the result indicates a peptide ‘footprint’ of 0.88 nm<sup>2</sup>. By assuming the model for thiol binding on reconstructed gold (111), the observed peptide coverage is illustrated, figure V.2A. The dimensions of the peptide are  $\sim 0.5 \times 0.5 \times 7$  nm. If the peptide was bound end on to the surface so that all thiol binding sites were occupied, the ‘footprint’ would be 0.16 nm<sup>2</sup>. A peptide bound parallel to the surface as such to block potential binding sites would have a larger ‘footprint’ of 3.5 nm<sup>2</sup> (the surface area of the peptide). The peptide, consisting of a straight chain of 19 amino acids, may bend and fold in different orientations. Therefore, it is reasonable to assume that the peptide would not occupy every possible binding site due to steric effects. The observed mass change indicates the peptide is protruding from the surface in agreement with a theoretical model<sup>[99]</sup> presented in figure V.2B.

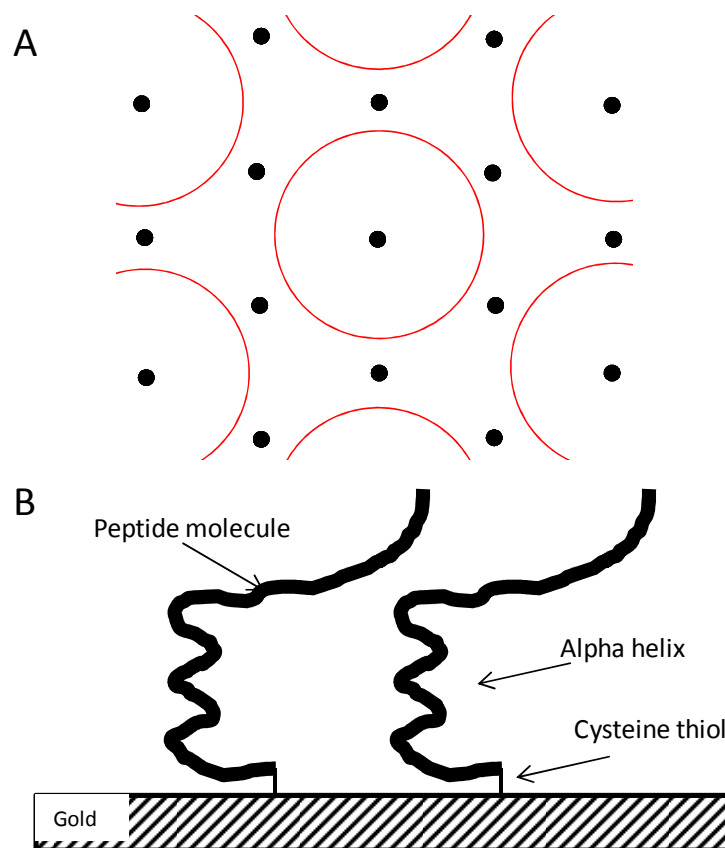


Figure V.2: (A) Proposed footprint area (red circles) of peptide PA22-2 on gold(111), black circles are possible thiol binding sites 0.497 nm apart. (B) Simulated theoretical conformation of PA22-2 on gold, when bound by the terminal cysteine, redrawn from<sup>[99]</sup>. The peptide region near the N terminus may form a helical conformation.

Despite many attempts, the instrument was found not to stabilise with ethanol as a test solution. Because ethanol was needed for the AUT thiol adsorption it was not possible to reliably measure the binding of AUT to gold with the QCM.

### V-3.2 Protein adsorption from culture media

The mass adsorption of components from the culture media onto various surfaces was determined by QCM. Gold coated QCM sensors were treated to produce AUT-gold, Peptide-gold, and AUT-PEG-Peptide-gold surfaces using the same surface preparation method described in chapter III. The frequency response and Sauerbrey mass gain due to the adsorption from *Neurobasal* and the *B27* supplement are presented in appendices 21-24.

The average Sauerbrey mass change resulting from adsorption are summarised in table V.2. The addition of the *B27* supplement results in more mass adsorption in comparison to *Neurobasal* alone, as observed on both the AUT-gold and Peptide-gold surfaces. The AUT-gold surface promoted the greatest adsorption from the supplement. The AUT-PEG-Peptide-gold surface has the least mass adsorption from the supplement.

Surface	Mass adsorbed (ng/cm <sup>2</sup> )	
	<i>Neurobasal</i>	<i>Neurobasal + B27</i>
AUT-gold	2 ±3	391 ±88
Peptide-gold	50 ±43	310 ±21
AUT-PEG-Peptide-gold	No data	70 ±24

Table V.2: Mass gain at 15 MHz, following exposure to *Neurobasal media* with and without the *B27* supplement.

On the AUT-gold, adsorption from *Neurobasal media* alone was marginal, ~ 2 ng/cm<sup>2</sup>, figure V.3. Once the supplement is added there is a more significant adsorption which remains after PBS wash, figure V.3. The *B27* supplement contains proteins and enzymes, whereas the *Neurobasal* component does not, table V.1. Consequently, the mass increase could be assigned to the adsorption of the proteins present in the supplement. The amount is estimated using the Sauerbrey equation to be ~ 391 ng/cm<sup>2</sup>. The culture media endothelial basal medium containing 2 % FBS resulted in ~ 290 ng/cm<sup>2</sup> mass adsorption on an AUT SAM<sup>[142]</sup>, using SPR. The AUT SAM had a WCA of ~ 51°, which was higher than the ~ 41° observed on the AUT SAM in this work. Although the culture media was different, significant adsorption from the media is observed on the AUT SAM. SPR was also used to

study the adsorption from *Neurobasal* + *B27* media onto peptide PA22-2 surfaces<sup>[143]</sup>. Two maleimide terminated disulfide molecules were used to form maleimide terminated SAMs on gold, one of the molecules contained a PEG chain 6 units long. The peptide was then coupled to the maleimide surface. Although the mass gain due to media adsorption was not predicted, a relative comparison was made between the PEG and non-PEG peptide coupled surfaces. The result indicated that both surfaces had similar responses to adsorption from the media. This result is in contrast to the results for the longer maleimide terminated PEG chain (over 100 PEG units, 5000 amu) used in this study for peptide coupling. Longer PEG chains have been shown to have greater resistance to protein adsorption<sup>[144]</sup>, which may explain the contrasting result of the shorter PEG chains protein adsorption.

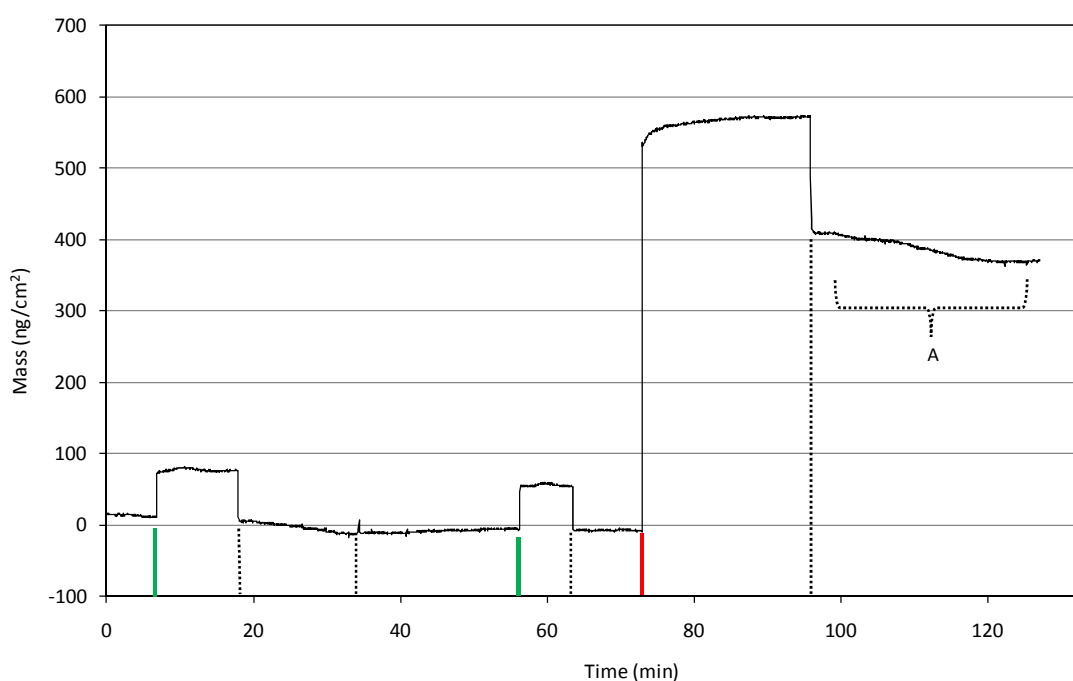


Figure V.3: QCM trace of mass adsorption from culture media to the AUT-gold surface at 15 MHz. Green line is *Neurobasal* addition. Red line is *Neurobasal+B27* addition. Dotted lines are PBS additions, (A) PBS additions ~ 2 minute intervals.

Several of the proteins in the supplement are negatively charged in the media. This can be inferred from the reported isoelectric point (pI) of each protein: Bovine serum albumin pI 4.9<sup>[145]</sup>; insulin pI 5.3<sup>[145]</sup>; superoxide dismutase pI 4.75<sup>[146]</sup>; catalase pI 5.8<sup>[147]</sup>; transferrin pI 5.85<sup>[148]</sup>. The isoelectric point is the pH ( $-\log[H^+]$ ) at which the protein has an overall neutral charge. The culture media is buffered at a pH of 7.4, so fewer hydrogen ions are present to balance the remaining negative charge of the proteins. Therefore, negatively charged proteins may adsorb to the surface via electrostatic interactions with any positively charged regions of the surface. This electrostatic adsorption could be an important factor in the high protein adsorption observed on the amine terminated AUT-gold surface. Although the electrostatic charge of the surfaces presented was not investigated, it is known that amine groups can be positively charged; PLL adsorbed to polystyrene results in a positively charged surface<sup>[149]</sup>.

In solution, the amine will exist in equilibrium between the un-protonated and protonated form. The equilibrium is described by the acid dissociation constant,  $K_a$ . The pH of a solution will affect the position of the equilibrium, described by pKa (the negative logarithm of  $K_a$ ). When the pH is below the pKa value the equilibrium shifts and the amine becomes protonated. In solutions with a pH above their pKa value the amines will remain un-protonated. Primary amine groups have high pKa values, making them bases (proton acceptors). For example, the pKa values for butylamine and undecylamine are approximately 10.6 and 10.7 respectively<sup>[150]</sup>. These values provide an estimate pKa value for amine groups of the aminopropyl silanes and aminoundecanethiol. However, the consideration that the amine groups are immobilised to the surface must be taken into account, as discussed below.

The buffered pH 7.4 of PBS used in this study is below the pKa value for the amine groups, indicating that the amine groups would be protonated. However, once a molecule has been immobilised on a surface the pKa value becomes less informative. The pKa for bases decreases<sup>[151]</sup>, requiring a more acidic environment to protonate the surface bound amines. The pKa for acids increases<sup>[152]</sup>, a more basic environment is required for dissociation. These studies determine the pH value at which half of the surface groups are ionised, a  $pK_{1/2}$  value. The trend is due to several factors. Firstly, the close proximity of charged groups of the same polarity is unfavourable due to electrostatic repulsion, hence more basic pH is required to drive

dissociation of acids, and a more acidic pH for protonation of amines<sup>[153]</sup>. Secondly, the acid and amine groups can form hydrogen bonds between neighbouring groups. Hydrogen bonding will favour close interaction of the terminal groups, opposing the charged alternative. Further, the ionic strength of the solution will influence the surface charge and  $pK_{1/2}$ . Ions can diffuse to the surface and compete with the electrostatic interactions, reducing electrostatic repulsion between terminal groups. Therefore, at high ionic strength, the difference between  $pK_a$  and  $pK_{1/2}$  is reduced<sup>[154]</sup>. Considering the above factors, the AUT surface at pH 7.4 will be significantly protonated, and have a net positive charge. This is further supported by the observation that negatively charged phosphate ions interact with the amine surface in neutral pH buffers<sup>[153]</sup>.

In contrast to the AUT surface, components from the *Neurobasal media* alone adsorbed onto the peptide surface,  $\sim 50 \text{ ng/cm}^2$ . This difference could be due to different structural characteristics of the AUT and peptide SAMs. The van der Waals forces between the alkyl chains of the AUT SAM may form stronger intermolecular forces than those within the peptide SAM. As a result, components of the media may penetrate and reside within the peptide SAM but not within the AUT SAM. The hydrophobic region of alkyl chains within the AUT SAM may also prevent polar components of the media penetrating the SAM. The interactions between the *Neurobasal* components and AUT SAM may then be overcome during the PBS washing step. In the case of the peptide SAM, the components which may reside within the layer are not completely removed during the PBS wash.

Similarly with the AUT SAM, the peptide SAM adsorbed components from the *B27* supplement. The different amino acids of the peptide will possess different electrostatic charges<sup>[1]</sup>; at pH 7.4 there are 5 positive, 1 negative, and 12 neutral amino acids present in the PA22-2 peptide sequence. These charges may contribute to the protein adsorption through electrostatic interactions with the peptide surface.

### **V-3.3 The effect of PEG on protein adsorption**

The AUT-PEG-Peptide surface has a reduced protein adsorption from the media, when compared with the peptide bound directly to gold. However, protein adsorption has not been completely eliminated. In a study where the peptide sequence RGD was bound to a protein resistant PEG surface, it was found that increasing the proportion of bound RGD peptide resulted in increased protein adsorption from 100% human serum<sup>[155]</sup>. The protein adsorption may occur through interactions with the terminal peptide. It is also possible that the smaller molecules present in the media could penetrate into the PEG layer, contributing to the mass gain. In comparison with the other modifications, the presence of the PEG chain between the peptide and AUT SAM has reduced protein adsorption from the *B27* supplement.

PEG surface modifications have been used to prevent protein adsorption, and as a result prevent cell adhesion<sup>[156,157]</sup>. The length and surface density of the PEG chains are important factors for the resulting protein resistance<sup>[139,158]</sup>. Longer PEG chains are more effective than shorter chains for preventing protein adsorption<sup>[144]</sup>. In solution, the PEG chains become hydrated forming random coils<sup>[159]</sup>. Water is bound tightly within the PEG layer, which may prevent protein interactions which involve the displacement of water. The hydrated coils are flexible and resist compression making adhesions unfavourable in terms of entropy<sup>[139]</sup>. The protein resistance of PEG surfaces may not last indefinitely under a constant protein and/or cellular environment<sup>[160,161]</sup>.

## **V-4 Summary**

The adsorption of components from the neural culture media *Neurobasal* and the *B27* supplement has been monitored using a QCM. Gold QCM sensors were pre-modified to form the AUT, peptide or AUT-PEG-Peptide surfaces, onto which protein adsorption was measured.

The AUT and peptide surfaces adsorbed the greatest mass from the *B27* supplemented *Neurobasal media*, in comparison to the *Neurobasal media* alone. Both *Neurobasal* and *B27* have a complex composition of small molecules such as vitamins, amino acids, and salts. However, only the *B27* contains proteins. The

higher mass adsorption in the presence of *B27* is attributed to the protein components.

The AUT-PEG-Peptide surface adsorbed fewer components of the *B27* supplemented *Neurobasal media* in comparison to the AUT and peptide SAMs. The reduced adsorption is attributed to PEG chain between the terminal peptide and the AUT SAM.

# VI Discussion

---

## VI-1 Introduction

The main goal of the work contained within this thesis was to modify the surface chemistry of glass and gold to support long term cultures of primary neurons. The aim of this section is to explain the results of the neuron culture (Ch. IV) in light of the surface chemical analysis (Ch. III) and protein adsorption study (Ch. V).

## VI-2 Protein adsorption and cell culture

Upon initial plating, smaller molecules will diffuse and interact with the surface quicker than the cells, which settle under gravity. This could be inferred from the QCM results, which showed an instantaneous mass adsorption at the point of introducing the media to the surface. The consideration that proteins in the cell culture media will adsorb to the surface before the cell is important. This is because the adsorbed proteins may mask the initial surface chemistry. When the adsorbed proteins display a cell adhesion domain, and are not denatured, the cells will adhere to the protein regardless of the original underlying surface chemistry. This is shown for proteins such as fibronectin and laminin which promotes cell adhesion on non-adherent substrates. In contrast, proteins that do not display cell adhesion domains will deter cell adhesion, albumin is one example. Once cells have attached to the surface, they may excrete proteins to produce an extracellular matrix over the original surface. This matrix provides extra adhesion sites for the cells.

The fact that not all the surfaces presented showed good cell adhesion, implies that the adsorbed media components alone are not enough to support healthy adherent neural cultures, and that the underlying surface chemistry is an important factor. The adsorbed components do not inhibit cell adhesion, shown by both the AUT-gold and peptide-gold surfaces, upon which neurons survived despite the adsorbed layer. It could be argued that the adsorbed media components can influence cell adhesion, but require the underlying surface chemistry to direct their adsorbed

orientation/conformation to do so. Although no evidence is presented here for the role of protein conformation on cell adhesion, evidence indicates a dynamic role between surface wettability and protein conformation<sup>[89,162,163]</sup>. Proteins can have complex structures, determined by interactions between amino acids, and with water molecules<sup>[164]</sup>. When a protein contacts a surface this structure may change as a result of more thermodynamically favourable interactions with the surface<sup>[39]</sup>. Proteins adsorb more strongly to hydrophobic surfaces, in comparison with hydrophilic surfaces<sup>[139]</sup>. This is a thermodynamically favourable adsorption, displacing water at the hydrophobic surfaces' interface; hydrophobic dehydration<sup>[39]</sup>. This adsorption may be too strong for other cell adhesion proteins to displace in order in order for cell adhesion, as shown for albumin<sup>[89,142]</sup>. The surfaces presented are hydrophilic, with WCA ranging from 31° to 67°, and so cell adhesion may occur through displacement of the adsorbed protein layer by cell adhesion proteins secreted by the cells, or through cell adhesion motifs which may be presented by the adsorbed protein layer.

It is difficult to suggest there is a correlation between 'WCA and protein adsorption', figure VI.1, due to the few data points presented here. It is important to note that the uppermost chemistry of the surface will determine the surface wettability. Different chemistries may show similar wettability but differ in protein adsorption due to other interactions such as electrostatic forces. For example, a PEG surface can have certain properties which resist protein adsorption, discussed in chapter V. A protein resistant PEG surface has a WCA of ~ 20°<sup>[165,166]</sup>. The peptide modified PEG surface presented here has a WCA of ~ 61°, and retains some resistance to protein adsorption. Thus, a correlation between WCA and protein adsorption may not be expected across the different surface chemistries investigated here.

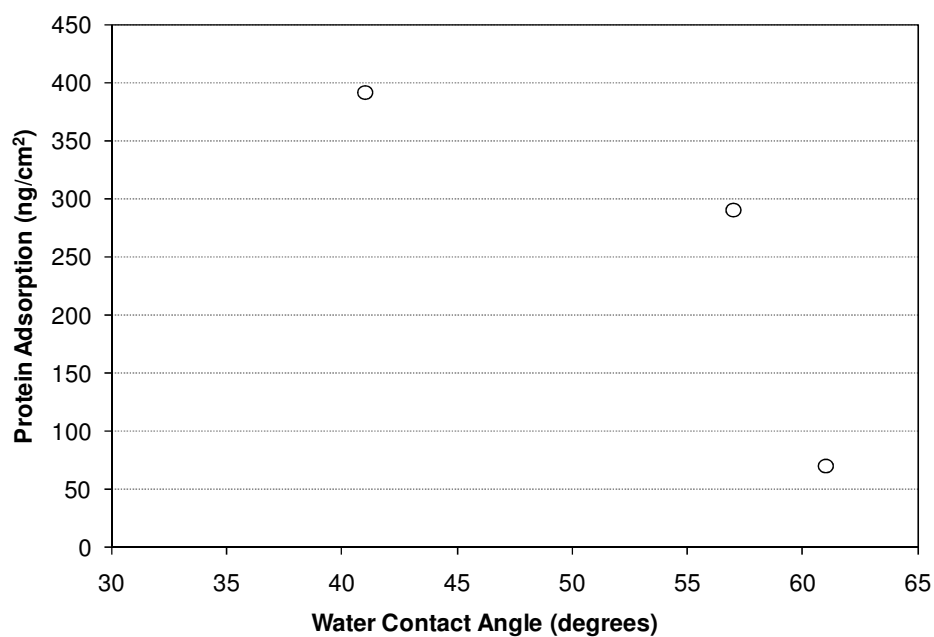


Figure V1.1: Protein adsorption vs water contact angle.

The results presented here show no correlation between ‘WCA and live cell numbers’ figure VI.2. Both successful and unsuccessful surfaces (in terms of neuron survival) displayed a range of wettability. Thus, when using the *Neurobasal* media and *B27* supplement, the quantity, identity and conformation of adsorbed media components due to surface wettability appears to have little effect on neuron adhesion to the surfaces in this study.

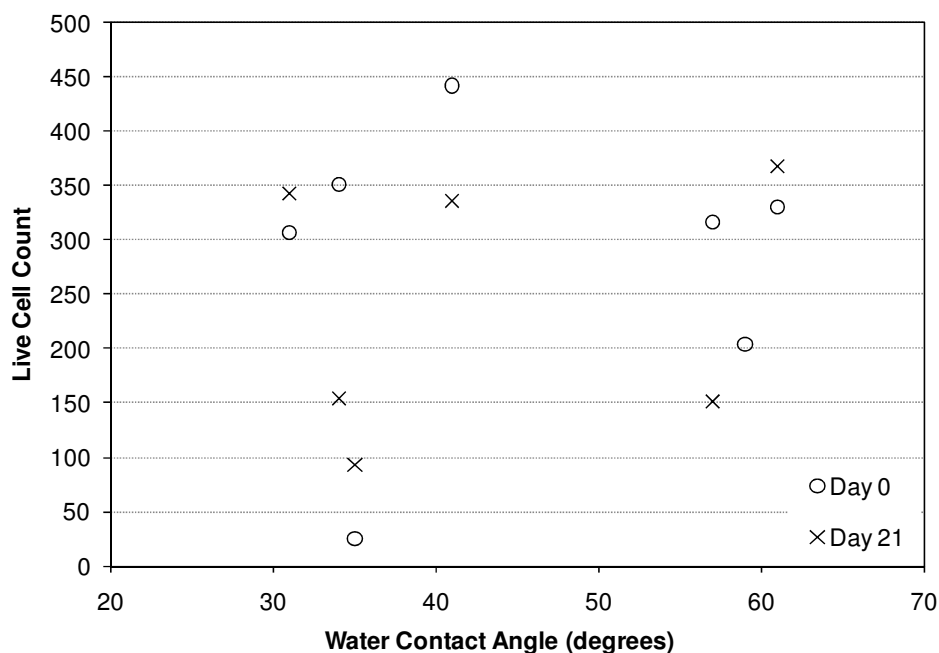


Figure VI.2: The number of live cells at day 0 and 21 vs water contact angle.

The amino terminated AUT-gold surface and Peptide-gold surface showed the highest protein adsorption. It was discussed in chapter V that protein adsorption could be due to electrostatic interactions between negatively charged proteins and the positively charged surface; amine groups of AUT, and certain amino acid residues of the peptide. This electrostatic driven protein adsorption has been observed on a PLL surface<sup>[149]</sup>. Therefore, protein adsorption maybe driven through electrostatic interactions between the protein and surface, for the surfaces presented. The mechanism of neuronal cell attachment to these surfaces may overcome the electrostatic force of protein adsorption, and displace the protein layer. A SAM of AUT on gold promoted cell adhesion (human umbilical vein endothelial cells and human cervical carcinoma cells) in the presence of a pre-adsorbed layer of albumin<sup>[142]</sup>. Indicating albumin is displaced by other cell adhesion proteins during the adhesion process, or that the conformation of the albumin presents some initial adhesion sites for the cell.

In comparison to the directly attached peptide-gold surface, the inclusion of the PEG linker promoted higher average live cell numbers, and reduced protein adsorption from the supplement. The protein resistant nature of PEG was discussed in chapter V. It is assumed that the cells are able to specifically bind the peptide

through integrin receptors. The reduced protein layer on PEG may allow the cells to interact with more peptide molecules, resulting in higher integrin binding, formation of adhesion complexes, and initiating internal cell signalling pathways required for survival. When directly bound to gold via the cysteine residue, the peptides will be constricted spatially and may exhibit steric hindrance during integrin binding. In contrast, due to the length of the PEG chain and its non-rigid nature, the accessibility of the peptide to integrin recognition maybe more favourable on the PEG coupled surface. The PEG layer introduces a softer mechanical stiffness in comparison to the directly adsorbed peptide, due to the hydrated PEG chains releasing water on compression<sup>[167]</sup>. A softer substrate may promote more viable neuronal cultures than harder substrates. Mechanical stiffness has not been investigated here, however, it is known that substrate stiffness can direct cell differentiation<sup>[168]</sup>; neuronal differentiation was favoured on a softer substrate<sup>[169]</sup>. Neurons, *in vivo*, are supported by other neurons and glial cells, which provide a mechanically soft surrounding. However, the implication of this affect on the cell viability results presented is unclear. It is more likely that the protein resistant properties of PEG enable the attached peptide to be more accessible for cell adhesion, improving viability over the peptide only surface.

### **VI-3 Surface chemistry and cell adhesion**

This section aims to explore how the surface chemistry influenced the cell viability.

The primary neuronal cell cultures survived on the AUT-gold, Peptide-gold, AUT-PEG-Peptide-gold, and on PLL-gold as well as the PLL-glass control surfaces. The evidence from surface characterisation with ToF-SIMS and XPS suggests these surfaces present the intended chemical modifications, chapter III.

Although neuronal cells adhered to APTMS-glass and APTMS-PEG-Peptide-glass surfaces, the cultures became clustered within the first week, and unsuitable for the comparison of cell viability. The APTMS treatment appeared to present surface amine groups as intended, chapter III. However, the PEG linker bound with a heterogeneous distribution to the APTMS. As a result, the subsequent peptide binding step followed the underlying distribution of the PEG linker, forming a

heterogeneous distribution of peptide at the surface. The lack of cell viability on the APTMS-PEG-Peptide surface could be attributed to the incomplete coverage of peptide at the surface. The clustering observed in these cultures indicates the neurons preferentially adhere to each other, due to lack of surface adhesion sites.

The neuronal cell cultures on APDES and APDES-PEG-Peptide surfaces were not viable. Evidence from the surface characterisation suggests the initial APDES silanisation did not present sufficient amine groups for the PEG linker to bind homogeneously. Due to the low amount of surface bound PEG linker, the addition of peptide resulted in an adsorbed layer rather than the intended PEG-Peptide coupled layer. Previous studies have shown cell attachment to peptide surfaces produced by adsorption from solution<sup>[114,170]</sup>. However, longer adsorption times and a drying/evaporation step were used, which is not required for the maleimide-peptide coupling used here. Evaporating a peptide solution will leave a peptide residue on the surface, which is likely to have a higher concentration of peptide in comparison to an adsorbed film from solution. Therefore, the amount of adsorbed peptide on the APDES-PEG-Peptide surface was insufficient to promote neuronal cell adhesion.

The Pearson correlation coefficient has been calculated between the elemental composition determined by XPS and the average live cell number, table VI.1, using data from the viable cultures only (PLL-glass, PLL-gold, AUT-gold, Peptide-gold and AUT-PEG-Peptide-gold). At day 0, carbon and oxygen show the greatest correlation with live cells. The positive correlation of carbon on cell growth is partly an artefact due to the alkyl chain of AUT. At day 21 the live cell numbers correlate negatively with the initial nitrogen content. Surfaces presenting methyl groups have reduced cell adhesion<sup>[142]</sup>, suggesting that the cell adhesion concerns the terminal amino groups rather than the underlying alkyl chain of AUT. Due to the analysis depth of XPS (~ 10 nm), the atomic composition may include contributions from underlying surface regions which do not influence cell adhesion. Therefore, the correlation between surface composition by XPS and cell response may not be an

Culture	Pearson Correlation Coefficient Element vs Av. Live Cell Number						
	Day	C	O	N	C/N	C/O	O/N
<b>0</b>		0.61	-0.56	0.06	0.25	0.96	-0.45
<b>21</b>		0.16	0.26	-0.69	0.96	0.36	0.37

Table VI.1: Correlation between XPS atomic percentages and average live cell numbers. Data from PLL, AUT and peptide surface modifications. accurate indicator of which elements influence cell viability.

The Pearson correlation coefficient has also been calculated between the ToF-SIMS ion fragment intensities and live cell counts, table VI.2. It is important to note that ToF-SIMS is not quantitative, the ion intensities may not be indicative of a particular fragments actual concentration at the surface. However, the greater sensitivity and smaller analysis depth (~ 2 nm), in comparison to XPS, may provide a more accurate indication of what chemical functionalities the cells encounter. At day 0, the ion fragments  $\text{CN}^-$ ,  $\text{CNO}^-$  and  $\text{C}_3\text{N}^-$  show a negative correlation, indicating nitrogen has a negative influence on cell viability. This negative correlation is also apparent at day 21. The significance of any correlations at day 21 is debatable, by this time cells may have excreted ECM factors masking the original surface. Previous studies have shown a positive correlation between cell adhesion and surface nitrogen content<sup>[35,142]</sup>. However, this trend has not been observed for the cell viability on the surfaces presented within. This is not a surprising result considering the variation of surface modifications used. The surfaces presenting only amino groups are then considered separately in section VI-3.1, because the surface functional groups are essentially the same a clearer correlation maybe observed.

Ion	Pearson Correlation Coefficient Ion vs Av. Live Cell Number	
	Day 0	Day 21
$\text{CH}_3^+$	-0.41	<b>0.73</b>
$\text{NH}_3^+$	0.23	-0.51
$\text{C}_2\text{H}_2^+$	-0.40	0.34
$\text{C}_3\text{H}_3^+$	0.15	0.48
$\text{C}_2\text{H}_5\text{O}^+$	-0.19	0.53
$\text{C}_2\text{H}_6\text{NO}^+$	-0.39	-0.53
$\text{C}_5\text{H}_{10}\text{N}^+$	-0.20	<b>-0.77</b>
$\text{O}^-$	-0.47	0.35
$\text{OH}^-$	-0.43	0.39
$\text{CN}^-$	<b>-0.60</b>	<b>-0.84</b>
$\text{CNO}^-$	<b>-0.64</b>	<b>-0.77</b>
$\text{C}_3\text{N}^-$	<b>-0.69</b>	-0.12
$\text{C}_2\text{H}_5\text{O}_2^-$	-0.19	0.49

Table VI.2: Correlation between ToF-SIMS normalised ion intensity and average live cell numbers. Data from PLL, AUT and peptide surface modifications.

### VI-3.1 Amino terminated surfaces

The PLL, AUT, APDES, and APTMS surfaces present terminal amine groups. Comparing the nitrogen content of these surfaces may correlate with the cell viability. The XPS analysis was not sensitive to the adsorbed layer of PLL on glass and gold. Ordering the remaining surfaces by nitrogen content from XPS analysis gives; APTMS (8.7%) > AUT (5.1%) > APDES (1.3%). This order is also reproduced by the normalised intensity of the  $\text{NH}_3^+$  and  $\text{CN}^-$  ion fragments, attributed to the surface amine groups, from ToF-SIMS analysis. The AUT surface promoted adhesion of neurons, and the long term culture of neurons. Whereas the APTMS and APDES surfaces, with the highest and lowest nitrogen content respectively, were not sufficient to support viable cultures. This result indicates that the amine content of the surface may influence the cell response. Furthermore, since the nitrogen content (% by XPS) of the AUT SAM is between the APTMS and APDES, there may be an optimal concentration of surface amino groups required for viable neural cultures. The number of positively charged amine groups may also influence the adhesion and growth of primary neural cultures<sup>[82]</sup>. The results of qualitative observations inferred that there is positive correlation between the amount of positively charged amines and the viability of the adherent culture. In a separate study, a mixed SAM of AUT and 1-dodecanthiol (DDT) on gold was used to investigate cell adhesion<sup>[142]</sup>. It was found that cell adhesion increased as the surface ratio of amine (AUT) to methyl (DDT) increased. Providing further evidence that amine groups have a positive influence of on cell adhesion. Given the above, although the APTMS surface has higher amine content, the AUT surface may present more accessible positively charged amine groups, resulting in better viability of neural cultures. Cell adhesion onto positively charged surfaces is thought to initially occur through electrostatic interactions with negatively charged molecules on the surface of the cell, such as glycoproteins.

## **VI-4 Surface treatments for neuronal culture**

Several of surfaces presented are suitable for culturing primary neurons. In particular cell viability on the AUT and AUT-PEG-Peptide modifications was better or comparable to cultures on PLL-glass over the 3 week long culture. Due to the gold-thiol bond, the surfaces modifications are stable over long periods of time. The PLL layer can be degraded by enzymes, which can result in reduced cell adhesion over several weeks in culture. As with PLL, peptides may also be degraded by enzymes<sup>[171]</sup>, reducing their long term application. In contrast to biological molecules which can be degraded by enzymes, the AUT SAM will be resistant to enzymatic degradation, providing a cell adhesion layer for long term culture applications.

## **VI-5 Neuronal culture death rate**

A high linear regression was observed for the dead cell counts, which was independent of the surface treatment and the number of live cells. This result implies that the death rate is inversely proportional to the number of live cells, and that soluble factors released by the cells could explain the observation, as discussed in chapter IV. Other studies have found that low density cultures require conditioned media or feeder cells of glia<sup>[172]</sup>, which provide the neurons with soluble growth factors in order to survive. A lower density of electrically active neurons can be achieved using conditioned media than with non conditioned media<sup>[75]</sup>.

## **VI-6 Current applications**

Investigating the electrical activity of neurons is one of the most important reasons for developing cell cultures. The gold surface modifications presented within offer suitable platforms upon which electrical activity can be monitored.

Multi-electrode arrays (MEAs) are used for recording action potentials, requiring that neurons are adhered in close proximity to the electrodes. MEAs can be made with gold electrodes. These electrodes can then be modified with the AUT or peptide modifications presented to promote cell adhesion onto the electrodes for recording neural activity.

The gold surface treatments are also compatible with surface plasmon resonance, an optical technique which is sensitive to changes in the refractive index of the medium within approximately ~ 100 nm of the gold surface. SPR has been used to detect neuron action potentials<sup>[25,53]</sup>. SPR imaging (SPRi) is made possible by the contrast in reflected light resulting from changes of refractive index on the surface. SPRi can be used to image cells in culture<sup>[173]</sup>. Low density neural networks coupled with SPR, could be used to develop a system where every action potential is recorded from all neurons, throughout the duration of the culture. This ability is not readily provided by existing approaches with MEAs, microelectrodes, or fluorescent dyes. As such, this system would make a valuable contribution to the fields of electrophysiology and neuroscience in general.

## **VI-7 Conclusions**

Gold surfaces have been successfully modified to support the neural cultures. The viability of neurons cultured on AUT and AUT-PEG-Peptide surface was higher than the PLL control over the first two weeks in culture, and comparable to PLL at the end of the third week. Both of these gold surface treatments are able to support viable cultures of neurons at low density. These surfaces will provide alternative treatments to promote neural adhesion onto gold electrodes or SPR sensors with the aim of recording electrical activity.

Generally, the gold surface treatments were more homogeneous than the glass surface treatments which were patchy for the PEG-Peptide equivalent treatments on APDES and APTMS. The process of surface silanisation can be difficult, involving the control of several variables for optimum performance. In contrast, alkanethiol SAMs on gold are generally more straightforward provided that the gold surface is clean. The poor cell viability observed on the glass surface modifications is attributed in part to their non uniform nature in comparison to the gold treatments.

Despite showing high adsorption from the culture media components the AUT and Peptide SAMs promoted neural cell adhesion, and the growth of viable cultures. It is understood that the adsorbed protein may provide initial adhesion sites for the cells. Further production of cell adhesion proteins by the cells may displace proteins

or mask non adhesive regions of the surface. The PEG-Peptide surface had the lowest adsorption of media components, which was attributed to the inclusion of the PEG chain. Cell viability was also maintained on the PEG-Peptide surface while the Peptide SAM started to decline by week 3, forming clustered neurons. This could be due to protein adsorption from the media masking the peptide layer and preventing cell adhesion. The PEG-Peptide surface, with reduced protein adsorption, may allow neural cells to adhere more specifically to the peptide. Thus, on PEG-Peptide surfaces there is less clustering after 21 days culture.

## **VI-8 Future Work**

Several of the surfaces discussed demonstrate the potential to support viable low-density cultures of primary hippocampal neurons. However, the electrical activity of the cultures has not been addressed. Cultures of adult neurons have been shown to require further addition of glutamate to the media to induce electrical activity <sup>[174]</sup>. Also, cultures of neurons at low density (as performed in this study) may have reduced electrical activity in comparison to more dense cultures <sup>[75]</sup>. Therefore, although the neurons are living, they may not be generating action potentials. Further, any electrical activity may not be characteristic of *in vivo* neurons. With respect to a ‘proof of concept’ or ‘device optimisation’ such as developing a surface plasmon based sensor to detect action potentials, initially, the electrical activity of the neuron cultures does not need to be optimum, but present at least. Several methods are commonly used to monitor the electrical activity of neurons in culture, these are; microelectrode recordings (e.g. patch clamping), MEAs, and fluorescent imaging (calcium imaging and voltage sensitive dyes). Microelectrode recordings are the most informative, providing direct measures of the cell resting potentials and action potentials over time. But patch clamping has inherent difficulties, such as requiring accurate manipulation of a delicate micropipette. This makes recordings from many cells impractical. MEAs provide a platform to monitor electrical activity at fixed points of a culture grown on top of the array. However, the surface chemistry of commercial MEAs is not compatible with the protocols used in this work. Finally, the calcium influx in neurons as a response to an action potential can be imaged with fluorescent molecules<sup>[175]</sup>. Hence, future work using calcium

imaging and microelectrode recordings would determine if the cultures show a characteristic electrophysiology and may also indicate how surface treatments influence the electrical activity of neurons.

Primary cell cultures have been shown to contain several cell types, including neurons and astrocytes. It would be useful to know the proportion of each cell type in the culture, specifically the numbers of neurons present in the culture over time. This would allow further refinement of the model proposed in chapter IV. Identification of cell types could be achieved using immunohistochemistry (IHC). IHC is a staining technique which can label proteins via specific antibody-antigen binding. The cell culture can be labelled with fluorescently tagged antibodies which bind cell-type specific markers, such as microtubule-associated protein 2, which is neuron specific. Using several different fluorescent markers in parallel would give a visual and quantitative comparison of the cell-types present in the culture.

The cultures presented are grown on uniformly treated surfaces. As a result the networks formed by the cultures grow over the entire surface. It would be interesting to constrain the neurons to pre-defined spatial patterns and study if this changes the electrical activity and viability of the neurons. One purpose of this study could be to mimic different structures of the *in vivo* brain in a 2D culture. Techniques such as micro-contact printing and photolithography could be used to pattern the surface chemistries presented in this thesis, and therefore direct the adhesion and formation of neuronal networks.

# References

---

1. Campbell, N.A. and J.B. Reece, *Biology*. 6 ed. 2002, San Francisco: Benjamin Cummings.
2. Ulman, A., *An Introduction to Ultrathin Organic Films from Langmuir-Blodgett to Self-Assembly*. 1991, London: Academic Press. 442.
3. Seshan, K., *Handbook of Thin Film Deposition - Techniques, Processes, and Technologies*. 2012, William Andrew.
4. Zhang, F., et al., *Chemical Vapor Deposition of Three Aminosilanes on Silicon Dioxide: Surface Characterization, Stability, Effects of Silane Concentration, and Cyanine Dye Adsorption*. *Langmuir*, 2010. **26**(18): p. 14648-14654.
5. Ulman, A., *Formation and structure of self-assembled monolayers*. *Chemical Reviews*, 1996. **96**(4): p. 1533-1554.
6. Brook, M.A., *Silicon in organic, organometallic, and polymer chemistry*. 2000, New York: Wiley Interscience.
7. Nagao, M., *Physisorption of water on zinc oxide surface*. *The Journal of Physical Chemistry*, 1971. **75**(25): p. 3822-3828.
8. Hair, M.L., ed. *The chemistry of biosurfaces*. Vol. 1. 1972, M Dekker: New York.
9. Chapman, B., *Glow discharge processes: sputtering and plasma etching*. 1980: Wiley interscience.
10. Agrawal, J.P. and R. Hodgson, *Organic Chemistry of Explosives*. 2007: John Wiley & Sons.
11. Vrancken, K.C., et al., *The physisorption and condensation of aminosilanes on silica gel*, in *Chemically modified surfaces*, J.J. Pesek and I.E. Leigh, Editors. 1994, Royal society of chemistry: Cambridge.
12. Blitz, J.P., R.S.S. Murthy, and D.E. Leyden, *The role of amine structure on catalytic activity for silylation reaction with cab-o-sil*. *Journal of Colloid and Interface Science*, 1988. **126**(2): p. 387-392.
13. Nuzzo, R.G. and D.L. Allara, *Adsorption Of Bifunctional Organic Disulfides On Gold Surfaces*. *Journal of the American Chemical Society*, 1983. **105**(13): p. 4481-4483.
14. Bain, C.D., et al., *Formation of monolayer films by the spontaneous assembly of organic thiols from solution onto gold*. *Journal of the American Chemical Society*, 1989. **111**(1): p. 321-335.
15. Kankate, L., A. Turchanin, and A. Golzhauser, *On the Release of Hydrogen from the S-H groups in the Formation of Self-Assembled Monolayers of Thiols*. *Langmuir*, 2009. **25**(18): p. 10435-10438.
16. Zharnikov, M., et al., *The effect of sulfur-metal bonding on the structure of self-assembled monolayers*. *Physical Chemistry Chemical Physics*, 2000. **2**(15): p. 3359-3362.

17. Shaporenko, A., et al., *Self-assembled monolayers of alkaneselenolates on (111) gold and silver*. Journal of Physical Chemistry B, 2005. **109**(9): p. 3898-3906.
18. Miller, D.C., et al., *Intrinsic stress development and microstructure evolution of Au/Cr/Si multilayer thin films subject to annealing*. Scripta Materialia, 2005. **52**(9): p. 873-879.
19. Saha, J.K., et al., *Small Size Limit to Self-Assembled Monolayer Formation on Gold(111)*. Journal of Physical Chemistry C, 2011. **115**(27): p. 13193-13199.
20. Boubour, E. and R.B. Lennox, *Insulating properties of self-assembled monolayers monitored by impedance spectroscopy*. Langmuir, 2000. **16**(9): p. 4222-4228.
21. Goes, M.S., et al., *A Dielectric Model of Self-Assembled Monolayer Interfaces by Capacitive Spectroscopy*. Langmuir, 2012. **28**(25): p. 9689-9699.
22. Heuschkel, M.O., et al., *A three-dimensional multi-electrode array for multi-site stimulation and recording in acute brain slices*. Journal of Neuroscience Methods, 2002. **114**(2): p. 135-148.
23. Seker, E., et al., *The fabrication of low-impedance nanoporous gold multiple-electrode arrays for neural electrophysiology studies*. Nanotechnology, 2010. **21**(12): p. 7.
24. Slaughter, G.E., et al., *Improving neuron-to-electrode surface attachment via alkanethiol self-assembly: An alternating current impedance study*. Langmuir, 2004. **20**(17): p. 7189-7200.
25. Kim, S.A., et al., *Optical measurement of neural activity using surface plasmon resonance*. Optics Letters, 2008. **33**(9): p. 914-916.
26. Zhang, S.J., et al., *Advances in surface plasmon resonance-based high throughput biochips*. Frontiers of Physics in China, 2009. **4**(4): p. 469-480.
27. Hynes, R.O., *The Extracellular Matrix: Not Just Pretty Fibrils*. Science, 2009. **326**(5957): p. 1216-1219.
28. Morgan, M.R., M.J. Humphries, and M.D. Bass, *Synergistic control of cell adhesion by integrins and syndecans*. Nature Reviews Molecular Cell Biology, 2007. **8**(12): p. 957-969.
29. Humphries, J.D., A. Byron, and M.J. Humphries, *Integrin ligands at a glance*. Journal of Cell Science, 2006. **119**(19): p. 3901-3903.
30. Berrier, A.L. and K.M. Yamada, *Cell-matrix adhesion*. Journal of Cellular Physiology, 2007. **213**(3): p. 565-573.
31. Groossmann, J., *Molecular mechanisms of "detachment-induced apoptosis—Anoikis"*. Apoptosis, 2002. **7**(3): p. 247-260.
32. Chiarugi, P. and E. Giannoni, *Anoikis: A necessary death program for anchorage-dependent cells*. Biochemical Pharmacology, 2008. **76**(11): p. 1352-1364.
33. Arnold, M., et al., *Activation of integrin function by nanopatterned adhesive interfaces*. Chemphyschem, 2004. **5**(3): p. 383-388.

34. Carey, D.J., *Syndecans: Multifunctional cell-surface co-receptors*. Biochemical Journal, 1997. **327**: p. 1-16.
35. Zelzer, M., et al., *Investigation of cell-surface interactions using chemical gradients formed from plasma polymers*. Biomaterials, 2008. **29**(2): p. 172-184.
36. Zelzer, M., M.R. Alexander, and N.A. Russell, *Hippocampal cell response to substrates with surface chemistry gradients*. Acta Biomaterialia, 2011. **7**(12): p. 4120-4130.
37. Iuliano, D.J., S.S. Saavedra, and G.A. Truskey, *Effect of the conformation and orientation of adsorbed fibronectin on endothelial cell spreading and the strength of adhesion*. Journal of Biomedical Materials Research, 1993. **27**(8): p. 1103-1113.
38. Burmeister, J.S., et al., *Effect of fibronectin amount and conformation on the strength of endothelial cell adhesion to HEMA/EMA copolymers*. Journal of Biomedical Materials Research, 1996. **30**(1): p. 13-22.
39. Norde, W., *My voyage of discovery to proteins in flatland ... and beyond*. Colloids and Surfaces B-Biointerfaces, 2008. **61**(1): p. 1-9.
40. Tzoneva, R., N. Faucheux, and T. Groth, *Wettability of substrata controls cell-substrate and cell-cell adhesions*. Biochimica et Biophysica Acta (BBA) - General Subjects, 2007. **1770**(11): p. 1538-1547.
41. Burmeister, J.S., et al., *Role of endothelial cell–substrate contact area and fibronectin–receptor affinity in cell adhesion to HEMA/EMA copolymers*. Journal of Biomedical Materials Research, 1999. **47**(4): p. 577-584.
42. Ranella, A., et al., *Tuning cell adhesion by controlling the roughness and wettability of 3D micro/nano silicon structures*. Acta Biomaterialia, 2010. **6**(7): p. 2711-2720.
43. Roach, P., et al., *Surface strategies for control of neuronal cell adhesion: A review*. Surface Science Reports, 2010. **65**(6): p. 145-173.
44. Khan, S. and G. Newaz, *A comprehensive review of surface modification for neural cell adhesion and patterning*. Journal of Biomedical Materials Research Part A, 2010. **93A**(3): p. 1209-1224.
45. Gomez, N., et al., *Immobilized nerve growth factor and microtopography have distinct effects on polarization versus axon elongation in hippocampal cells in culture*. Biomaterials, 2007. **28**(2): p. 271-284.
46. Roach, P., et al., *A bio-inspired neural environment to control neurons comprising radial glia, substrate chemistry and topography*. Biomaterials Science, 2013. **1**(1): p. 83-93.
47. Mesulam, M.M., *From sensation to cognition*. Brain, 1998. **121**: p. 1013-1052.
48. Seth, A.K., B.J. Baars, and D.B. Edelman, *Criteria for consciousness in humans and other mammals*. Consciousness and Cognition, 2005. **14**(1): p. 119-139.

49. Baker, B.J., et al., *Imaging brain activity with voltage- and calcium-sensitive dyes*. Cellular and Molecular Neurobiology, 2005. **25**(2): p. 245-282.
50. Carter, M. and J. Shieh, *Guide to Research Techniques in Neuroscience*. 2009: Academic Press.
51. Hamill, O.P., et al., *Improved Patch-clamp Techniques For High-resolution Current Recording From Cells And Cell-free Membrane Patches*. Pflugers Archiv-European Journal of Physiology, 1981. **391**(2): p. 85-100.
52. Gu, Y., et al., *High-resolution scanning patch-clamp: new insights into cell function*. The FASEB Journal, 2002.
53. Zhang, J.Y., T. Atay, and A.V. Nurmikko, *Optical Detection of Brain Cell Activity Using Plasmonic Gold Nanoparticles*. Nano Letters, 2009. **9**(2): p. 519-524.
54. Kim, S.A., et al., *In vivo optical neural recording using fiber-based surface plasmon resonance*. Optics Letters, 2012. **37**(4): p. 614-616.
55. Hodgkin, A.L. and A.F. Huxley, *A Quantitative Description Of Membrane Current And Its Application To Conduction And Excitation In Nerve*. Journal of Physiology-London, 1952. **117**(4): p. 500-544.
56. Wedeen, V.J., et al., *The Geometric Structure of the Brain Fiber Pathways*. Science, 2012. **335**(6076): p. 1628-1634.
57. Abbott, L.F. and W.G. Regehr, *Synaptic computation*. Nature, 2004. **431**(7010): p. 796-803.
58. Gasser, U.E. and M.E. Hatten, *Neuron-glia interactions of rat hippocampal cells-in vitro - glial-guided neuronal migration and neuronal regulation of glial differentiation*. Journal of Neuroscience, 1990. **10**(4): p. 1276-1285.
59. Perea, G., M. Navarrete, and A. Araque, *Tripartite synapses: astrocytes process and control synaptic information*. Trends in Neurosciences, 2009. **32**(8): p. 421-431.
60. Stern, P.R., *The Adult Astrocyte Is Different*. Sci. Signal., 2013. **6**(258): p. ec17-.
61. Baumann, N. and D. Pham-Dinh, *Biology of oligodendrocyte and myelin in the mammalian central nervous system*. Physiological Reviews, 2001. **81**(2): p. 871-927.
62. Bez, A., et al., *Neurosphere and neurosphere-forming cells: morphological and ultrastructural characterization*. Brain Research, 2003. **993**(1-2): p. 18-29.
63. Zeng, H.C., et al., *Studying the formation of large cell aggregates in patterned neuronal cultures*. Journal of Neuroscience Methods, 2007. **165**(1): p. 72-82.
64. Sorkin, R., et al., *Compact self-wiring in cultured neural networks*. Journal of Neural Engineering, 2006. **3**(2): p. 95-101.
65. Yang, H., et al., *Long-Term Primary Culture of Highly-Pure Rat Embryonic Hippocampal Neurons of Low-Density*. Neurochemical Research, 2010. **35**(9): p. 1333-1342.

66. Banker, G. and K. Goslin, eds. *Culturing Nerve Cells*. 2 ed. 1998, MIT Press.
67. Lesuisse, C. and L.J. Martin, *Long-term culture of mouse cortical neurons as a model for neuronal development, aging, and death*. *Journal of Neurobiology*, 2002. **51**(1): p. 9-23.
68. Kummer, T.T., et al., *Spotted substrates for focal presentation of proteins to cells*. *Biotechniques*, 2002. **33**(5): p. 1018-+.
69. Brewer, G.J., et al., *Optimised survival of hippocampal-neurons in B27-supplemented neurobasal(TM), a new serum-free medium combination*. *Journal of Neuroscience Research*, 1993. **35**(5): p. 567-576.
70. Evans, M.S., M.A. Collings, and G.J. Brewer, *Electrophysiology of embryonic, adult and aged rat hippocampal neurons in serum-free culture*. *Journal of Neuroscience Methods*, 1998. **79**(1): p. 37-46.
71. Perry, S.W., et al., *Antioxidants are required during the early critical period, but not later, for neuronal survival*. *Journal of Neuroscience Research*, 2004. **78**(4): p. 485-492.
72. Ray, J., et al., *Proliferation, Differentiation, And Long-term Culture Of Primary Hippocampal-neurons*. *Proceedings of the National Academy of Sciences of the United States of America*, 1993. **90**(8): p. 3602-3606.
73. Bottenstein, J.E. and G.H. Sato, *Growth of rat neuroblastoma cell line in serum-free supplemented medium*. *Proceedings of the National Academy of Sciences of the United States of America*, 1979. **76**(1): p. 514-517.
74. Staines, D. and P. Price, *Perspectives in cell culture: Managing serum requirements for cell culture*. 2003, Invitrogen Corporation, Gibco™ Cell Culture.
75. Ito, D., et al., *Minimum neuron density for synchronized bursts in a rat cortical culture on multi-electrode arrays*. *Neuroscience*, 2010. **171**(1): p. 50-61.
76. Segev, R., et al., *Formation of electrically active clusterized neural networks*. *Physical Review Letters*, 2003. **90**(16).
77. Li, J. and E.S. Yeung, *Real-Time Single-Molecule Kinetics of Trypsin Proteolysis*. *Analytical Chemistry*, 2008. **80**(22): p. 8509-8513.
78. Tsuyuki, E., H. Tsuyuki, and M.A. Stahmann, *Synthesis and enzymatic hydrolysis of poly-d-lysine*. *Journal of Biological Chemistry*, 1956. **222**(1): p. 479-485.
79. Yavin, E. and Z. Yavin, *Attachment and culture of dissociated cells from rat embryo cerebral hemispheres on polylysine-coated surface*. *Journal of Cell Biology*, 1974. **62**(2): p. 540-546.
80. Deloulme, J.C., J. Baudier, and M. Sensenbrenner, *Establishment of pure neuronal cultures from fetal-rat spinal-cord and proliferation of the neuronal precursor cells in the presence of fibroblast growth-factor*. *Journal of Neuroscience Research*, 1991. **29**(4): p. 499-509.

81. Kim, Y.H., et al., *Enhancement of neuronal cell adhesion by covalent binding of poly-d-lysine*. Journal of Neuroscience Methods, 2011. **202**(1): p. 38-44.
82. Stenger, D.A., et al., *Surface determinants of neuronal survival and growth on self-assembled monolayers in culture*. Brain Research, 1993. **630**(1-2): p. 136-147.
83. Powell, S.K., et al., *Neural cell response to multiple novel sites on laminin-1*. Journal of Neuroscience Research, 2000. **61**(3): p. 302-312.
84. Tashiro, K., et al., *A synthetic peptide deduced from the sequence in the cross-region of laminin-a chain mediates neurite outgrowth, cell attachment and heparin-binding*. Biochemical Journal, 1994. **302**: p. 73-79.
85. Colognato, H. and P.D. Yurchenco, *Form and function: The laminin family of heterotrimers*. Developmental Dynamics, 2000. **218**(2): p. 213-234.
86. Sanes, J.R., *Extracellular-matrix molecules that influence neural development*. Annual Review of Neuroscience, 1989. **12**: p. 491-516.
87. Dekeyser, C.M., et al., *A rough morphology of the adsorbed fibronectin layer favors adhesion of neuronal cells*. Journal of Biomedical Materials Research Part A, 2008. **87A**(1): p. 116-128.
88. Freire, E., et al., *Structure of laminin substrate modulates cellular signaling for neuritogenesis*. Journal of Cell Science, 2002. **115**(24): p. 4867-4876.
89. Zelzer, M., et al., *The Role of Albumin and Fibronectin in the Adhesion of Fibroblasts to Plasma Polymer Surfaces*. Plasma Processes and Polymers, 2012. **9**(2): p. 149-156.
90. Thanos, S., et al., *Survival and axonal elongation of adult-rat retinal ganglion-cells - invitro effects of lesioned sciatic-nerve and brain derived neurotrophic factor*. European Journal of Neuroscience, 1989. **1**(1): p. 19-26.
91. Ruoslahti, E., *RGD and other recognition sequences for integrins*. Annual Review of Cell and Developmental Biology, 1996. **12**: p. 697-715.
92. Ruoslahti, E. and M.D. Pierschbacher, *New perspectives in cell-adhesion - RGD and integrins*. Science, 1987. **238**(4826): p. 491-497.
93. Pierschbacher, M.D. and E. Ruoslahti, *Cell attachment activity of fibronectin can be duplicated by small synthetic fragments of the molecule*. Nature, 1984. **309**(5963): p. 30-33.
94. Huber, M., et al., *Modification of glassy carbon surfaces with synthetic laminin-derived peptides for nerve cell attachment and neurite growth*. Journal of Biomedical Materials Research, 1998. **41**(2): p. 278-288.
95. Yu, L.M.Y., N.D. Leipzig, and M.S. Shoichet, *Promoting neuron adhesion and growth*. Materials Today, 2008. **11**(5): p. 36-43.
96. Liesi, P., et al., *Identification of a neurite outgrowth-promoting domain of laminin using synthetic peptides*. Febs Letters, 1989. **244**(1): p. 141-148.

97. Agius, E., et al., *Antibodies directed against the beta 1-integrin subunit and peptides containing the IKVAV sequence of laminin perturb neurite outgrowth of peripheral neurons on immature spinal cord substrata*. *Neuroscience*, 1996. **71**(3): p. 773-786.
98. Srikanth, M., et al., *Nanofiber-mediated inhibition of focal adhesion kinase sensitizes glioma stemlike cells to epidermal growth factor receptor inhibition*. *Neuro-Oncology*, 2013. **15**(3): p. 319-329.
99. Heller, D.A., et al., *Patterned networks of mouse hippocampal neurons on peptide-coated gold surfaces*. *Biomaterials*, 2005. **26**(8): p. 883-889.
100. Palyvoda, O., C.C. Chen, and G.W. Auner, *Culturing neuron cells on electrode with self-assembly monolayer*. *Biosensors & Bioelectronics*, 2007. **22**(9-10): p. 2346-2350.
101. Wenzel, R.N., *Resistance of solid surfaces to wetting by water*. *Industrial and Engineering Chemistry*, 1936. **28**: p. 988-994.
102. Bain, C.D. and G.M. Whitesides, *Depth sensitivity of wetting - monolayers of omega-mercapto ethers on gold*. *Journal of the American Chemical Society*, 1988. **110**(17): p. 5897-5898.
103. Adamson, A.W., *Physical chemistry of surfaces*. 5 ed. 1990, New York: Wiley interscience.
104. Friedbacher, G., H. Bubert, and H. Jenett, eds. *Surface and thin film analysis. A compendium of principles, instrumentation and applications*. 2 ed. 2011, Wiley-VCH.
105. Briggs, D., *Surface analysis of polymers by XPS and static SIMS*. 1998, Cambridge: Cambridge University Press.
106. Watts, J.F. and J. Wolstenholme, *An introduction to surface analysis by XPS and AES*. 2003, Chichester: J. Wiley.
107. RoentDek, MCP delay line detector manual, 2010, Version 9.22.1003.1, RoentDek Handels GmbH.
108. Binnig, G., C.F. Quate, and C. Gerber, *Atomic force microscope*. *Physical Review Letters*, 1986. **56**(9): p. 930-933.
109. Takano, H., et al., *Chemical and biochemical analysis using scanning force microscopy*. *Chemical Reviews*, 1999. **99**(10): p. 2845-+.
110. Rodahl, M., et al., *QUARTZ-CRYSTAL MICROBALANCE SETUP FOR FREQUENCY AND Q-FACTOR MEASUREMENTS IN GASEOUS AND LIQUID ENVIRONMENTS*. *Review of Scientific Instruments*, 1995. **66**(7): p. 3924-3930.
111. Zernike, F., *Phase contrast, a new method for the microscopic observation of transparent objects*. *Physica*, 1942. **9**: p. 686-698.
112. Zernike, F., *Phase contrast, a new method for the microscopic observation of transparent objects Part II*. *Physica*, 1942. **9**: p. 974-986.
113. Gaugain, B., et al., *DNA Bifunctional Intercalators .2. Fluorescence Properties And DNA Binding Interaction Of An Ethidium Homodimer And An Acridine Ethidium Heterodimer*. *Biochemistry*, 1978. **17**(24): p. 5078-5088.

114. Tashiro, K., et al., *A synthetic peptide containing the IKVAV sequence from the  $\alpha$ -chain of laminin mediates cell attachment, migration, and neurite outgrowth.* Journal of Biological Chemistry, 1989. **264**(27): p. 16174-16182.
115. Silva, G.A., et al., *Selective differentiation of neural progenitor cells by high-epitope density nanofibers.* Science, 2004. **303**(5662): p. 1352-1355.
116. Harder, P., et al., *Molecular conformation in oligo(ethylene glycol)-terminated self-assembled monolayers on gold and silver surfaces determines their ability to resist protein adsorption.* Journal of Physical Chemistry B, 1998. **102**(2): p. 426-436.
117. Sofia, S.J., V. Premnath, and E.W. Merrill, *Poly(ethylene oxide) grafted to silicon surfaces: Grafting density and protein adsorption.* Macromolecules, 1998. **31**(15): p. 5059-5070.
118. Goss, C.A., D.H. Charych, and M. Majda, *Application of (3-mercaptopropyl)trimethoxysilane as a molecular adhesive in the fabrication of vapour-deposited gold electrodes on glass substrates.* Analytical Chemistry, 1991. **63**(1): p. 85-88.
119. Behrens, S.H. and D.G. Grier, *The charge of glass and silica surfaces.* Journal of Chemical Physics, 2001. **115**(14): p. 6716-6721.
120. Ling, T.G.I., et al., *Fabrication and characterization of a molecular adhesive layer for micro- and nanofabricated electrochemical electrodes.* Microelectronic Engineering, 2003. **67-68**(0): p. 887-892.
121. Giesbers, M., J.M. Kleijn, and M.A. Cohen Stuart, *The Electrical Double Layer on Gold Probed by Electrokinetic and Surface Force Measurements.* Journal of Colloid and Interface Science, 2002. **248**(1): p. 88-95.
122. Wagner, M.S. and D.G. Castner, *Characterization of adsorbed protein films by time-of-flight secondary ion mass spectrometry with principal component analysis.* Langmuir, 2001. **17**(15): p. 4649-4660.
123. Rangarajan, S. and B.J. Tyler, *Topography in secondary ion mass spectroscopy images.* Journal of Vacuum Science & Technology A, 2006. **24**(5): p. 1730-1736.
124. Brewer, N.J., et al., *Photooxidation of self-assembled monolayers by exposure to light of wavelength 254 nm: A static SIMS study.* Journal of Physical Chemistry B, 2005. **109**(22): p. 11247-11256.
125. Gregory, C.D. and J.D. Pound, *Microenvironmental influences of apoptosis in vivo and in vitro.* Apoptosis, 2010. **15**(9): p. 1029-1049.
126. Shanley, D.K. and A.M. Sullivan, *Alterations in cellular phenotypes differentiating from embryonic rat brain neurosphere cultures by immunoselection of neuronal progenitors.* Brain Research, 2006. **1067**(1): p. 85-94.
127. Cheyne, J.E., et al., *Synaptic integration of newly generated neurons in rat dissociated hippocampal cultures.* Molecular and Cellular Neuroscience, 2011. **47**(3): p. 203-214.

128. Cheung, Z.H. and N.Y. Ip, *Neurotrophins - players in the regulation of neuronal survival and apoptosis*. *Current Science*, 2008. **95**(9): p. 1237-1251.
129. Skehan, P. and S.J. Friedman, *Non-exponential growth by mammalian-cells in culture*. *Cell and Tissue Kinetics*, 1984. **17**(4): p. 335-343.
130. Attiah, D.G., R.A. Kopher, and T.A. Desai, *Characterization of PC12 cell proliferation and differentiation-stimulated by ECM adhesion proteins and neurotrophic factors*. *Journal of Materials Science-Materials in Medicine*, 2003. **14**(11): p. 1005-1009.
131. LaPlaca, M.C., et al., *Three-Dimensional Neuronal Cultures*. *Methods in Bioengineering: 3d Tissue Engineering*, ed. F. Berthiaume and J. Morgan. 2010, Norwood: Artech House. 187-204.
132. Allen, S.J. and D. Dawbarn, *Clinical relevance of the neurotrophins and their receptors*. *Clinical Science*, 2006. **110**(2): p. 175-191.
133. Berg, D.K., *New neuronal growth-factors*. *Annual Review of Neuroscience*, 1984. **7**: p. 149-170.
134. Kim, J.A. and M.J. Druse, *Deficiency of essential neurotrophic factors in conditioned media produced by ethanol-exposed cortical astrocytes*. *Developmental Brain Research*, 1996. **96**(1-2): p. 1-10.
135. Yoshida, M., H. Saito, and H. Katsuki, *Neurotropic effects of conditioned media of astrocytes isolated from different brain-regions on hippocampal and cortical-neurons*. *Experientia*, 1995. **51**(2): p. 133-136.
136. Watanabe, M., et al., *Glutamine is involved in the dependency of brain neuron survival on cell plating density in culture*. *Neuroreport*, 1998. **9**(10): p. 2353-2357.
137. Chalazonitis, A., et al., *Neurotrophin-3 induces neural crest-derived cells from fetal-rat gut to develop in-vitro as neurons or glia*. *Journal of Neuroscience*, 1994. **14**(11): p. 6571-6584.
138. Arden, N. and M.J. Betenbaugh, *Life and death in mammalian cell culture: strategies for apoptosis inhibition*. *Trends in Biotechnology*, 2004. **22**(4): p. 174-180.
139. Ratner, B.D., et al., eds. *Biomaterials science: an introduction to materials in medicine*. 2 ed. 2004, Elsevier Academic Press: San Diego.
140. Veleva, A.N., et al., *Selective endothelial cell attachment to peptide-modified terpolymers*. *Biomaterials*, 2008. **29**(27): p. 3656-3661.
141. Grinnell, F. and M.K. Feld, *Initial adhesion of human fibroblasts in serum-free medium: Possible role of secreted fibronectin*. *Cell*, 1979. **17**(1): p. 117-129.
142. Arima, Y. and H. Iwata, *Effect of wettability and surface functional groups on protein adsorption and cell adhesion using well-defined mixed self-assembled monolayers*. *Biomaterials*, 2007. **28**(20): p. 3074-3082.

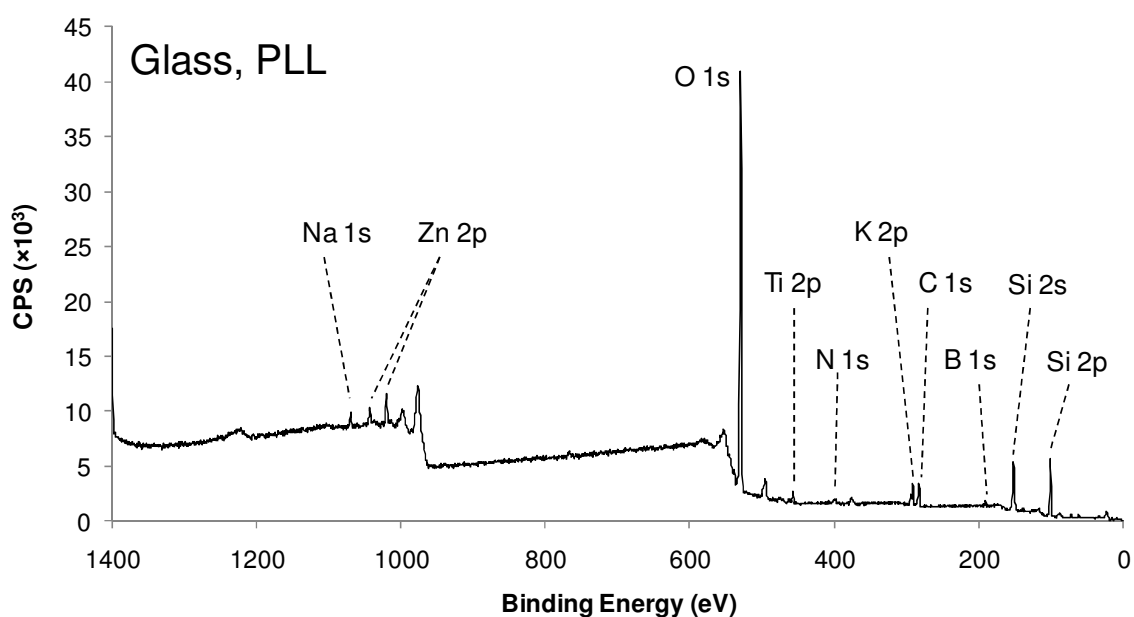
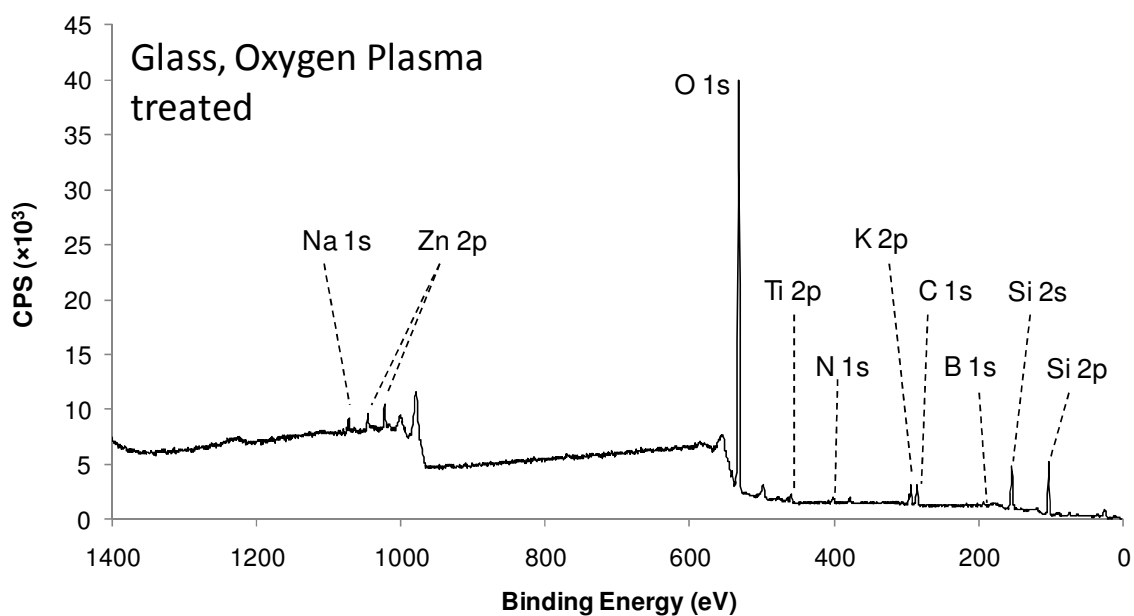
143. Jans, K., et al., *Chemical and Biological Characterization of Thiol SAMs for Neuronal Cell Attachment*. Langmuir, 2009. **25**(8): p. 4564-4570.
144. Gombotz, W.R., et al., *Protein adsorption to poly(ethylene oxide) surfaces*. Journal of Biomedical Materials Research, 1991. **25**(12): p. 1547-1562.
145. Conway-Jacobs, A. and L.M. Lewin, *Isoelectric focusing in acrylamide gels: Use of amphoteric dyes as internal markers for determination of isoelectric points*. Analytical Biochemistry, 1971. **43**(2): p. 394-400.
146. Andersen, R.A., et al., *Biochemical characteristics of rat superoxide dismutase and the effect caused by paraquat injection on the enzyme activity in various tissues*. General Pharmacology: The Vascular System, 1984. **15**(3): p. 205-210.
147. Caruso, F., et al., *Enzyme Encapsulation in Layer-by-Layer Engineered Polymer Multilayer Capsules*. Langmuir, 2000. **16**(4): p. 1485-1488.
148. Schreiber, G., et al., *The synthesis and secretion of rat transferrin*. Journal of Biological Chemistry, 1979. **254**(23): p. 2013-2019.
149. Dewez, J.L., et al., *Competitive adsorption of proteins: Key of the relationship between substratum surface properties and adhesion of epithelial cells*. Biomaterials, 1999. **20**(6): p. 547-559.
150. Hoerr, C.W., M.R. McCorkle, and A.W. Ralston, *Studies on high molecular weight aliphatic amines and their salts X Ionization constants of primary and symmetrical secondary amines in aqueous solution*. Journal of the American Chemical Society, 1943. **65**: p. 328-329.
151. Nitzan, B. and S. Margel, *Surface modification .2. Functionalization of solid surfaces with vinylic monomers*. Journal of Polymer Science Part a-Polymer Chemistry, 1997. **35**(1): p. 171-181.
152. White, H.S., et al., *Voltammetric measurement of interfacial acid/base reactions*. Journal of Physical Chemistry B, 1998. **102**(16): p. 2930-2934.
153. Marmisolle, W.A., et al., *Self-Assembled Monolayers of NH<sub>2</sub>-Terminated Thiolates: Order, pK(a), and Specific Adsorption*. Langmuir, 2013. **29**(17): p. 5351-5359.
154. Scavetta, E., et al., *Electrochemical characterization of self assembled monolayers on flexible electrodes*. Electrochimica Acta, 2012. **65**: p. 159-164.
155. VandeVondele, S., J. Voros, and J.A. Hubbell, *RGD-Grafted poly-L-lysine-graft-(polyethylene glycol) copolymers block non-specific protein adsorption while promoting cell adhesion*. Biotechnology and Bioengineering, 2003. **82**(7): p. 784-790.
156. Yoshimoto, K., M. Ichino, and Y. Nagasaki, *Inverted pattern formation of cell microarrays on poly(ethylene glycol) (PEG) gel patterned surface and construction of hepatocyte spheroids on unmodified PEG gel microdomains*. Lab on a Chip, 2009. **9**(9): p. 1286-1289.

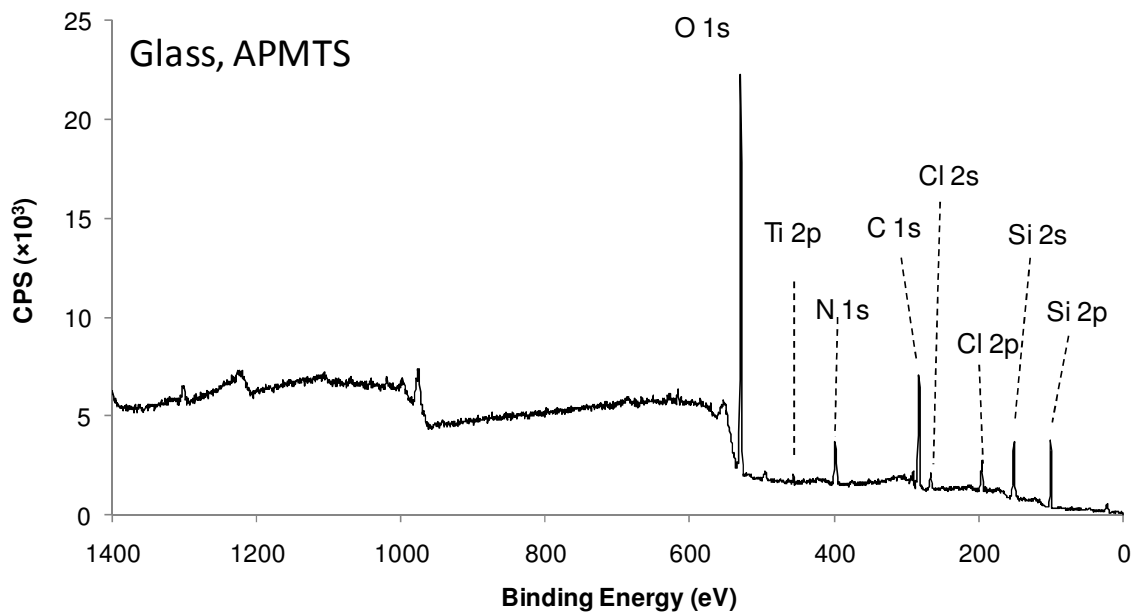
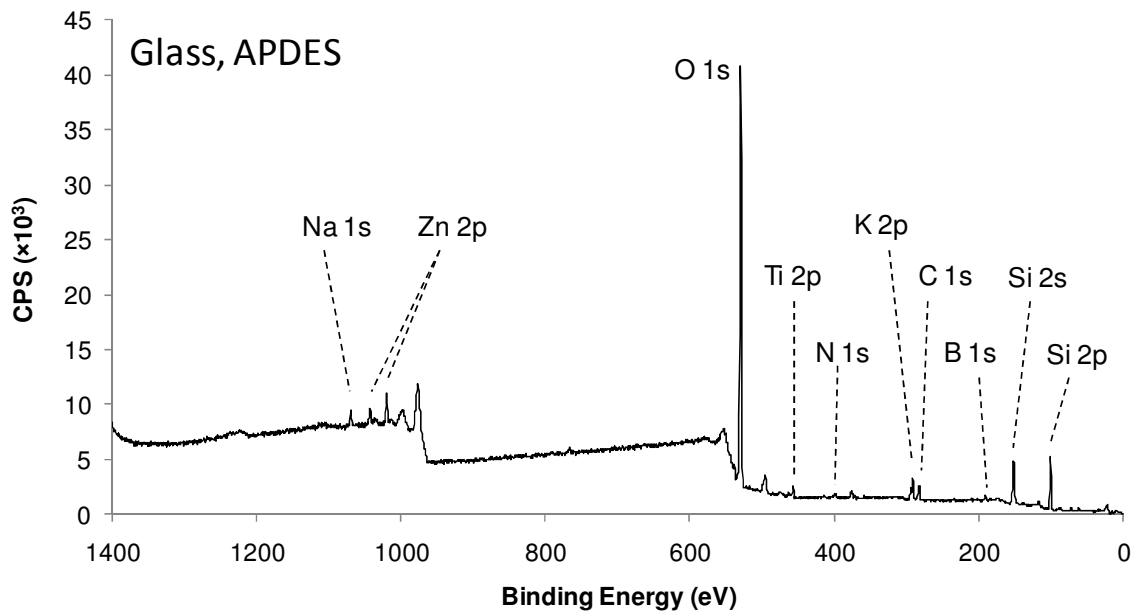
157. Saneinejad, S. and M.S. Shoichet, *Patterned glass surfaces direct cell adhesion and process outgrowth of primary neurons of the central nervous system*. Journal of Biomedical Materials Research, 1998. **42**(1): p. 13-19.
158. Unsworth, L.D., H. Sheardown, and J.L. Brash, *Protein-resistant poly(ethylene oxide)-grafted surfaces: Chain density-dependent multiple mechanisms of action*. Langmuir, 2008. **24**(5): p. 1924-1929.
159. Alessi, M.L., et al., *Helical and coil conformations of poly(ethylene glycol) in isobutyric acid and water*. Macromolecules, 2005. **38**(22): p. 9333-9340.
160. Branch, D.W., et al., *Long-term stability of grafted polyethylene glycol surfaces for use with microstamped substrates in neuronal cell culture*. Biomaterials, 2001. **22**(10): p. 1035-1047.
161. Lussi, J.W., et al., *Pattern stability under cell culture conditions - A comparative study of patterning methods based on PLL-g-PEG background passivation*. Biomaterials, 2006. **27**(12): p. 2534-2541.
162. Roach, P., D. Farrar, and C.C. Perry, *Interpretation of protein adsorption: Surface-induced conformational changes*. Journal of the American Chemical Society, 2005. **127**(22): p. 8168-8173.
163. Llopis-Hernandez, V., et al., *Role of Surface Chemistry in Protein Remodeling at the Cell-Material Interface*. Plos One, 2011. **6**(5): p. 11.
164. Chaplin, M., *Do we underestimate the importance of water in cell biology?* Nat Rev Mol Cell Biol, 2006. **7**(11): p. 861-866.
165. Papra, A., et al., *Microfluidic Networks Made of Poly(dimethylsiloxane), Si, and Au Coated with Polyethylene Glycol for Patterning Proteins onto Surfaces*. Langmuir, 2001. **17**(13): p. 4090-4095.
166. Han, J.-H. and J.-Y. Yoon, *Reusable, polyethylene glycol-structured microfluidic channel for particle immunoassays*. Journal of Biological Engineering, 2009. **3**(1): p. 6.
167. Pasche, S., et al., *Relationship between interfacial forces measured by colloid-probe atomic force microscopy and protein resistance of poly(ethylene glycol)-grafted poly(L-lysine) adlayers on niobia surfaces*. Langmuir, 2005. **21**(14): p. 6508-6520.
168. Engler, A.J., et al., *Matrix Elasticity Directs Stem Cell Lineage Specification*. Cell, 2006. **126**(4): p. 677-689.
169. Leipzig, N.D. and M.S. Shoichet, *The effect of substrate stiffness on adult neural stem cell behavior*. Biomaterials, 2009. **30**(36): p. 6867-6878.
170. Richard, B.L., et al., *Identification of Synthetic Peptides Derived from Laminin  $\hat{I}\pm 1$  and  $\hat{I}\pm 2$  Chains with Cell Type Specificity for Neurite Outgrowth*. Experimental Cell Research, 1996. **228**(1): p. 98-105.
171. Hersel, U., C. Dahmen, and H. Kessler, *RGD modified polymers: biomaterials for stimulated cell adhesion and beyond*. Biomaterials, 2003. **24**(24): p. 4385-4415.

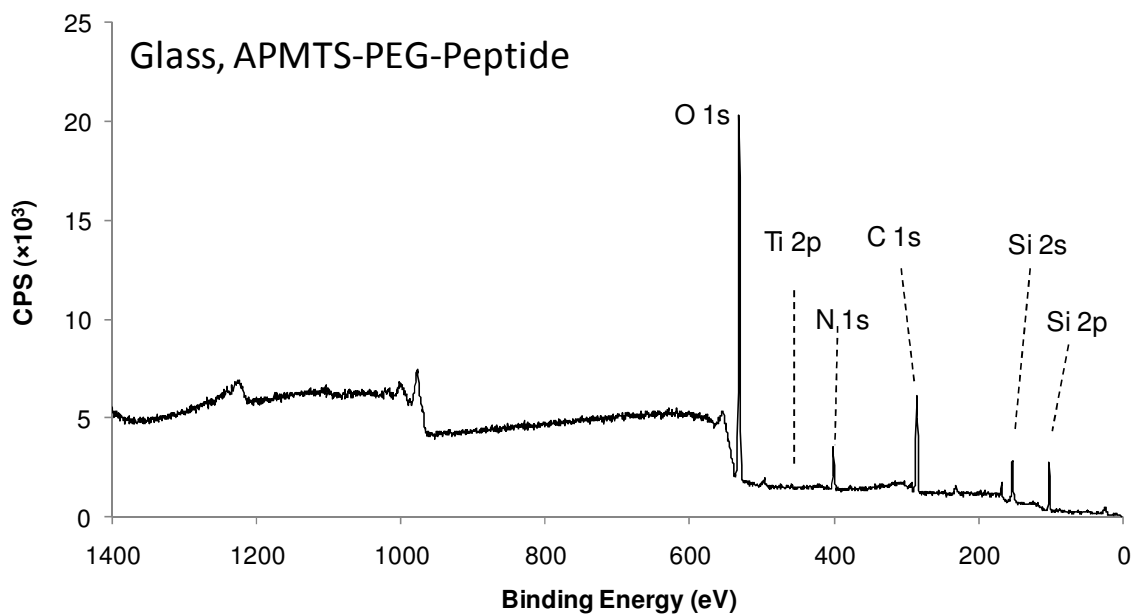
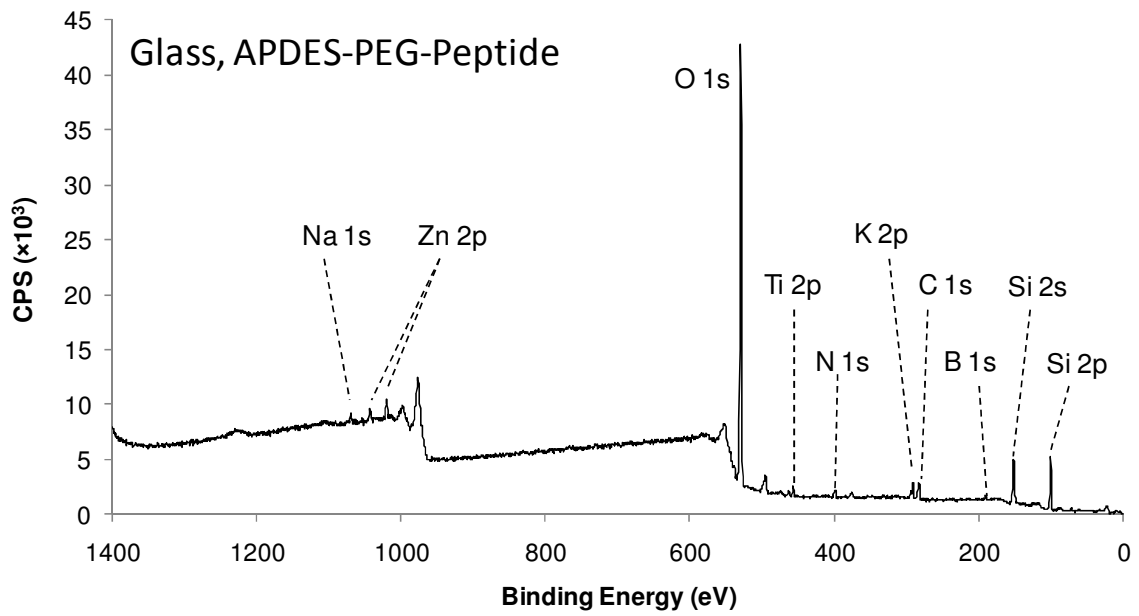
172. Banker, G.A., *Trophic interactions between astroglial cells and hippocampal-neurons in culture*. Science, 1980. **209**(4458): p. 809-810.
173. Webb, K.F. and N.A. Russell, *Label-free Cellular Imaging by Wide-Field Surface Plasmon Resonance Microscopy*. Journal of General Physiology, 2010. **136**(1): p. 13A-13A.
174. Edwards, D., et al., *Addition of glutamate to serum-free culture promotes recovery of electrical activity in adult hippocampal neurons in vitro*. Journal of Neuroscience Methods, 2010. **190**(2): p. 155-163.
175. Grienberger, C. and A. Konnerth, *Imaging Calcium in Neurons*. Neuron, 2012. **73**(5): p. 862-885.

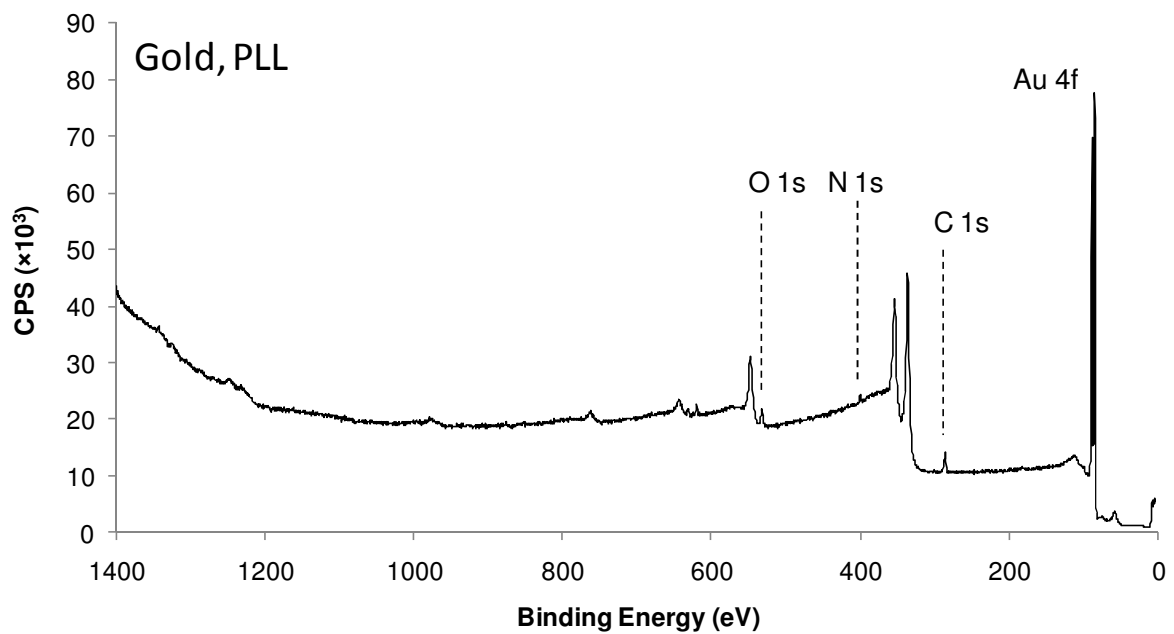
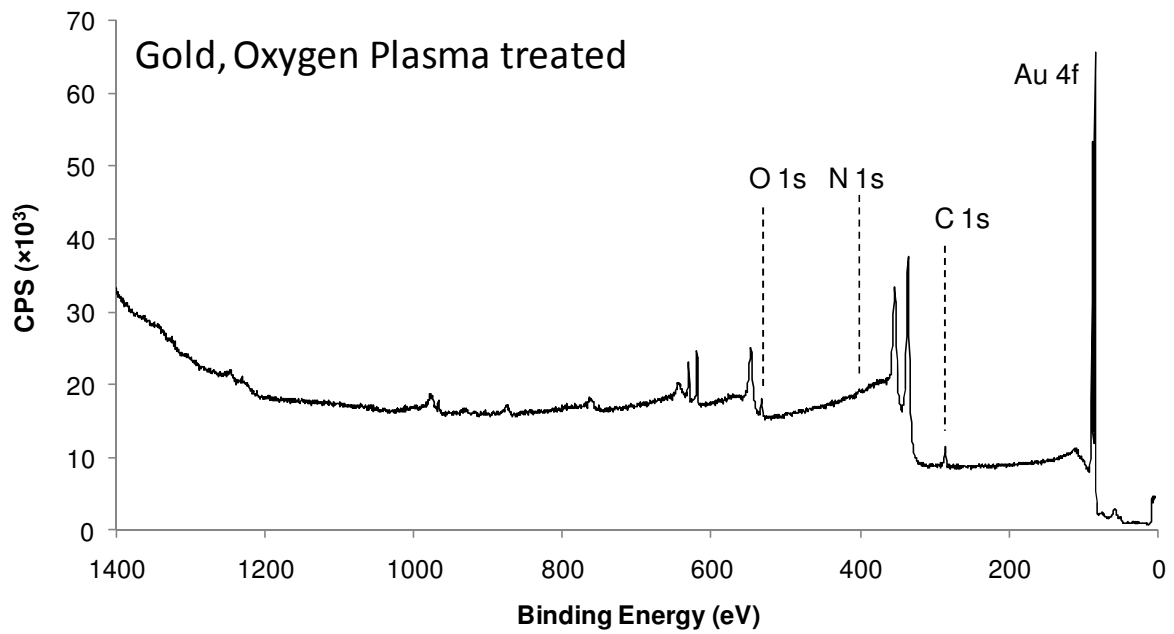
# Appendices

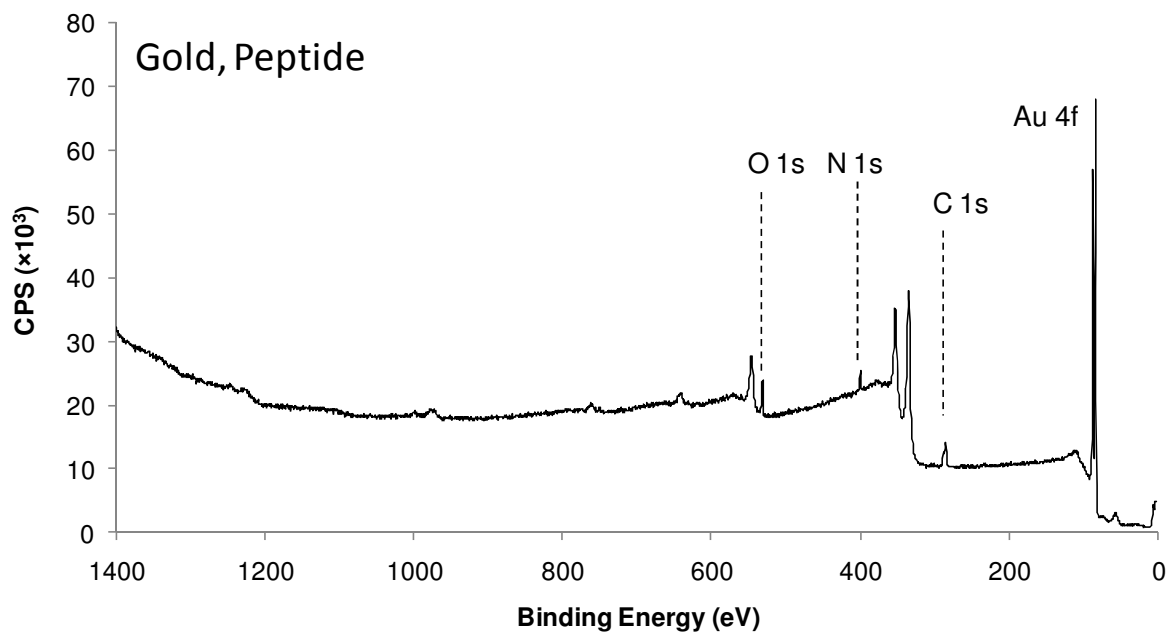
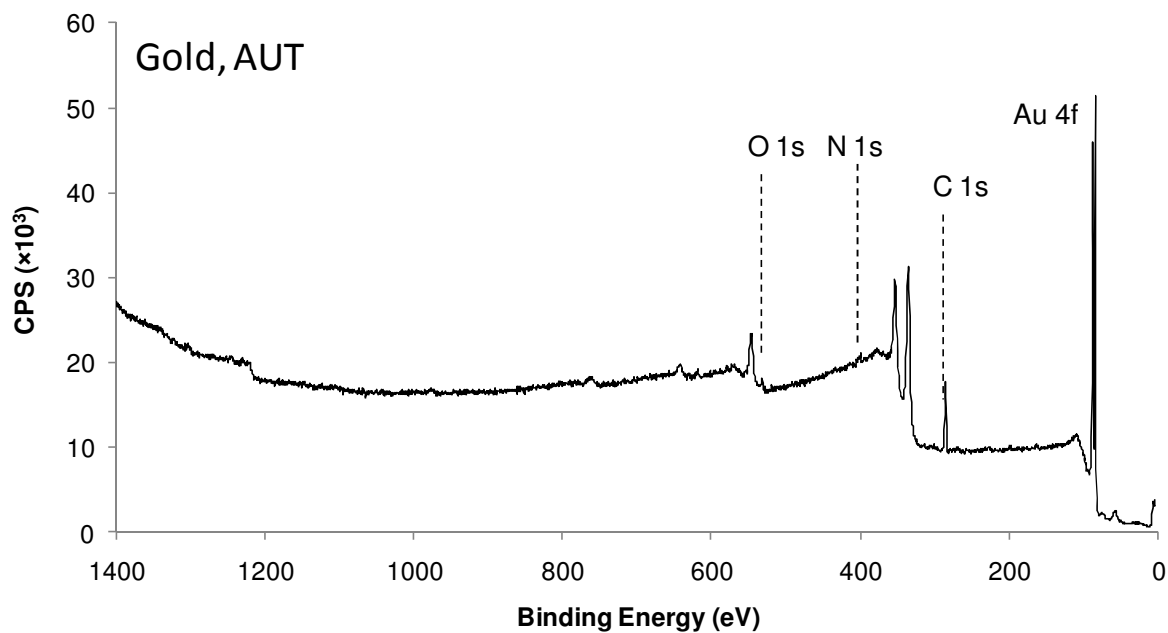
Appendix 1: XPS wide scan spectra of glass and gold surface modifications. All spectra were recorded in the same run with a mono-chromated Al  $\kappa\alpha$  X-ray source. Pass energy was 80 eV. Dwell time was 429 ms per point, the step was 500 meV.

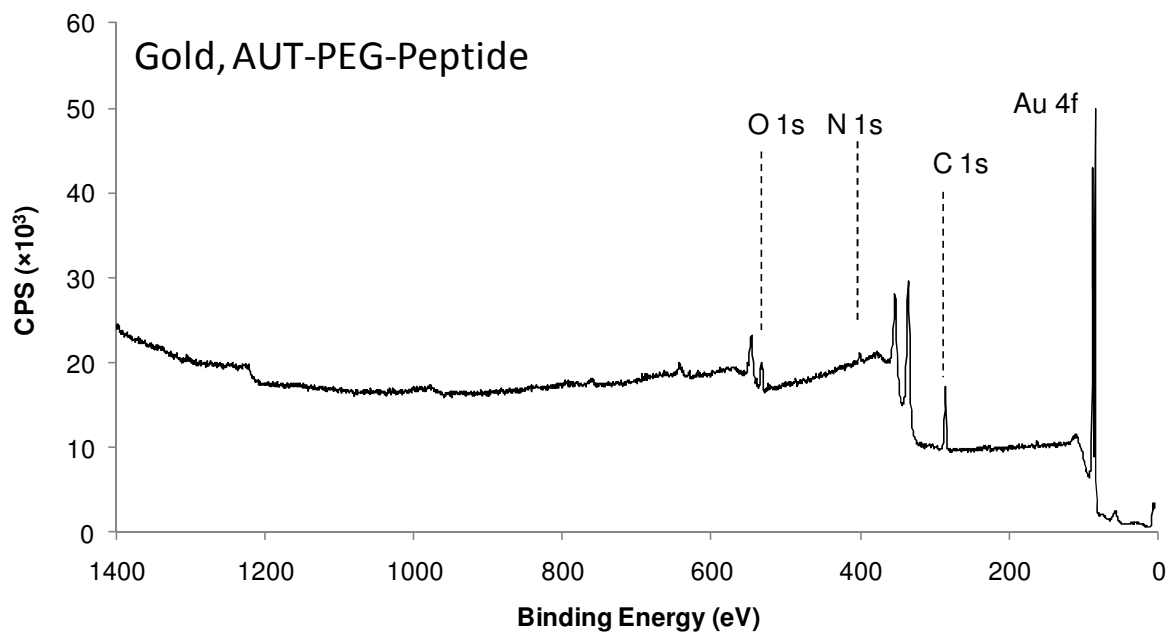




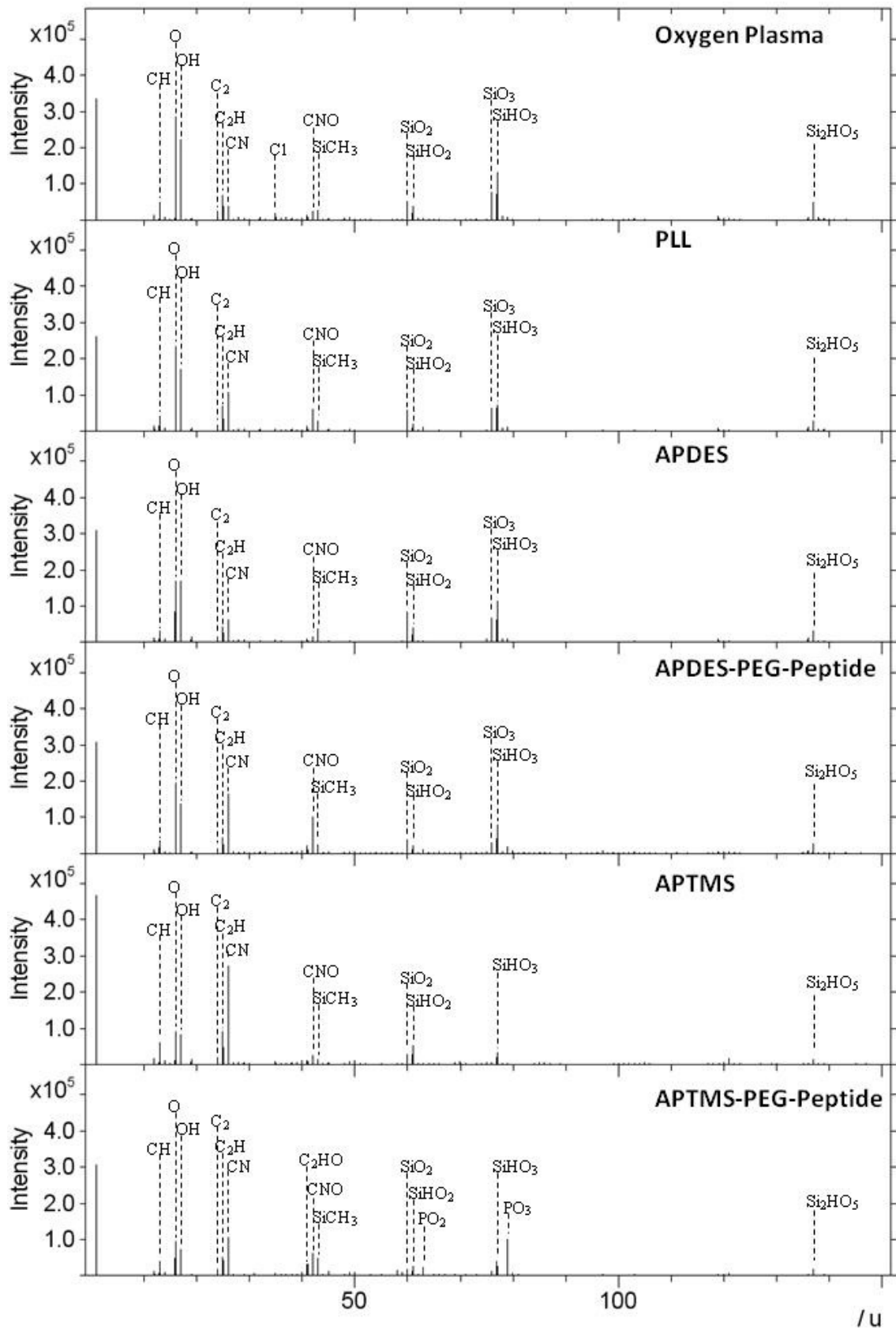




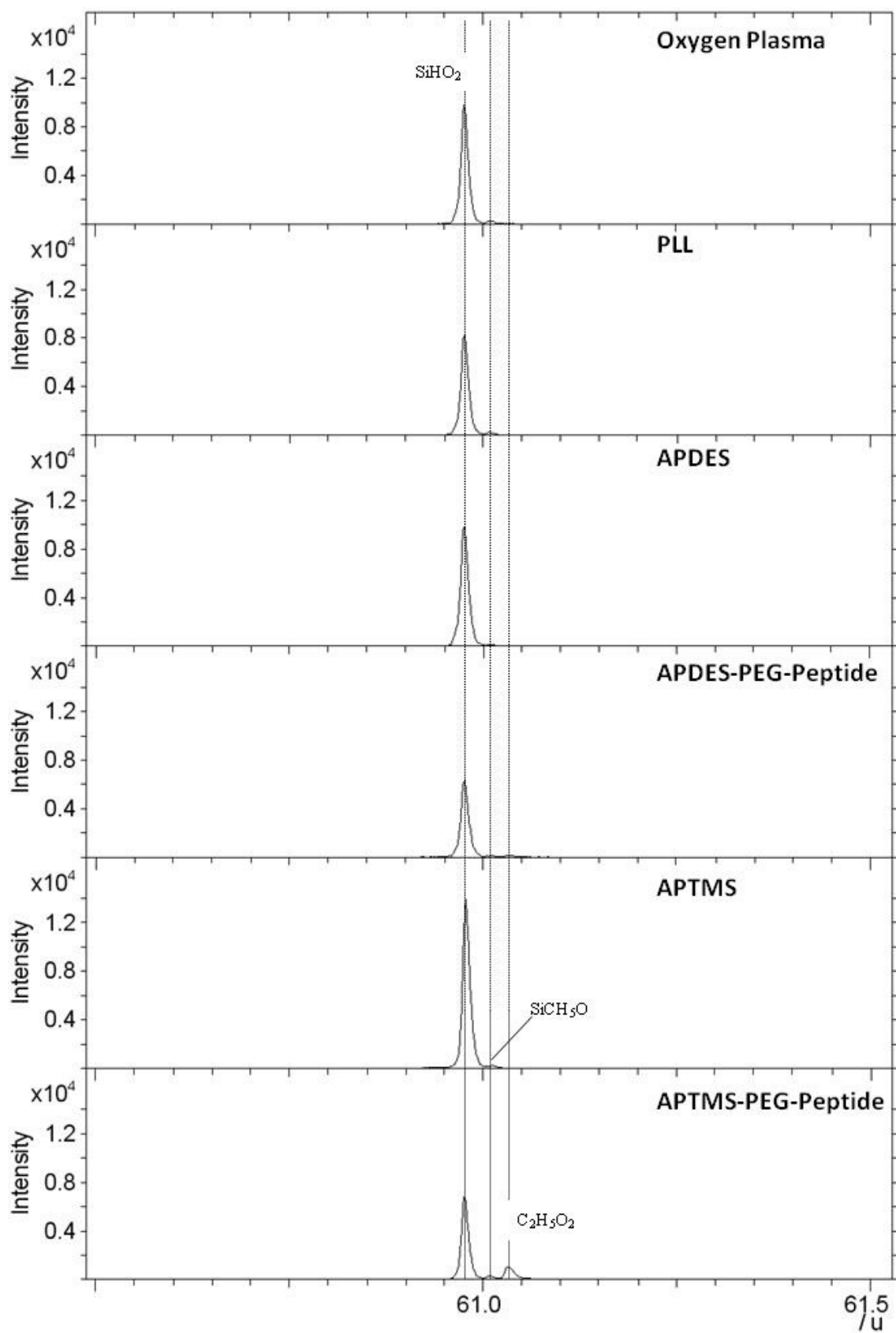




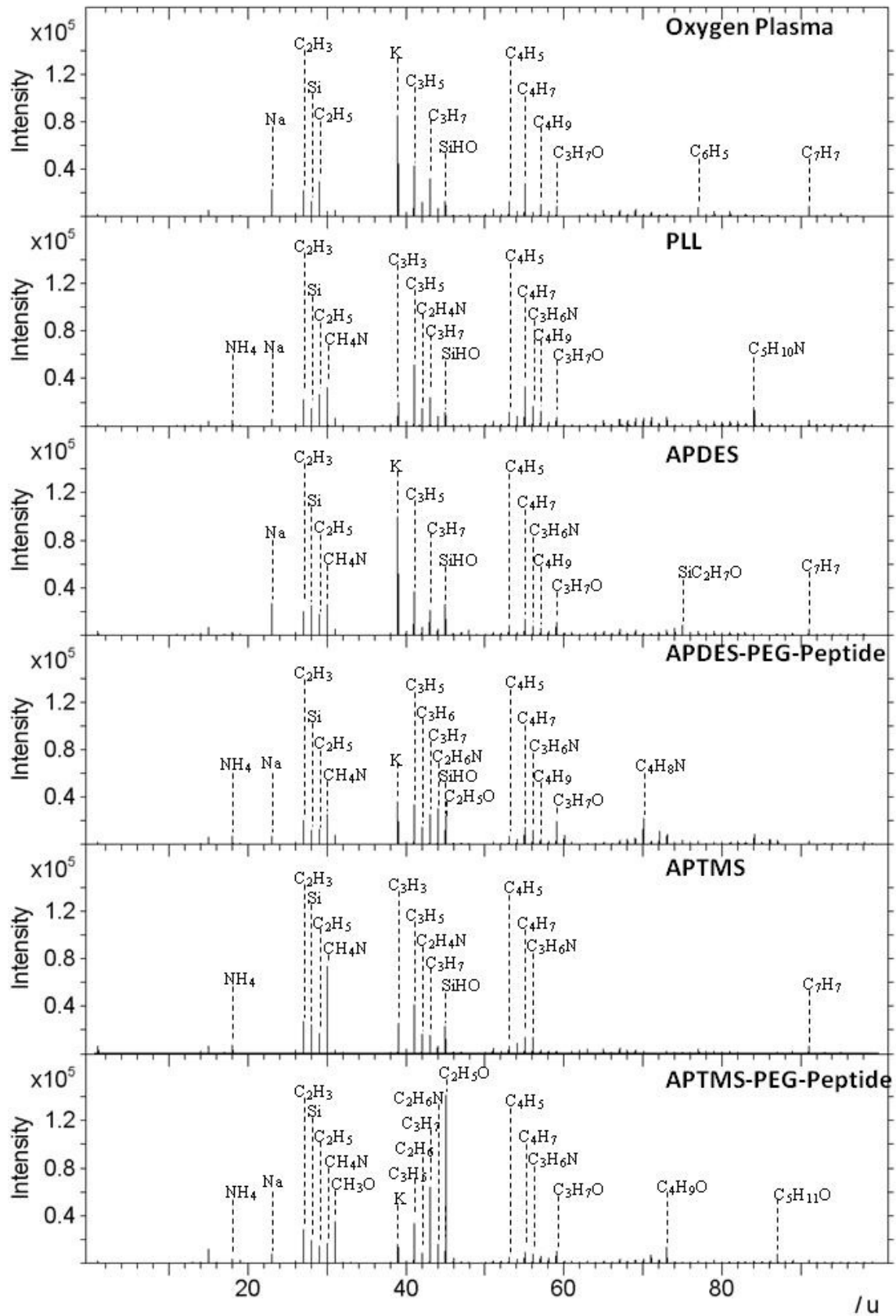
Appendix 2: ToF-SIMS Negative Ion Spectra: Glass surface modifications.



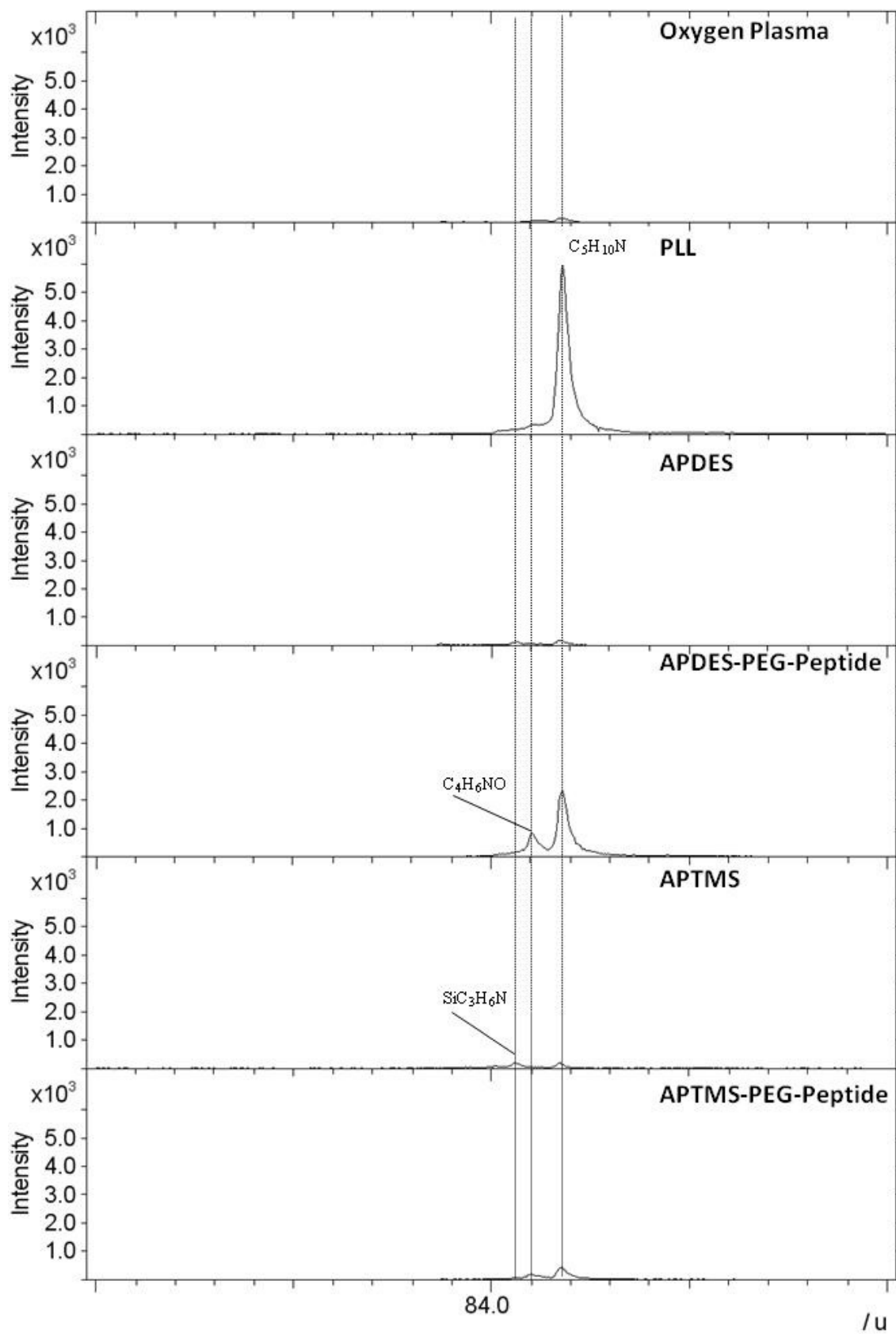
Appendix 3: ToF-SIMS Negative Ion Spectra: Glass surface modifications.  $C_2H_5O_2^-$  fragment attributed to PEG chain.



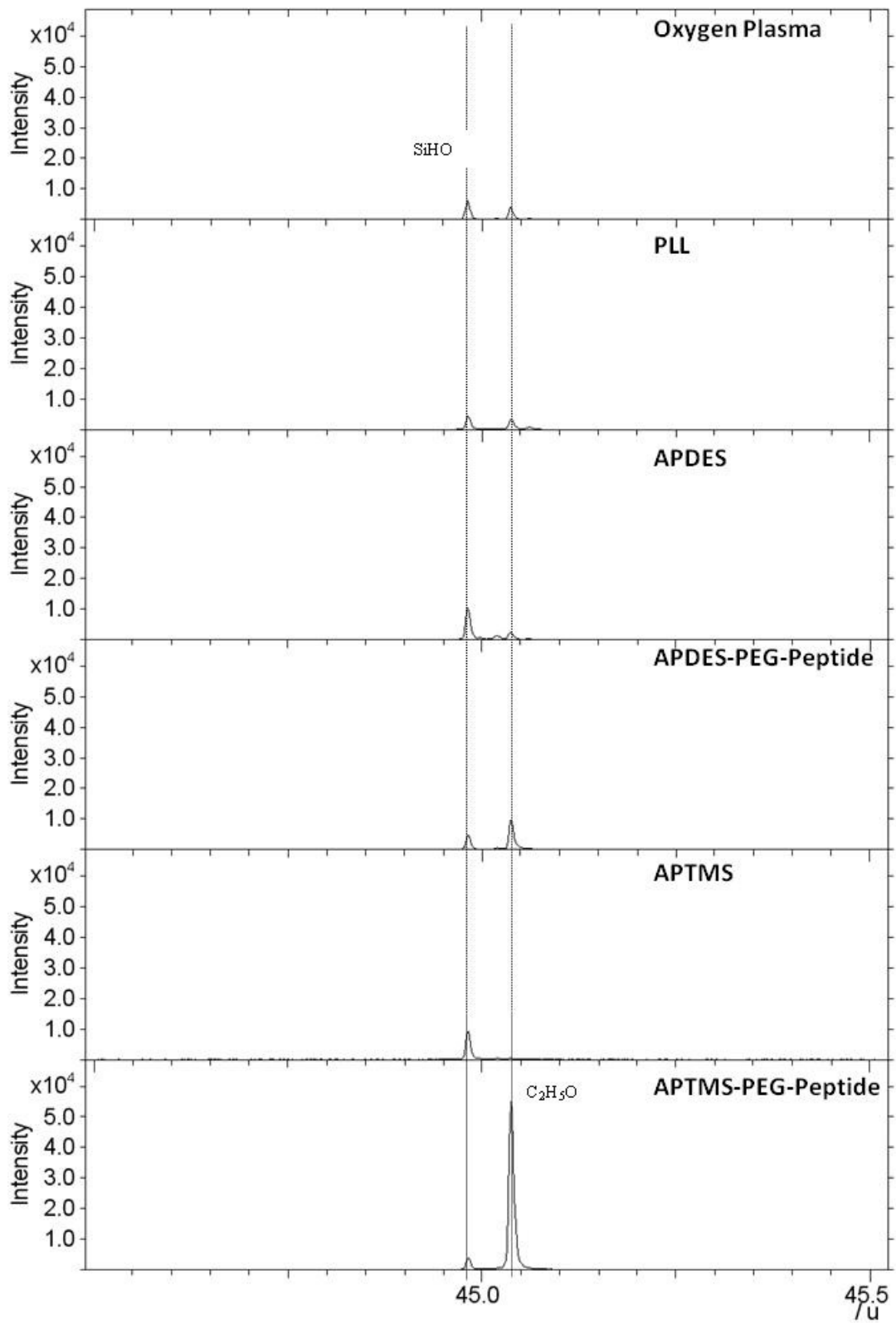
Appendix 4: ToF-SIMS Positive Ion Spectra: Glass surface modifications.



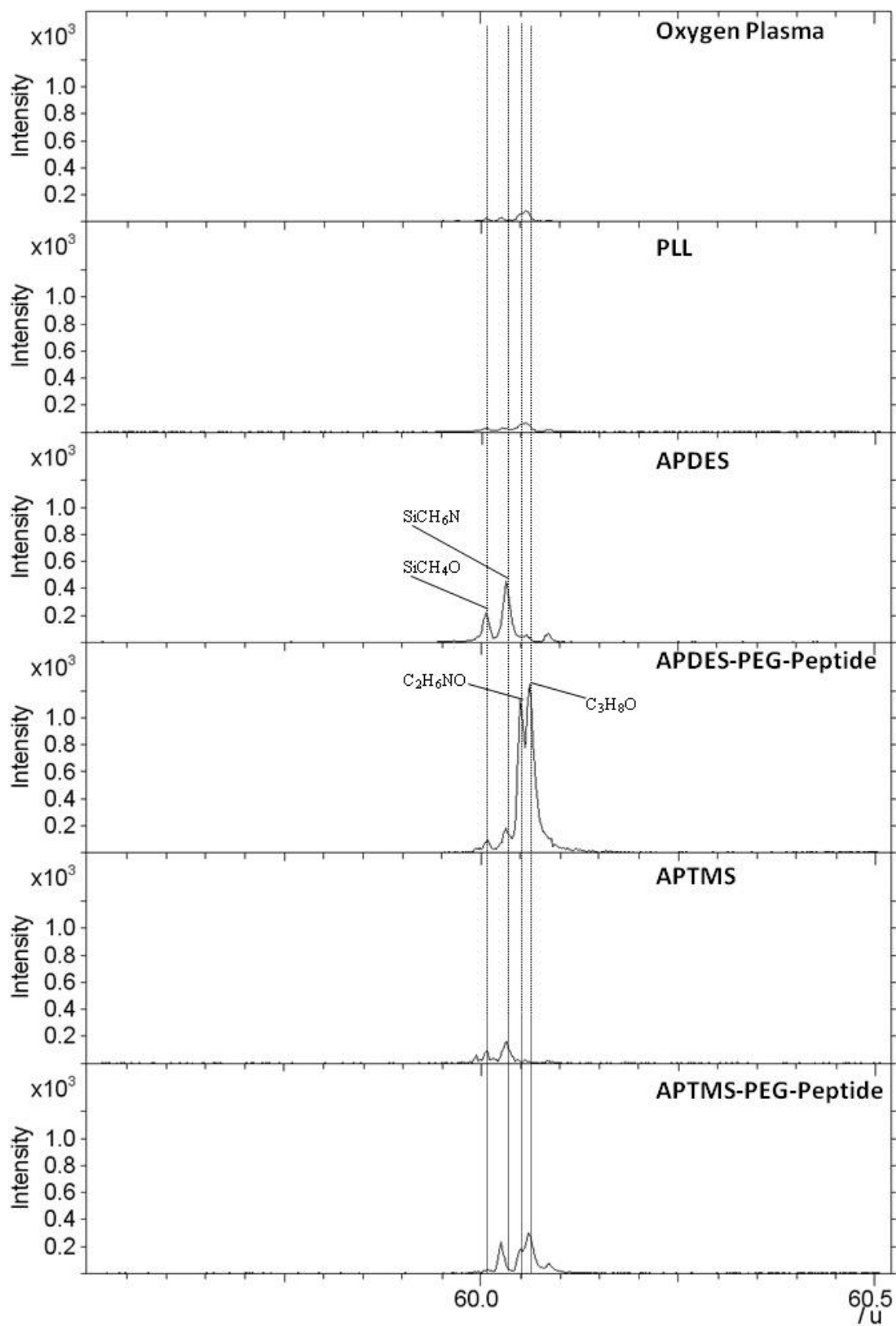
Appendix 5: ToF-SIMS Positive Ion Spectra: Glass surface modifications.  $C_4H_6NO^+$  fragment attributed to lysine.



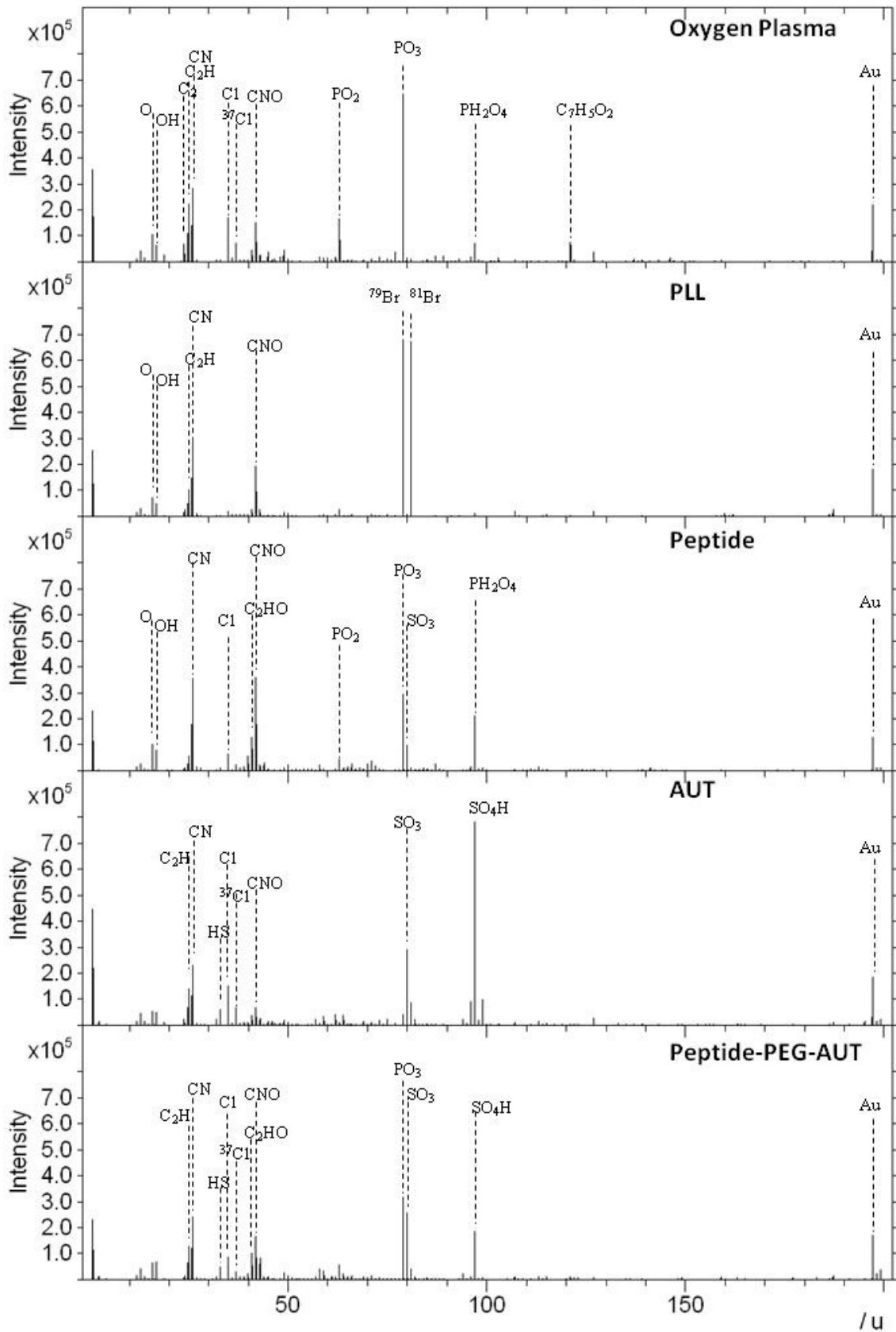
Appendix 6: ToF-SIMS Positive Ion Spectra: Glass surface modifications.  $C_2H_5O^+$  fragment attributed to PEG chain.



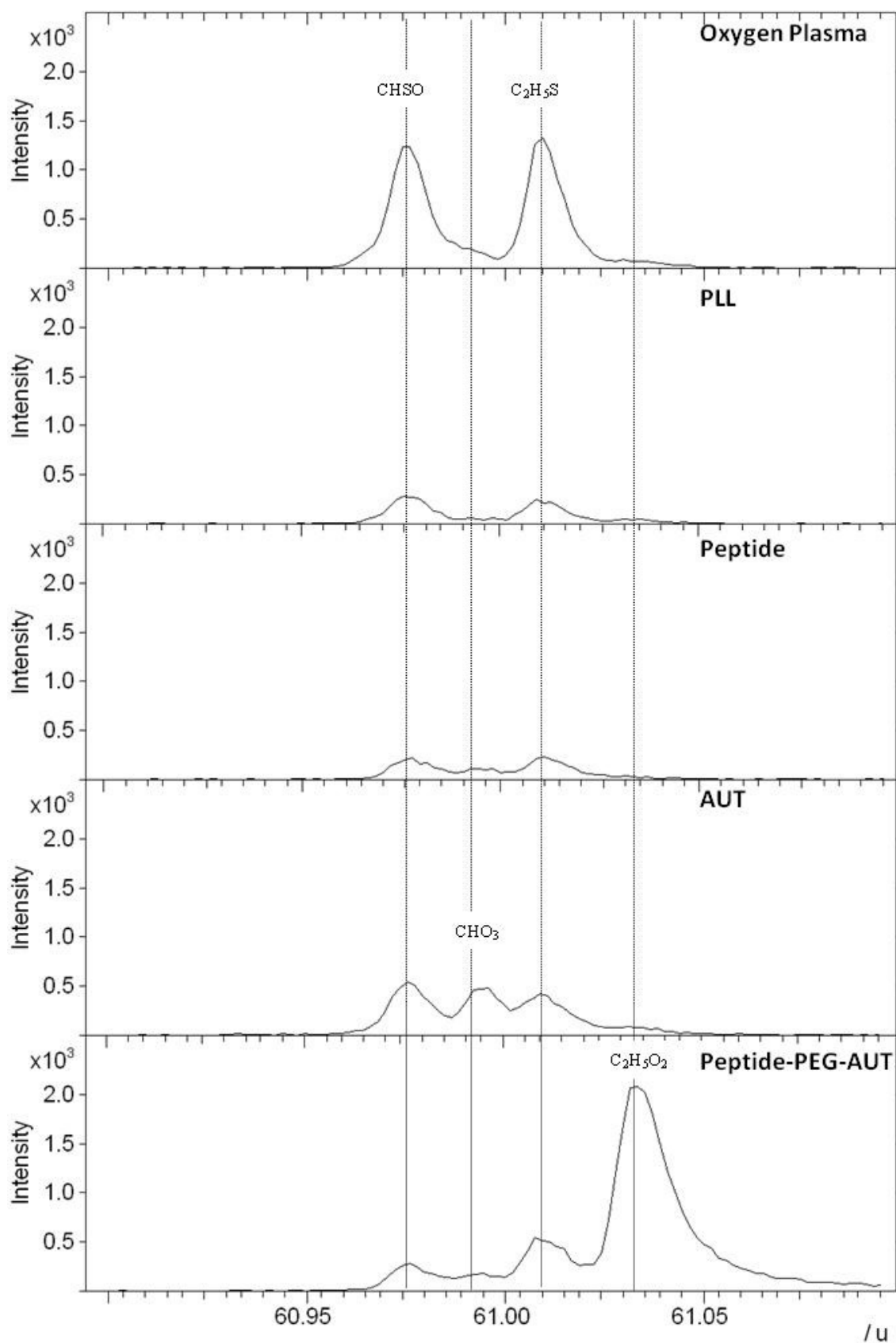
Appendix 7: ToF-SIMS Positive Ion Spectra: Glass surface modifications.  $C_2H_6NO^+$  fragment attributed to serine.



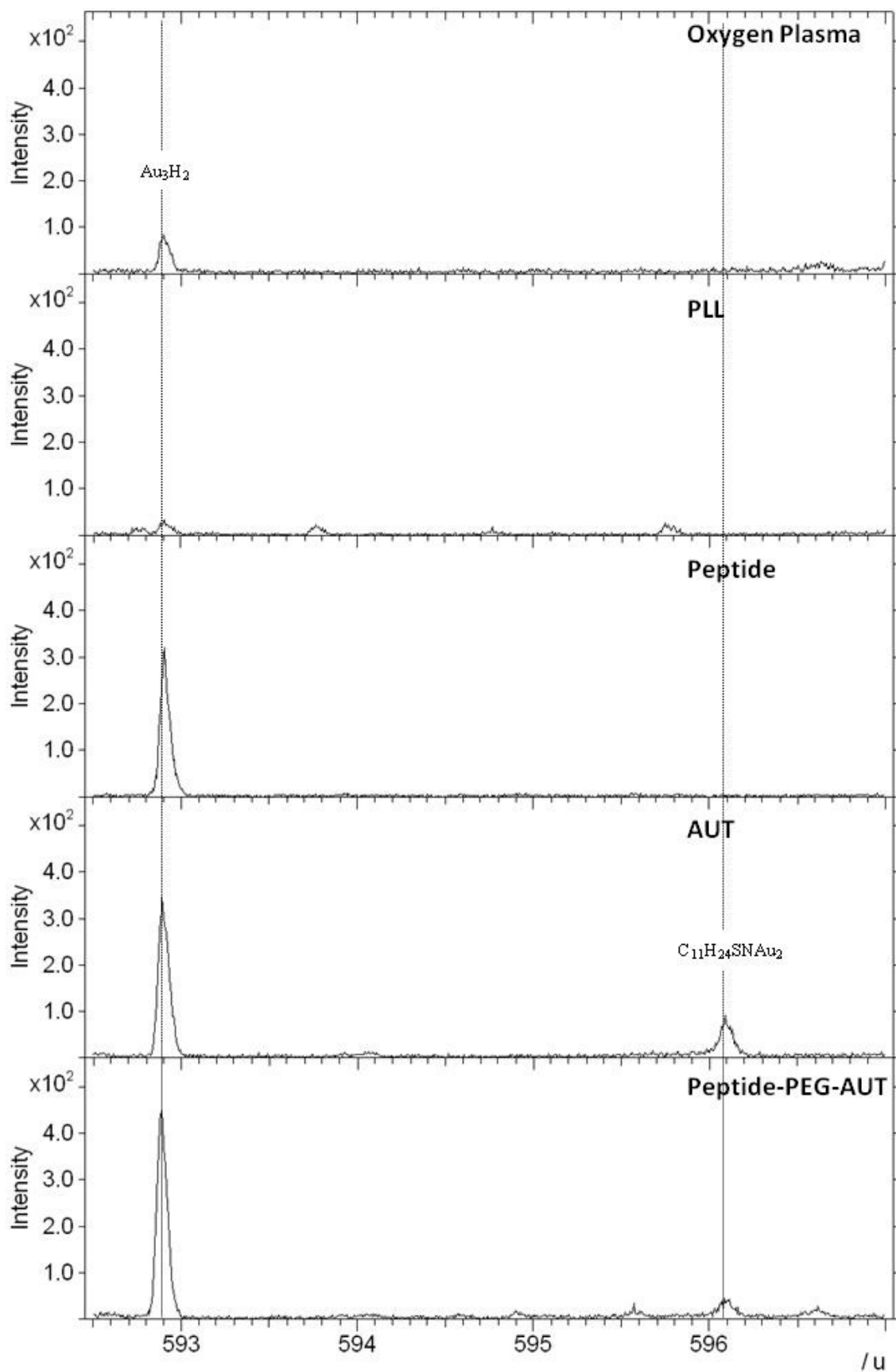
Appendix 8: ToF-SIMS Negative Ion Spectra: Gold surface modifications.



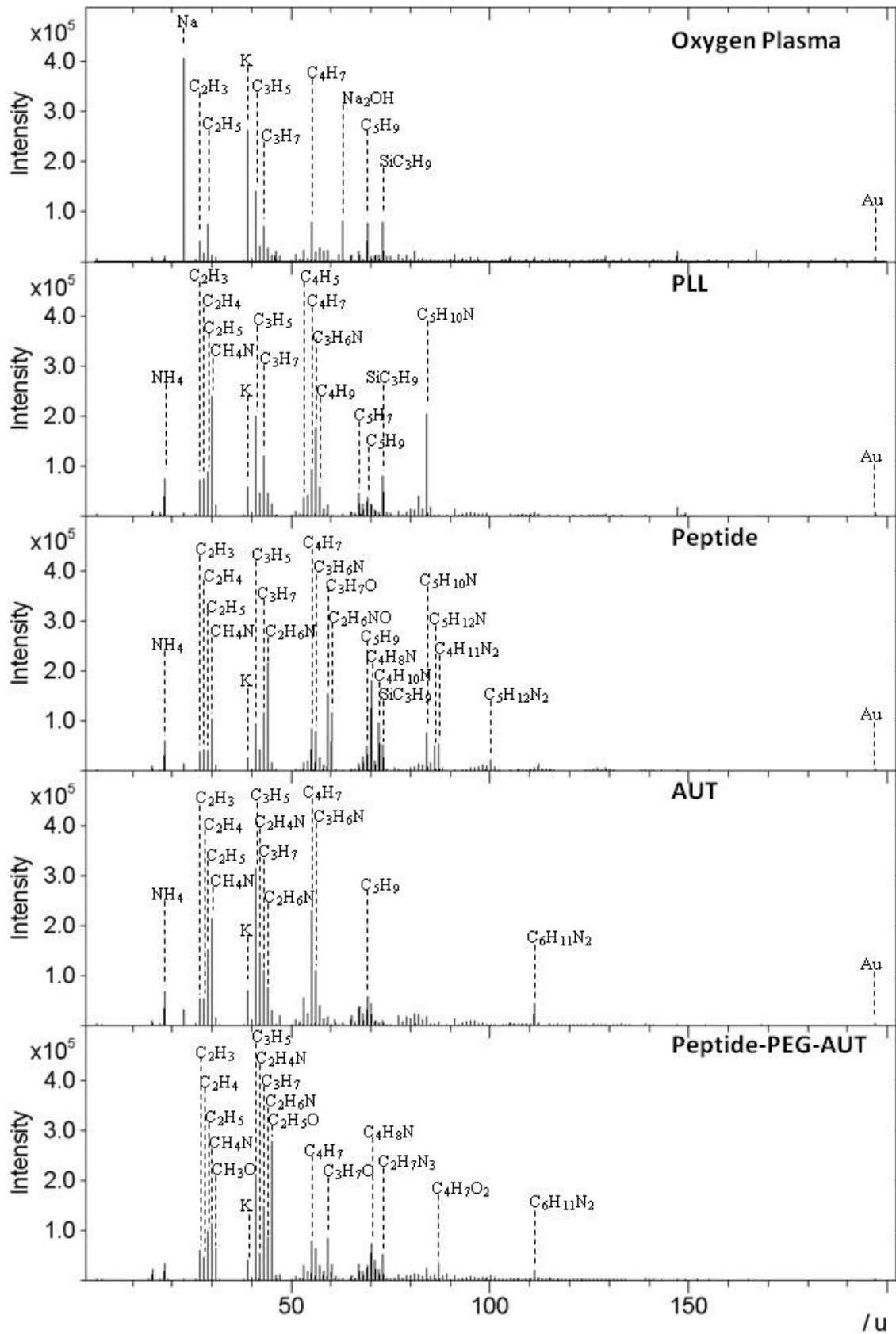
Appendix 9: ToF-SIMS Negative Ion Spectra: Gold surface modifications.  $C_2H_5O_2^-$  fragment attributed to PEG chain.



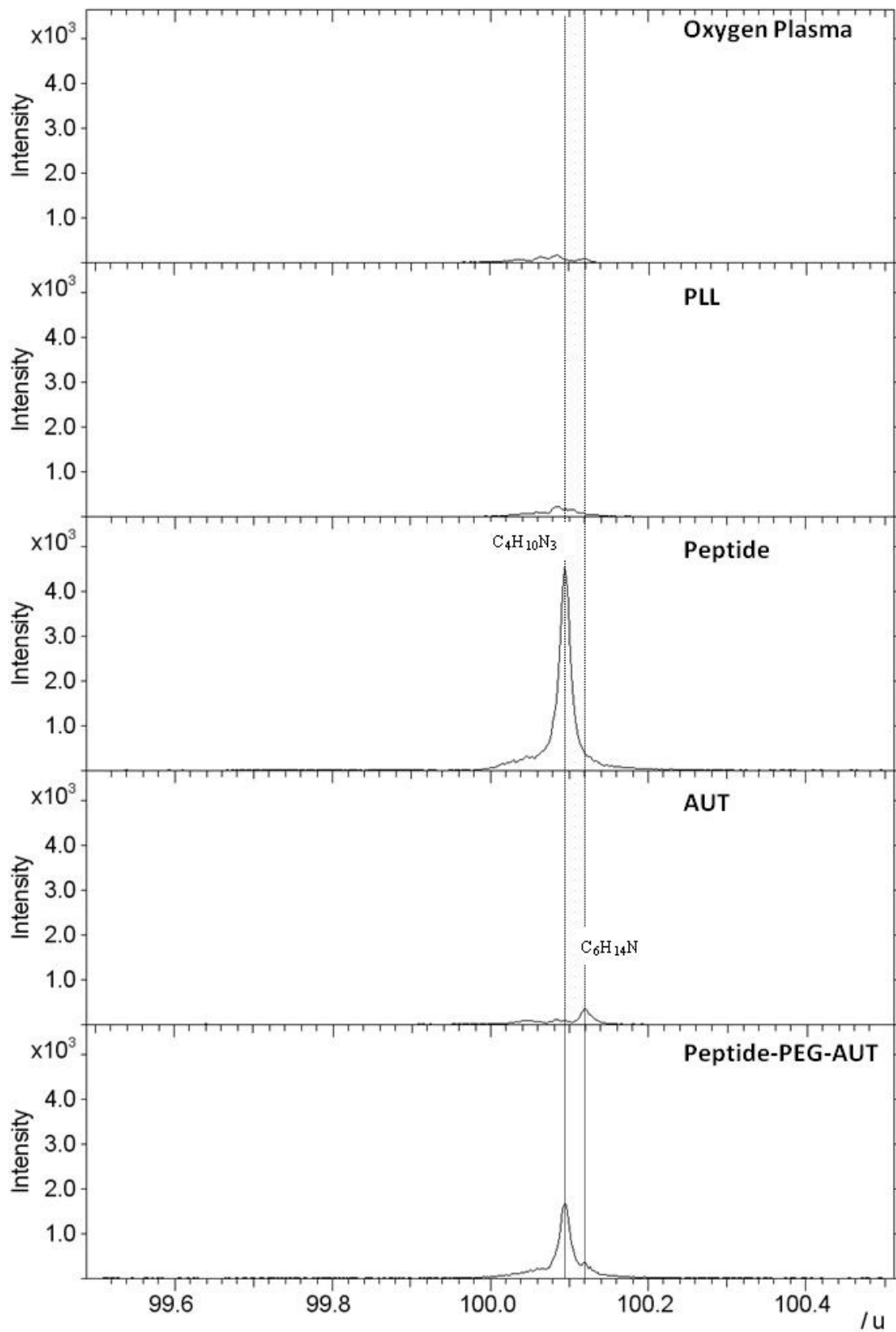
Appendix 10: ToF-SIMS Negative Ion Spectra: Gold surface modifications.  $C_{11}H_{24}SNAu_2^-$  fragment attributed to AUT.



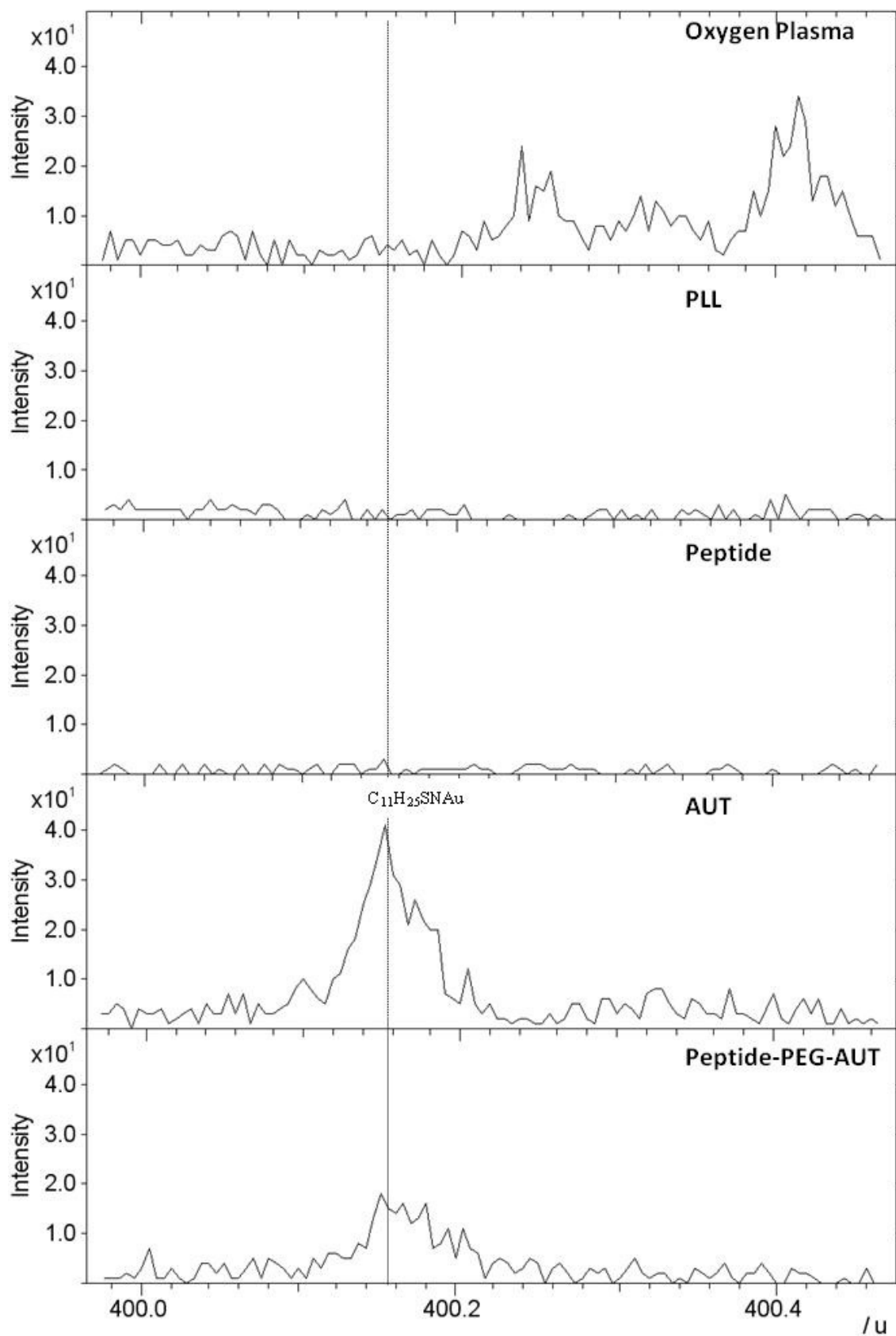
Appendix 11: ToF-SIMS Positive Ion Spectra: Gold surface modifications.



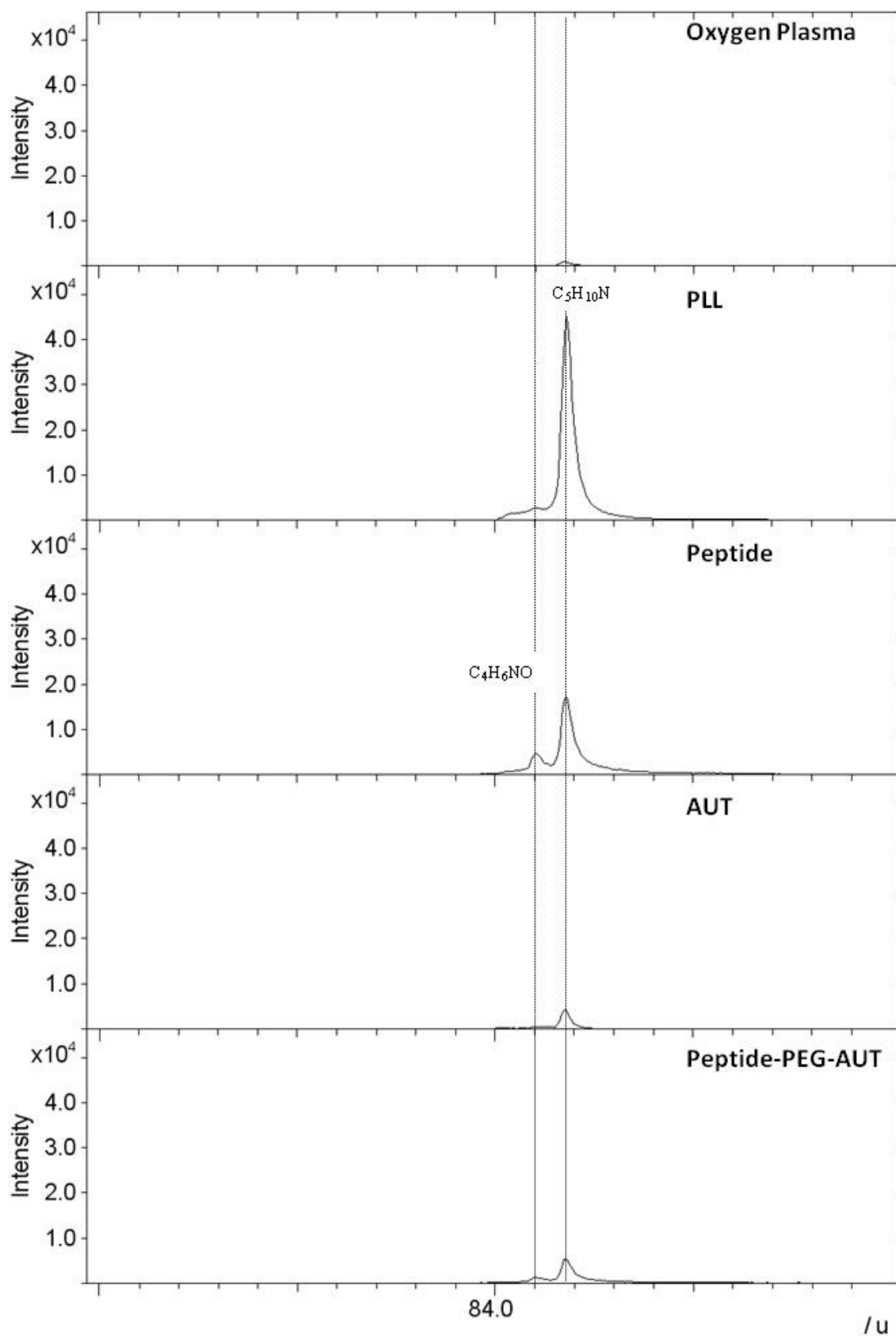
Appendix 12: ToF-SIMS Positive Ion Spectra: Gold surface modifications.  $C_4H_{10}N_3^+$  fragment attributed to arginine.



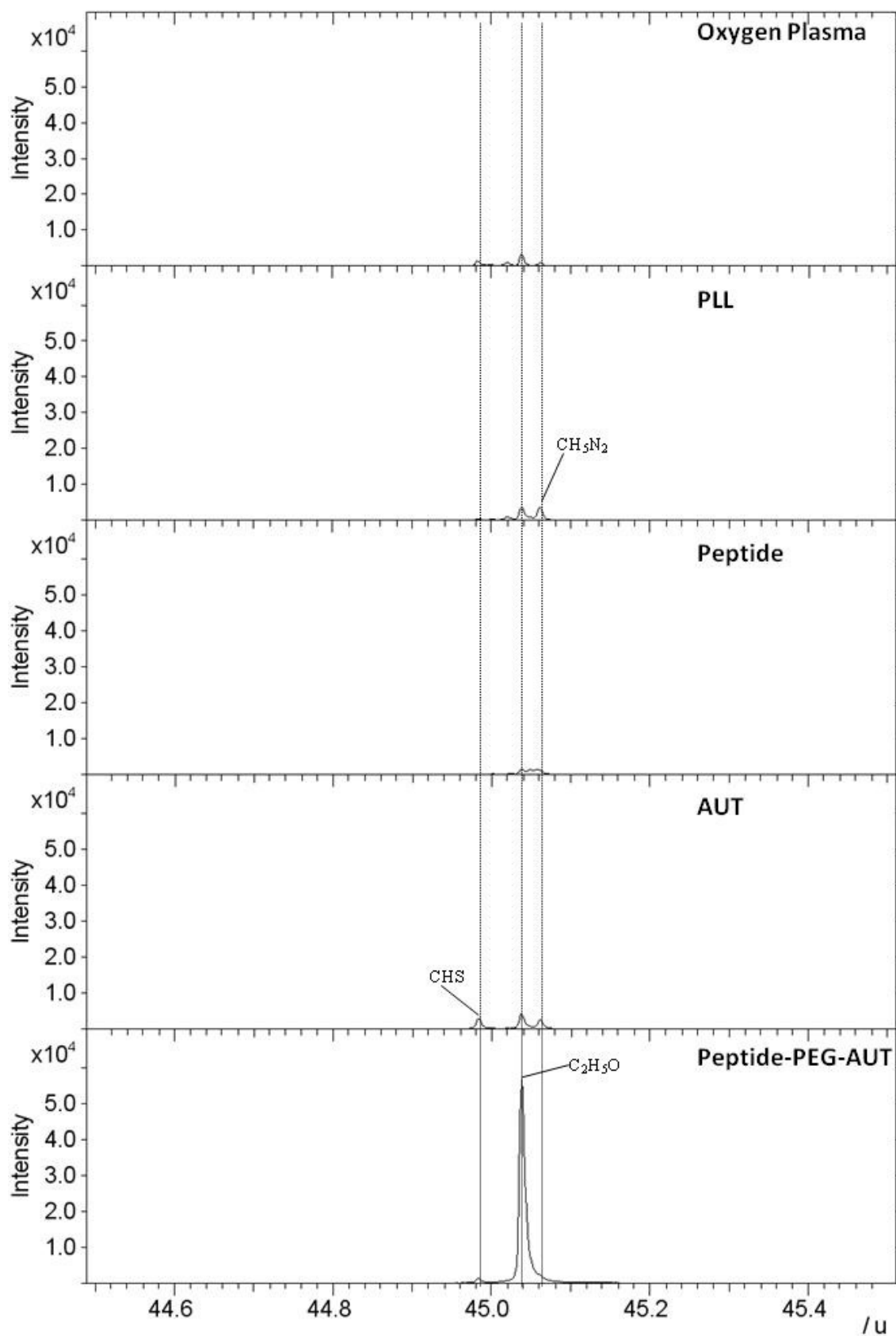
Appendix 13: ToF-SIMS Positive Ion Spectra: Gold surface modifications.  $C_{11}H_{25}SNAu^+$  fragment attributed to AUT.



Appendix 14: ToF-SIMS Positive Ion Spectra: Gold surface modifications.  $C_4H_6NO^+$  fragment attributed to lysine.



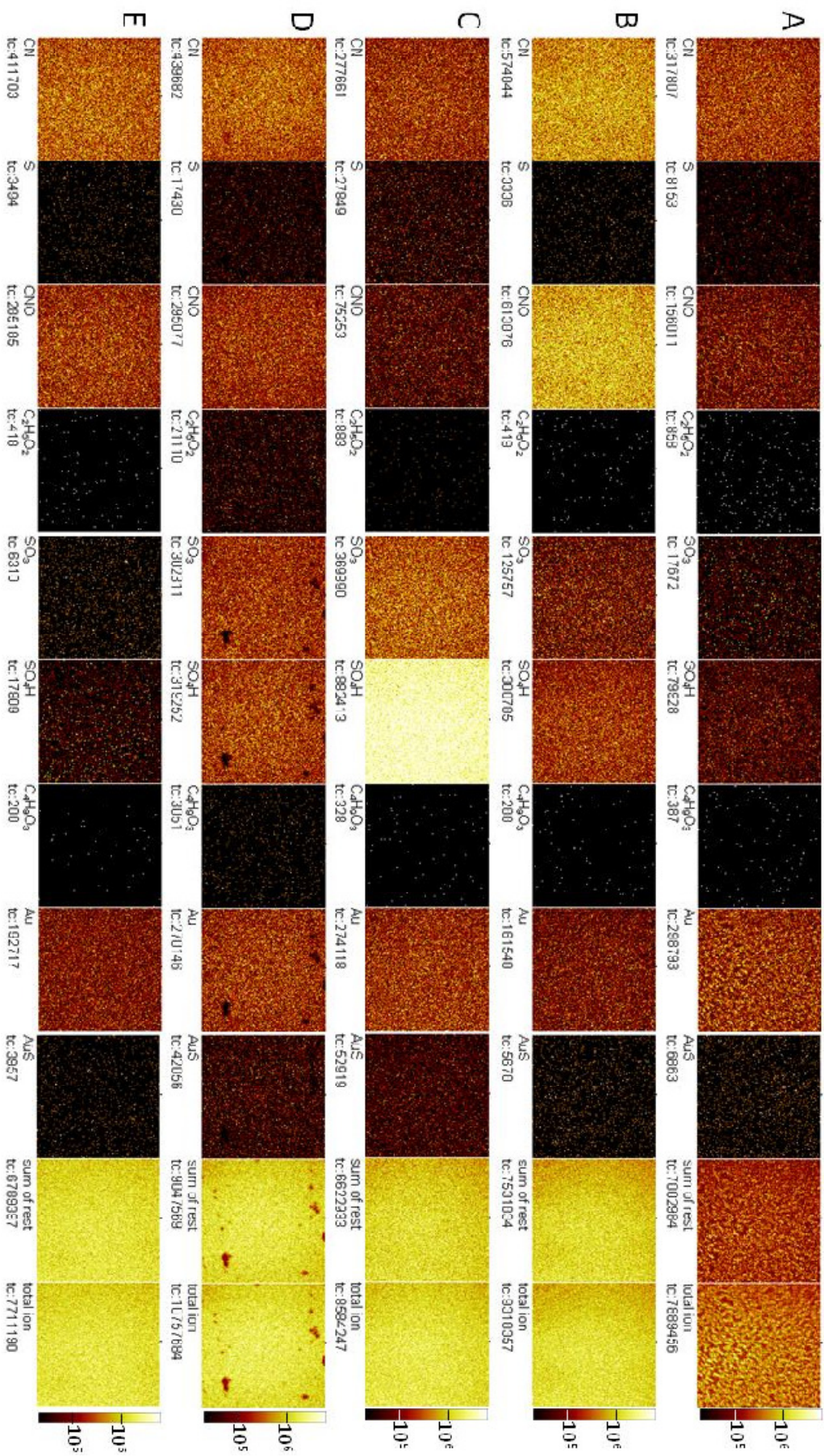
Appendix 15: ToF-SIMS Positive Ion Spectra: Gold surface modifications.  $C_2H_5O^+$  fragment attributed to PEG chain.



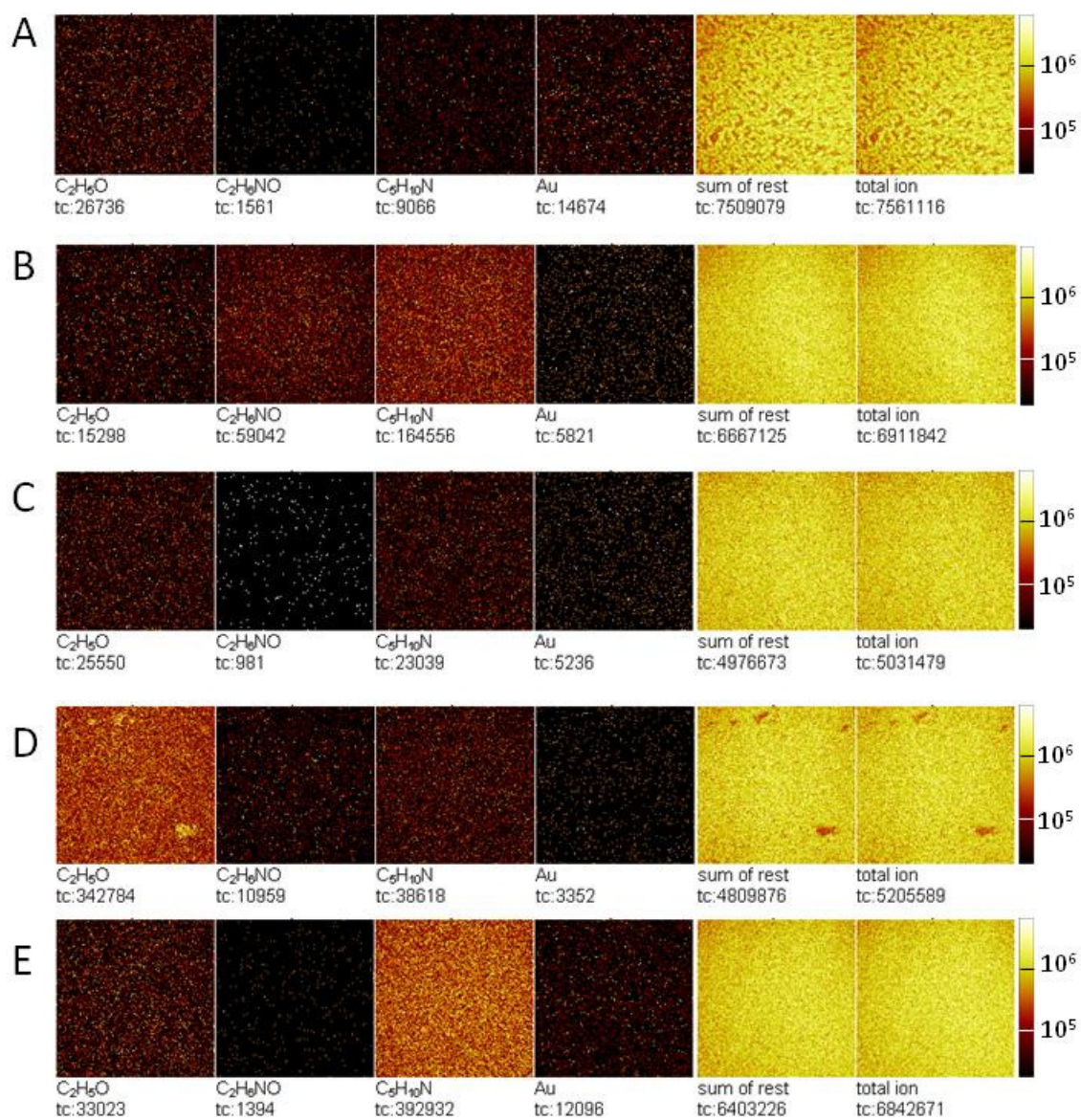
---

Appendix 16: ToF-SIMS negative ion images, 500×500 μm, of gold surface modifications:

A) Oxygen plasma etched; B) Peptide; C) AUT; D) AUT-PEG-Peptide; E) PLL.

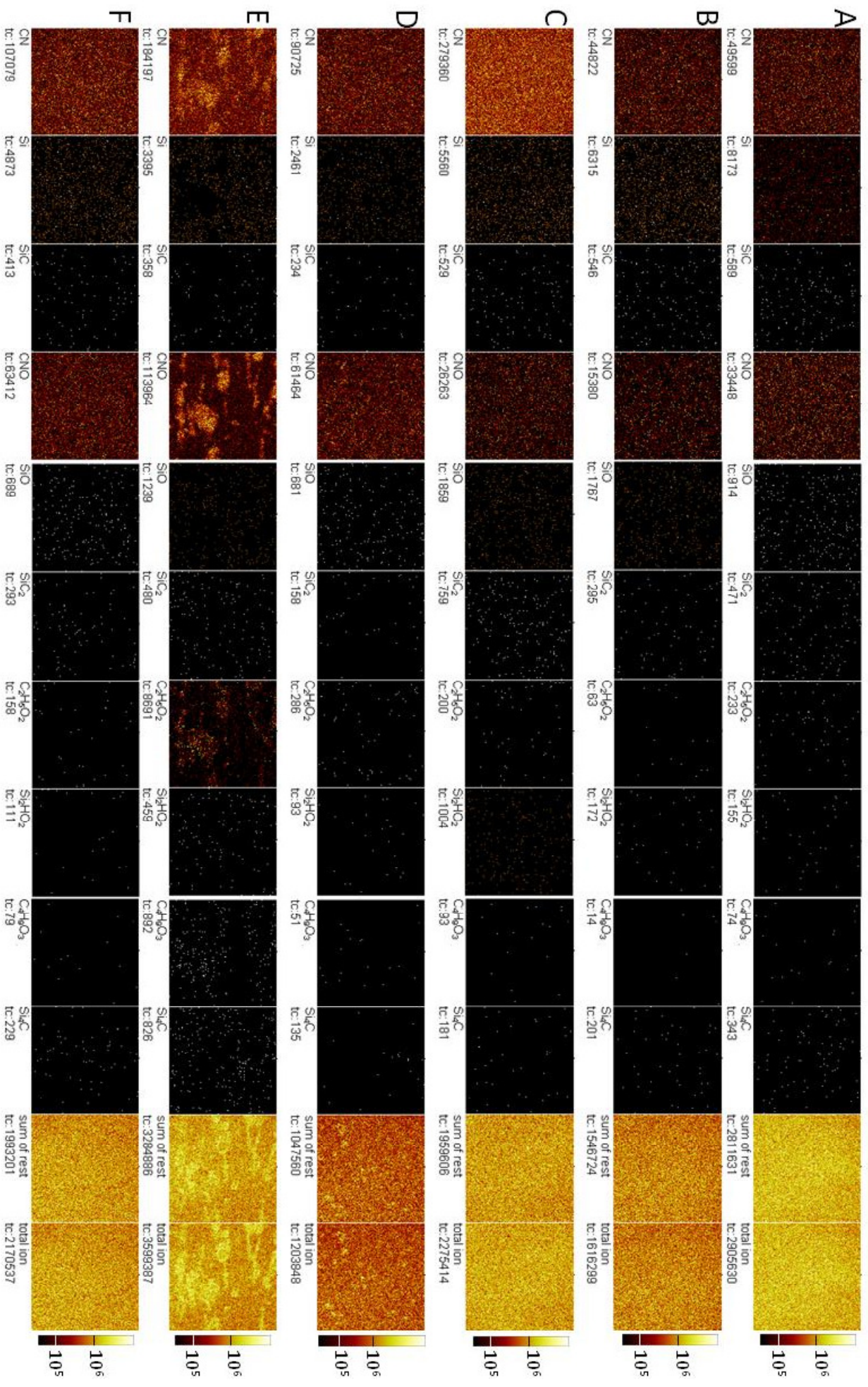


Appendix 17: ToF-SIMS positive ion images, 500×500 μm, of gold surface modifications: A) Oxygen plasma etched; B) Peptide; C) AUT; D) AUT-PEG-Peptide; E) PLL.



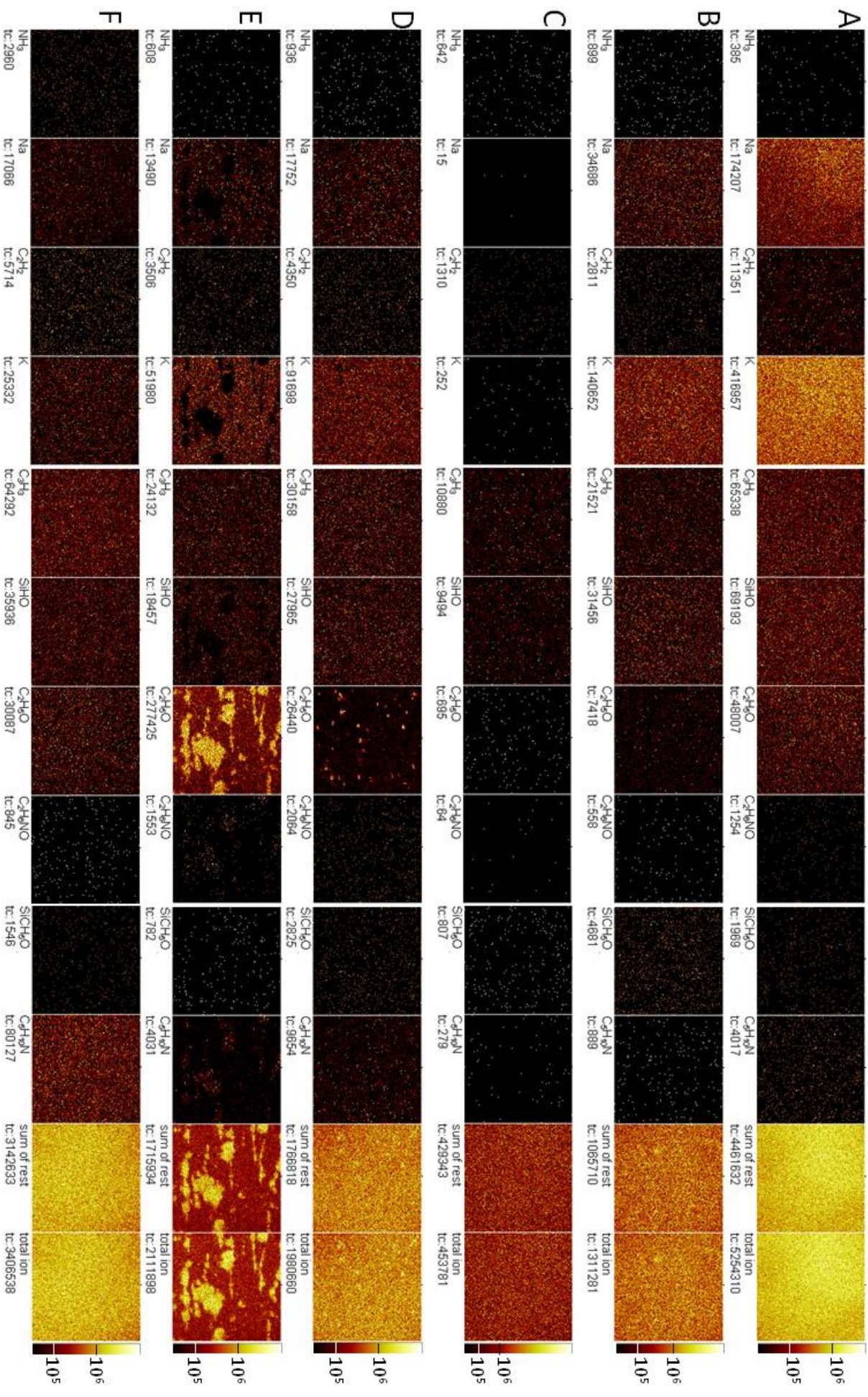
---

Appendix 18: ToF-SIMS negative ion images, 500×500 μm, of glass surface modifications:  
A) Oxygen plasma etched; B) APDES; C) APTMS; D) APDES-PEG-Peptide; E) APTMS-  
PEG-Peptide; F) PLL.

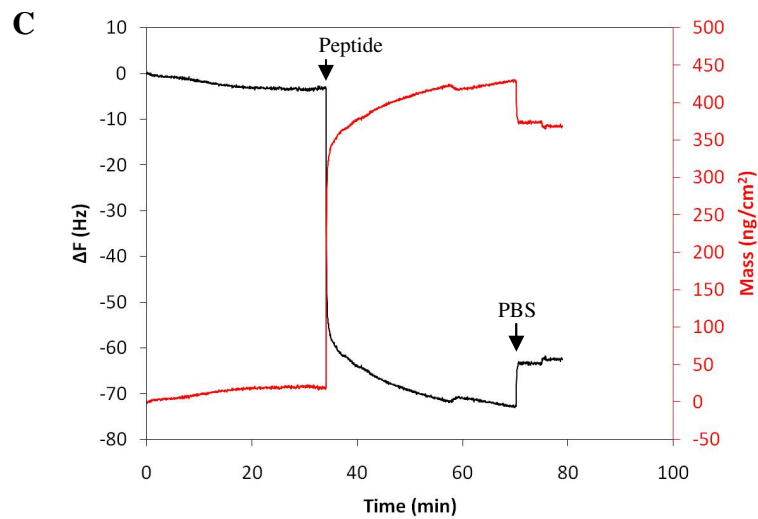
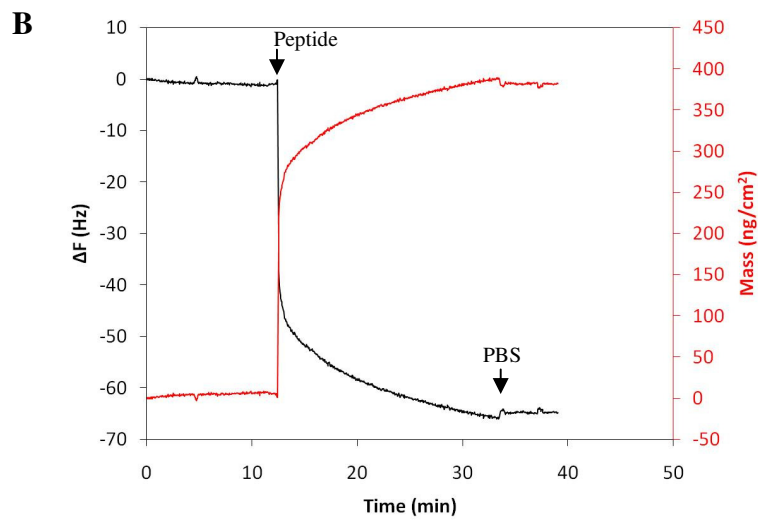
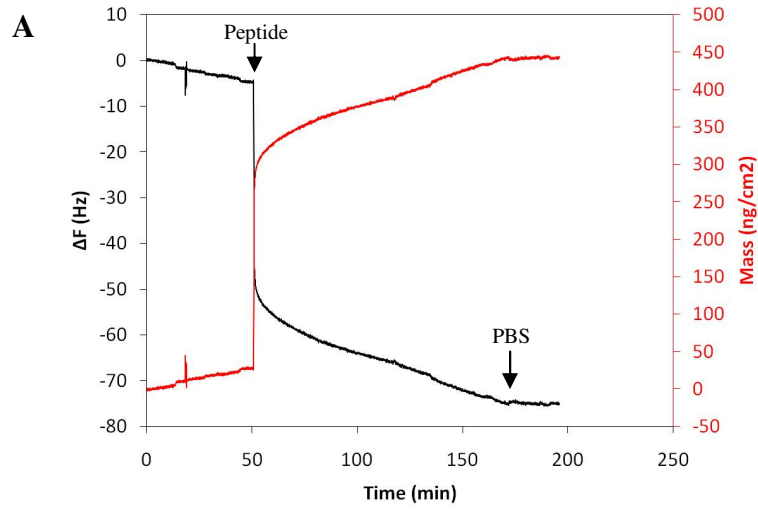


---

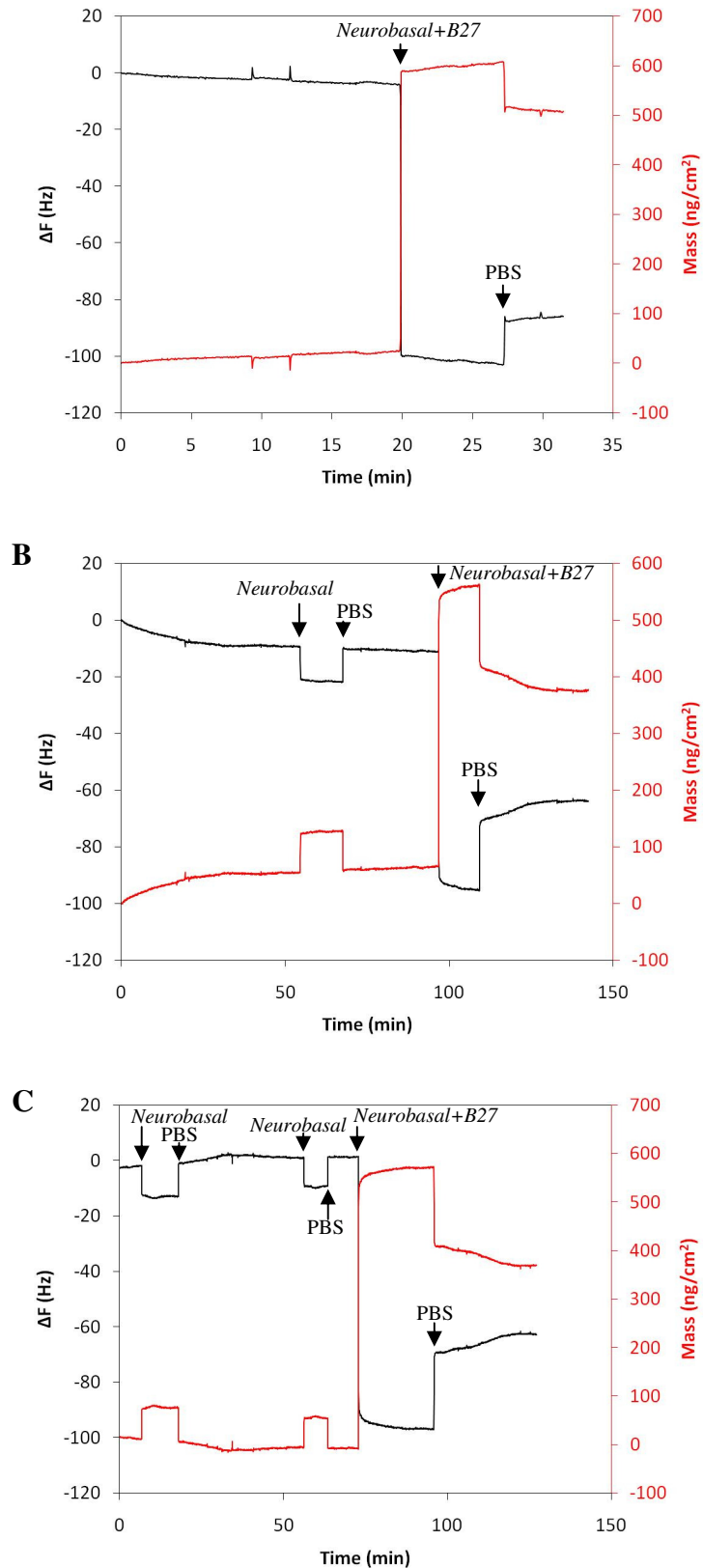
Appendix 19: ToF-SIMS positive ion images, 500×500 μm, of glass surface modifications:  
A) Oxygen plasma etched; B) APDES; C) APTMS; D) APDES-PEG-Peptide; E) APTMS-  
PEG-Peptide; F) PLL.



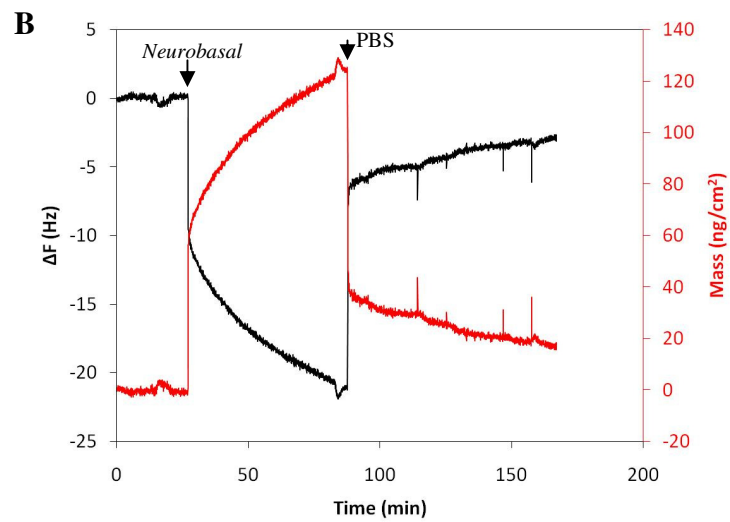
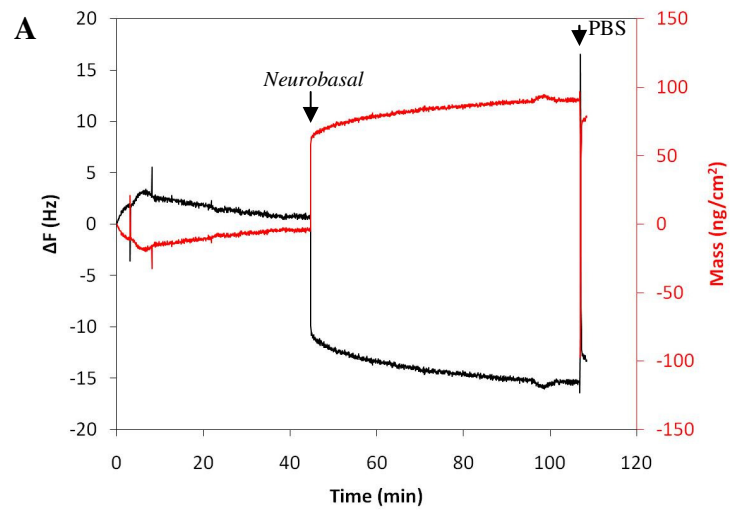
Appendix 20: QCM frequency and Sauerbrey mass plot: PA22-2 peptide (0.1mM in PBS) adsorption onto a gold sensor. Mass change of A) 414 ng/cm<sup>2</sup>; B) 375 ng/cm<sup>2</sup>; C) 349 ng/cm<sup>2</sup>.



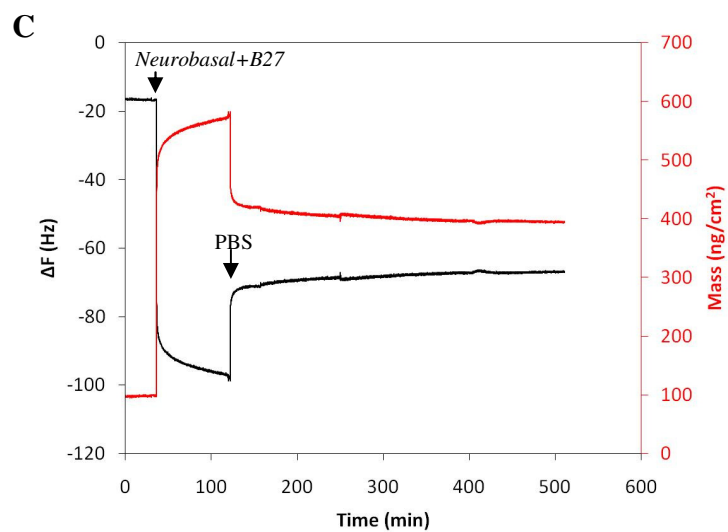
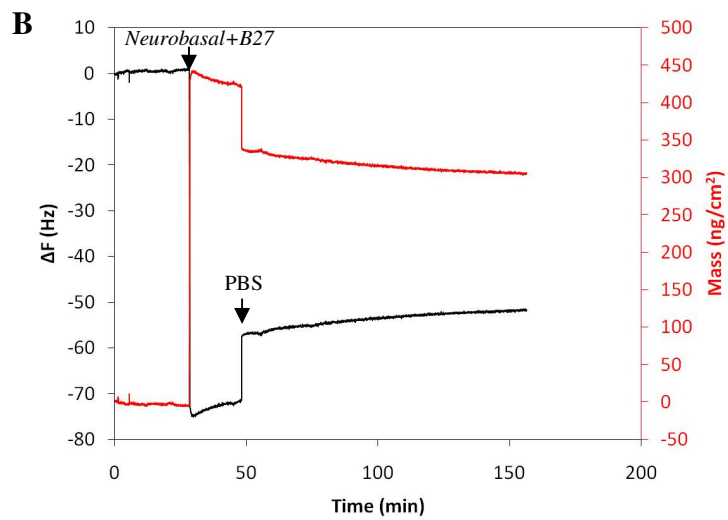
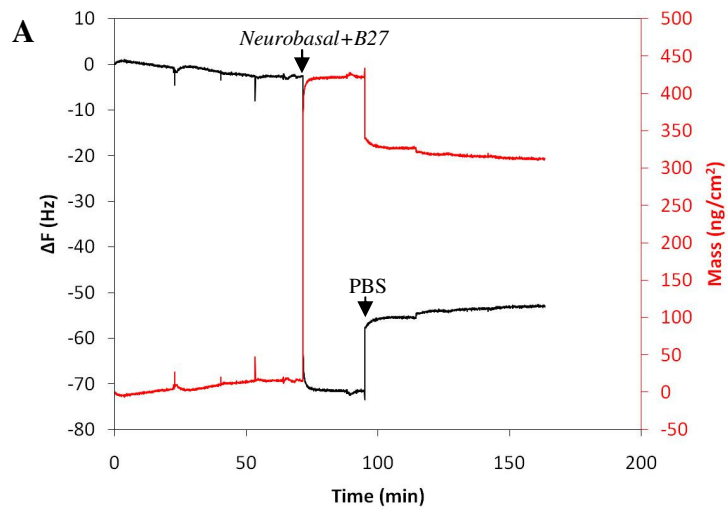
Appendix 21: QCM frequency and Sauerbrey mass plot: *Neurobasal* + *B27* adsorption on AUT-gold. Mass change of A) 485 ng/cm<sup>2</sup>; B) *Neurobasal* 5 ng/cm<sup>2</sup>, *Neurobasal*+*B27* 311 ng/cm<sup>2</sup>; C) *Neurobasal* -1 ng/cm<sup>2</sup>, *Neurobasal* 2 ng/cm<sup>2</sup>, *Neurobasal*+*B27* 377 ng/cm<sup>2</sup>.



Appendix 22: QCM frequency and Sauerbrey mass plot: *Neurobasal* adsorption onto Peptide-gold. Mass change of A) 80 ng/cm<sup>2</sup>; B) 19 ng/cm<sup>2</sup>.



Appendix 23: QCM frequency and Sauerbrey mass plot: *Neurobasal* + *B27* adsorption on Peptide-gold. Mass change of A) 298 ng/cm<sup>2</sup>; B) 334 ng/cm<sup>2</sup>; C) 297 ng/cm<sup>2</sup>.



Appendix 24: QCM frequency and Sauerbrey mass plot: *Neurobasal + B27* adsorption onto AUT-PEG-Peptide. Mass change of A) 46 ng/cm<sup>2</sup>; B) 93 ng/cm<sup>2</sup>; C) 71 ng/cm<sup>2</sup>.

